# Antimycobacterial characterisation of *Nα*-aroyl-*N*-aryl phenylalanine amides with focus on *Mycobacterium abscessus*


Dissertation

zur Erlangung des

Doktorgrades der Naturwissenschaften (*Dr. rer. nat.*)

Der

Naturwissenschaftlichen Fakultät I

– Biowissenschaften –

der Martin-Luther-Universität Halle-Wittenberg,

vorgelegt

von Dipl.-Pharm. Lea Mann

| | |
|---|---|
| Dekan: | Prof. Dr. Markus Pietzsch |
| Gutachter: | 1. Prof. Dr. Peter Imming |
| | 2. Prof. Dr. Gary Sawers |
| | 3. PD Dr. Norbert Reiling |
| Datum der Disputation: | 23.04.2025 in Halle (Saale) |

## Danksagung

Insbesondere möchte ich mich bei Professor Dr. Peter Imming und Dr. Adrian Richter bedanken. Für die Aufnahme in die Arbeitsgruppe, die hervorragende Betreuung und das entgegengebrachte Vertrauen. Die Ermöglichung der Auslandsaufenthalte im Rahmen von Konferenzbesuchen ist nicht selbstverständlich, hat aber die persönliche Entwicklung, die Motivation und die Zusammenarbeit in der Arbeitsgruppe entscheidend geprägt.

Mein Dank gilt den Mitgliedern der AG Imming für ihre Kooperation: Adrian, Andi, Christoph, Fabienne, Franzi, Johannes, Julia, Markus, Paul, Rana und Ruth, die die familiäre, fröhliche Atmosphäre und Kulinarik des Sozialraums auch über Kontinente hinweg getragen haben und eine unersetzliche fachliche, aber auch freundschaftliche Unterstützung bedeuteten.

Unseren Kooperationspartnern, der Gruppe um Professor Dr. Thomas Dick, sowie Professor Dr. Elizabeth Campbell und Dr. Barbara Bosch danke ich für all die anregenden Diskussionen in 2D und die produktiven Treffen in 3D. Danke auch an Professor Dr. Courtney Aldrich für die hilfsbereite, fördernde Zusammenarbeit bei den Besuchen in unserer Arbeitsgruppe.

An dieser Stelle möchte ich mich auch bei Dr. Nadine Taudte, Nadine Jänckel und Dr. Jens-Ulrich Rahfeld für die Unterstützung bei den Arbeiten in den Sicherheitslabors bedanken.

Auch danke ich Caroline für die Durchsicht der Arbeit und für alles was Sie mir über die englische Sprache beigebracht hat.

Mein Dank gilt auch der Deutschen Forschungsgemeinschaft für die finanzielle Förderung dieses Projektes (Nr. 432291016).

Meiner Familie, insbesondere meinen Eltern und Moritz danke ich für ihre Ermutigung und Beistand. Ohne eure Liebe, Geduld und Unterstützung wäre dieser Weg undenkbar gewesen.

## Table of Contents

## List of Abbreviations

| | |
|---|---|
| AAPs | *N*α-aroyl-*N*-aryl-phenylalanine amides |
| ADS | albumin, dextrose, sodium chloride |
| CFU | colony forming unit |
| COPD | chronic obstructive pulmonary disease |
| DAPI | 4′,6-diamidin-2-phenylindol |
| DprE1 | Decaprenylphosphoryl-β-D-ribofuranose 2′-oxidase |
| FICI | fractional inhibitory concentration index |
| GPL | glycopeptidolipid |
| *M. abscessus* | *Mycobacterium abscessus* |
| *M. avium* | *Mycobacterium avium* |
| *M. intracellulare* | *Mycobacterium intracellulare* |
| *M. smegmatis* | *Mycobacterium smegmatis* |
| *M. tuberculosis* | *Mycobacterium tuberculosis* |
| MBC | minimum bactericidal concentration |
| MIC | minimum inhibitory concentration |
| MmpL | mycobacterial membrane protein Large |
| NTM | non-tuberculous mycobacteria |
| OADC | oleic acid, albumin, dextrose, catalase |
| PD | pulmonary disease |
| R | rough (morphotype of *M. abscessus*) |
| RFP | red fluorescent protein |
| RNAP | RNA polymerase |
| ROS | reactive oxygen species |
| S | smooth (morphotype of *M. abscessus*) |
| TNF | tumour necrosis factor |
| 3HC-2-Tre | 2-(6-(diethylamino)benzofuran-2-yl)-3-hydroxy-4*H*-chromen-4-one-conjugated trehalose |

## List of Figures



## List of Tables

# 1 Introduction

## 1.1 Non-tuberculous Mycobacteria

Non-tuberculous mycobacteria (NTM) are referred to as environmental mycobacteria, atypical mycobacteria and mycobacteria other than tuberculosis. They are one group of three in the genus mycobacteria, belonging to the phylum of actinobacteria (Johansen, Herrmann and Kremer, 2020). The other two species of mycobacteria are *Mycobacterium tuberculosis* complex and *Mycobacterium leprae* (Table 1). Approximately 200 species of mycobacteria are known.

### 1.1.1 Systematics of Mycobacteria

The phylogenetic trees of bacteria are generated on the basis of 16S rRNA sequencing (Johnson *et al.*, 2019). Additionally, phenotypic criteria can be used to describe and identify a strain. These include morphology (e.g. staining pattern, see section 1.1.3), susceptibility towards antibiotics, ecological niche, causative disease and immunology (Fritsche, 2016). An accepted species concept is the "phylo-phenetic species concept" (Rosselló-Mora, 2001). It describes: "A monophyletic and genomically coherent cluster of individual organisms that show a high degree of overall similarity in many independent characteristics, and is diagnosable by a discriminative phenotypic property" (Chun, 2017).

According to current publications, the identification of a mycobacterial species is based on molecular methods. For this purpose, 16S rRNA sequencing is used, or identification is carried out using the rpoB and hsp65 genes (Forbes, 2017, Armstrong, Eisemann and Parrish, 2023, Aziz *et al.*, 2017). In addition, there are different criteria for classifying mycobacteria: Runyon's characterisation takes into account not only the growth rate, but also the production of yellow pigment and whether this pigment is produced with or without exposure to light (Photochromogenicity) (Rogall *et al.*, 1990).

However, NTM are usually classified according to their growth-rate. A distinction is made between mycobacteria that form colonies on the agar medium in less than seven days (rapid-growing) and mycobacteria that form visible colonies on agar in more than seven days (slow-growing). A classification of some specific mycobacteria is given in Table 1. It should be noted that most pathogenic mycobacteria belong to the group of slow-growing mycobacteria (Johansen, Herrmann and Kremer, 2020).

**Table 1** *Rapid-growing and slow-growing mycobacteria.*

| Non-tuberculous mycobacteria | | Other species |
|---|---|---|
| Rapid-growing mycobacteria | Slow-growing mycobacteria | |
| *M. abscessus*<br>subsp. *abscessus*<br>subsp. *bolletii*<br>subsp. *massiliense* | *M. marinum* | *M. tuberculosis* complex |
| | *M. ulcerans* | *M. leprae* |
| | *M. avium* complex*<br>*M. avium*<br>*M. intracellulare*<br>*M. chimera* | |
| *M. chelonae* | | |
| *M. fortuitum* | | |
| *M. smegmatis* | *M. kansasii* | |
| *M. vaccae* | *M. xenopi* | |

| |
|---|
| true pathogens |
| opportunistic pathogens |

Table adapted from (Johansen, Herrmann and Kremer, 2020). *The *M. avium* complex currently consists of 12 species, shortened here to three for the sake of clarity (van Ingen *et al.*, 2018; Wengenack *et al.*, 2024).

Taxonomic nomenclature

In 2018 a new nomenclature for mycobacteria was validated and published by the International Journal of Systematic and Evolutionary Microbiology(Oren and Garrity, 2018). Therefore, two nomenclatural names coexist: *Mycobacterium/ Mycobacteroides abscessus*. They can be used synonymously. To avoid confusion, leading researchers suggest continuing to use the name *Mycobacterium abscessus* (Tortoli *et al.*, 2019).

### 1.1.2 Epidemiology of NTM infections

Reliable information on the epidemiology of NTM infections is difficult to obtain because of under-reporting and lack of differentiation of mycobacterial pathogens. The American Thoracic Society/Infectious Disease Society of America guidelines provide a definition of a case of NTM pulmonary disease (NTM-PD) based on specific microbiological, radiological and clinical criteria. However, a case of infection can be defined differently for epidemiological counts (Prevots *et al.*, 2023). This makes it difficult to consistently count NTM-PD cases worldwide and to compare NTM-PD case numbers. In addition, there is no obligation to report NTM infections. NTM species vary between regions and countries, but microbiological data indicate a global increase in cases of *Mycobacterium avium* and *Mycobacterium abscessus.* The two pathogens are responsible for 80-85 % of NTM lung infections worldwide (Prevots and Marras, 2015).

As in Germany, infections with *Mycobacterium tuberculosis/africanum* or *Mycobacterium leprae* and *Mycobacterium bovis* are notifiable (Infektionsschutzgesetz §7),

but not cases of infection with NTM. Data from two studies are cited below to assess the epidemiology in Germany.
A Delphi study compared prevalence rates in Europe between France, Germany, Spain and the United Kingdom. The prevalence rates in Europe for NTM-PD ranged from 6.1/100,000 to 6.6/100,000 (Prevots *et al.*, 2023). A retrospective epidemiological study evaluated diagnostic data from 22 German laboratories over a 5-year period (2016-2020). The calculated laboratory incidence and prevalence of NTM obtained from respiratory samples in the German population were 4.5 to 4.9 and 5.3 to 5.8/100,000 inhabitants, respectively, and remained stable over the five years (Corbett *et al.*, 2023). In comparison, the incidence of *M. tuberculosis* infections in Germany in 2020 was 5.0/100,000 (Brodhun *et al.*, 2020).

To obtain a realistic picture of the number of NTM infections, a pulmonologist from one of four hospitals in a large city with a population of around 200,000 was consulted. Prof. Dr. Wolfgang Schütte, Medical Director and Chief Physician of the Clinic for Internal Medicine II and Pneumology at the Martha-Maria Hospital in Halle-Dölau, encounters about 15 cases of new diagnoses of atypical mycobacteria per year, including one to two infections with *M. abscessus*.

### 1.1.3 Characteristics of Mycobacteria

Non-tuberculous mycobacteria are categorised as Gram-positive bacteria, due to the structure of their cell envelope and RNA-analysis. They are rod-shaped, do not form spores, and are known as obligate aerobes. During evolution, saprophytic bacteria living in soil and water have developed a rapid and effective ability to adapt to different habitats. Together with the ability to form biofilms on different surfaces, the ability to adapt to the environment plays a key role in their pathogenesis.

Mycobacterial cell envelope

The waxy lipid-rich layer contributes to the high resistance to environmental influences and acts as an important barrier to antibiotics (Dulberger, Rubin and Boutte, 2020). The schematic structure of a mycobacterial cell wall is shown in Figure 1.
From the inside out, the periplasmic space is followed by a layer of peptidoglycan (murein) adjacent to the cytoplasmic membrane. This is a lattice structure consisting of linear chains of two alternatively linked amino sugar, *N*-acetylglucosamine and *N*-acetylmuramic acid. The alternating sugars are connected by a β-(1,4)-glycosidic linkage. These in turn are linked by peptides between the *N*-acetylmuramic acid molecules to form the aforementioned lattice structure. Covalently linked to the peptidoglycan layer is a layer of arabinogalactan, a layer of branched arabinose and galactose molecules. This is followed by the outer membrane,

whose mycolic acid components are covalently linked to the arabinogalactan layer. The mycomembrane is also composed of lipids, glycolipids and proteins. Externally, it consists mainly of mycolic acids, which may be free or bound to trehalose sugars (Dulberger, Rubin and Boutte, 2020).

The mycolic acid in the cell wall of mycobacteria prevents the penetration of hydrophilic dyes, so the cell envelope does not absorb the Gram stain. Instead, acid-fast stains such as Ziehl-Neelsen or fluorescent stains (eg. auramine–rhodamine stain) can be used to identify the bacteria (Cudahy and Shenoi, 2016). As shown in Figure 1, the mycomembrane consists of a number of different molecules such as lipoglycans and lipids. Some of these molecules such as glycopeptidolipids, trehalose dimycolate, trehalose monomycolate and phosphatidyl-inositol mannoside are clinically relevant as changes and regulation can be observed during pathogenesis (Parmar and Tocheva, 2023). In particular, trehalose dimycolate, known as cord factor, can prevent the fusion of phospholipid vesicles such as phagosomes and lysosomes (Poirier and Av-Gay, 2015). In addition, mycobacterial membrane protein Large (MmpL) proteins embedded in the cytoplasmic membrane are shown in Figure 1. MmpLs play a role in intrinsic resistance mechanisms as they can act as efflux pumps (Boudehen and Kremer, 2021). It is worth noting that different transpeptidases are expressed in *M. abscessus* compared to *M. tuberculosis* for the linkage of peptidoglycan, leading to differences in the efficacy of β-lactams (Kumar *et al.*, 2017).

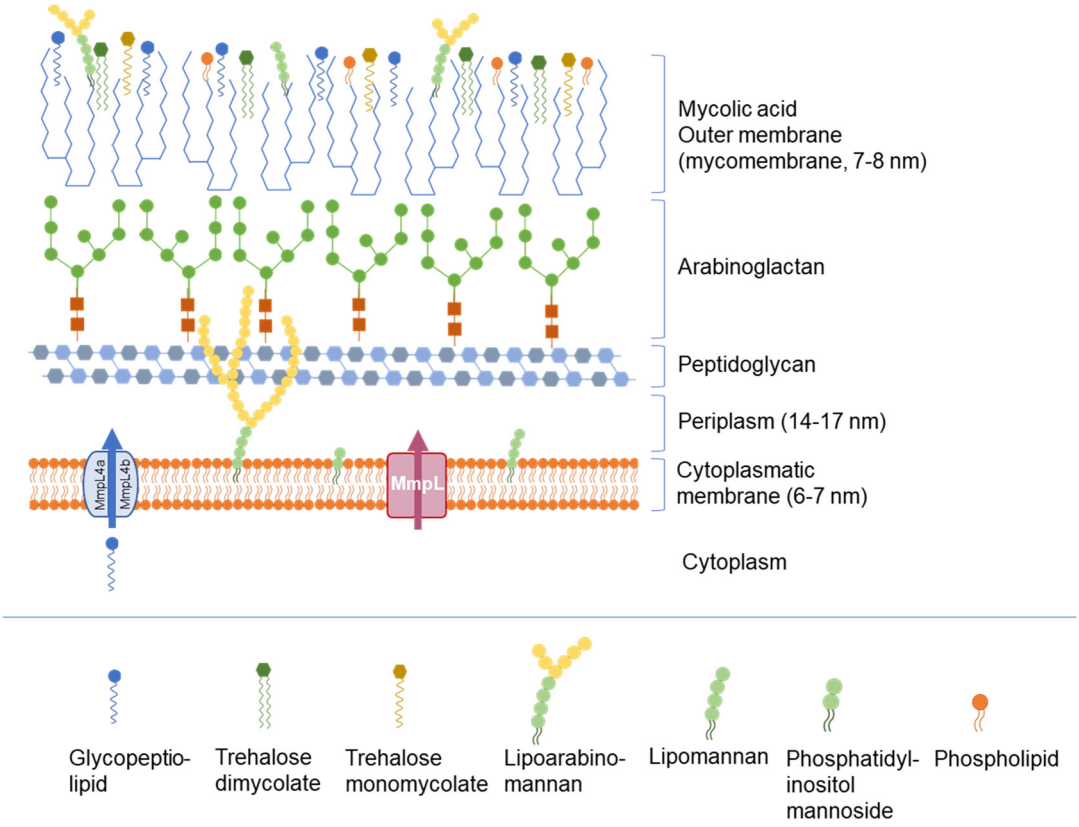


**Figure 1** *Schematic of the mycobacterial cell envelope.*
*Figure based on (Boudehen and Kremer, 2021; Parmar and Tocheva, 2023).*

Different Morphotypes

Several NTM species, including *M. abscessus* and *M. avium,* can grow in colonies with either a smooth (S) ("shiny") or a rough (R) ("stringy") morphotype (Belisle and Brennan, 1989; Agustí *et al.*, 2008; Rüger *et al.*, 2014; Bernut *et al.*, 2016). Figure 2 shows images of *M. abscessus* and *M. aurum* colonies grown on agar with visible differences in their appearance. The *M. abscessus* colonies clearly look not shiny, having a rough texture, while the *M. aurum* colonies look shiny having a smooth shape.

Furthermore, for *M. abscessus* the change in morphology results in significant changes in physiology and virulence, as the rough variant is associated with higher virulence in humans and animals. The transition from the smooth to the rough variant is caused by reduced levels of glycopeptidolipids (GPLs) in the outer membrane of the cell and can occur in the host during infection (Boudehen and Kremer, 2021; Victoria *et al.*, 2021). Indels in genes involved in the biosynthesis or transport (Proteins MmpL4a und MmpL4b, see Figure 1) of GPLs are thought to be responsible for the different morphologies. The low concentration of GPLs in the outer membrane of the rough variants leads to aggregation, clumping and cord formation. Extracellular cords that exceed the size of immune cells cannot be phagocytised. The increased hydrophobicity promotes biofilm formation of rough *M. abscessus* (Johansen, Herrmann and Kremer, 2020; Parmar and Tocheva, 2023).

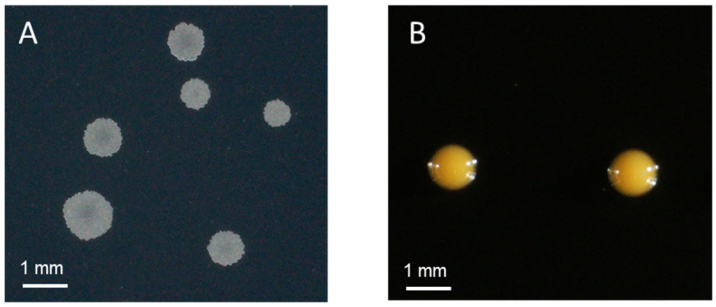


**Figure 2** *Smooth and rough colonies of NTM.*
***A**: rough colonies of M. abscessus* ATCC 19977, ***B**: smooth colonies of Mycobacterium aurum DSM 43999.*
*(Colonies grown on: 7H10 supplemented with 10% OADC, glycerol, active coal. Pictured with: TOMLOV DM602 Pro 10.1 Inch HDMI Digital Microscope by Lea Mann, 2024).*

Formation of Biofilms

NTM can form biofilms which constitute a kind of persistence strategy in which the bacterial cells adhere to each other and to surfaces. Within the biofilm, in part due to reduced penetration into a biofilm, the tolerance of bacteria to acidic pH, disinfectants, and antimicrobial agents is enhanced (Johansen, Herrmann and Kremer, 2020; Parmar and Tocheva, 2023). Bacteria in a biofilm are characterised by increased virulence and resistance. They exist in close proximity to each other and tend to exchange genes horizontally, facilitating the transfer of mutations. The bacteria within the biofilm can slow down their growth rate and become "persisters" (Gómara and Ramón-García, 2019). In co-diseases of the lung, like cystic fibrosis and chronic obstructive pulmonary disease, the microorganisms can be embedded in biofilms. The fact that bacterial tolerance to antimicrobial agents in biofilms is increasing is seen as a threat to public health (Johansen, Herrmann and Kremer, 2020).

### 1.1.4 Pathology

Once in the body, bacteria such as *M. abscessus* are normally phagocytised by immune cells such as macrophages and neutrophils. However, under certain conditions (described below) *M. abscessus* can resist intracellular destruction, leading to the activation and recruitment of immune cells and the formation of a granuloma. As the granuloma matures, the adaptive immune response is activated so that B and T lymphocytes are mobilised to envelop the granuloma (Johansen, Herrmann and Kremer, 2020). How mycobacteria enter the body and in which cases an infection occurs is described in the following sections.

#### 1.1.4.1 Aetiology of NTM infections

Environmental risk factors

As mycobacteria are found in soil, dust and water, including the domestic water supply, they are with us every day. Infections occur when NTM enter the respiratory tract of a susceptible host. The possibility of infection with NTM through contact with soil or water should not be underestimated. The bacteria form biofilms in shower heads, in rainwater barrels or in swimming pools, causing subsequent exposure through aerosols (Feazel *et al.*, 2009; Thomson *et al.*, 2013). NTM have been found in aerosols created by watering potting soil. The predominant bacteria in these patient-derived potting soil samples correlated with the clinically detected mycobacteria from the isolate of the same patient (De Groote *et al.*, 2006). This supports the possibility of infection through gardening.

Host risk factors

There are many factors that can make a human host susceptible to NTM. Lung diseases such as bronchiectasis, chronic obstructive pulmonary disease (COPD) and interstitial lung disease are associated with increased NTM infections. Of note is cystic fibrosis, which is a strong risk factor for NTM-PD. In some cases, person-to-person transmission between people with cystic fibrosis has been observed. However, person-to-person transmission without a history of cystic fibrosis is not known (Cowman *et al.*, 2019; Johansen, Herrmann and Kremer, 2020).

Other factors that increase the risk of NTM disease include treatment with immunosuppressive drugs, such as tumour necrosis factor alpha therapy and oral corticosteroids. The use of inhaled corticosteroids is associated with NTM-PD. Immunodeficiency in AIDS favours infections, for example the reduced CD4+ count favours infections with NTM species such as *M. avium* complex. Similarly, the risk of infection with certain NTM such as *M. avium* and *M. abscessus* can be increased by mutations in the interferon-γ pathway (Collins, 1988; Cowman *et al.*, 2019). Gastro-oesophageal diseases should be mentioned and especially those that cause the recurrent aspiration of stomach contents. Examples of conditions that can promote NTM infection include gastro-oesophageal reflux disease, achalasia or recurrent vomiting (Jarand *et al.*, 2011; Kim *et al.*, 2023). However, risk factors independent of previous disease include increasing age, smoking or a low body mass index, which is associated with a risk of faster disease progression and higher all-cause mortality (Johansen, Herrmann and Kremer, 2020; Yan, Brode and Marras, 2023).

### 1.1.4.2 Growth inside macrophages

It has been demonstrated that *M. tuberculosis* and various NTM species such as *M. avium* or *M. abscessus* are able to infect and survive in macrophages (Johansen, Herrmann and Kremer, 2020). The intracellular bacteria have developed mechanisms to compensate for the host's immune defence strategies. These strategies include the acidification of the phagolysosome and the induction of toxic antimicrobial effectors such as nitric oxide and reactive oxygen species (ROS). The access of bacteria to essential nutrients such as fatty acids, iron or amino acids is limited in macrophages. (Weiss and Schaible, 2015). Figure 3 schematically shows differences in processes that happen after phagocytosis of mycobacteria and other pathogens. Figure 4 shows an image of an infection of macrophages with *M. abscessus* cells.

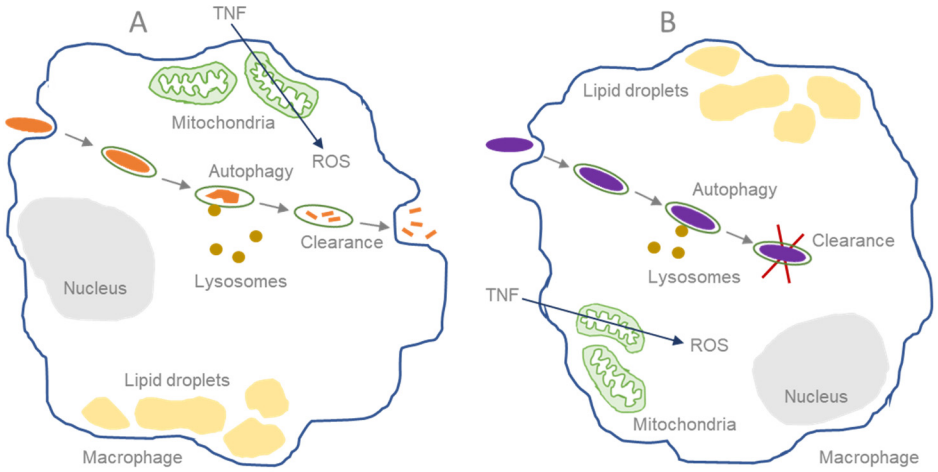


**Figure 3** *Simplified scheme of phagocytosis.*
*A: A bacterium is taken up by a macrophage by phagocytosis, a phagosome is formed. After fusing with lysosomes to form a phagolysosome, the pathogen is dissolved by enzymes. Dissolved material is then excreted.*
*B: A mycobacterium is taken up by a macrophage by phagocytosis and a phagosome is formed. Within the phagosome, mechanisms of the host cell are modulated by the bacterium.*
*As a pro-inflammatory cytokine, the tumour necrosis factor (TNF) leads to the production of ROS in the mitochondria* (Machelart *et al.*, 2017).

In addition, there are differences in the phagocytic processes depending on which morphological type of *M. abscessus* infects the macrophage. Phagosomes infected with the S morphotype of *M. abscessus* are usually lone phagosomes containing a single bacterium, whereas phagosomes with the R morphotype are usually social phagosomes containing at least two bacteria. The R and S morphotypes of *M. abscessus* differ in how they reside within the macrophage (Wu *et al.*, 2018; Johansen, Herrmann and Kremer, 2020). The smooth type survives longer in phagosomes, can prevent phagosome maturation, induces less apoptosis and blocks autophagy. A zone known as electron-transparent is described, which is created by the close attachment of the phagosome membrane to the bacterial surface. If the smooth variant remains in the macrophage for a long time, it can recruit phagocytes and trigger

granuloma formation. The rough type, on the other hand, fuses with the lysosome, leading to acidification of the phagosomes and activation of apoptosis and autophagy. This type can trigger the formation of granulomas; the activation of apoptosis releases the bacteria, causing extracellular growth, which can be accompanied by tissue destruction and inflammation. (Roux *et al.*, 2016).

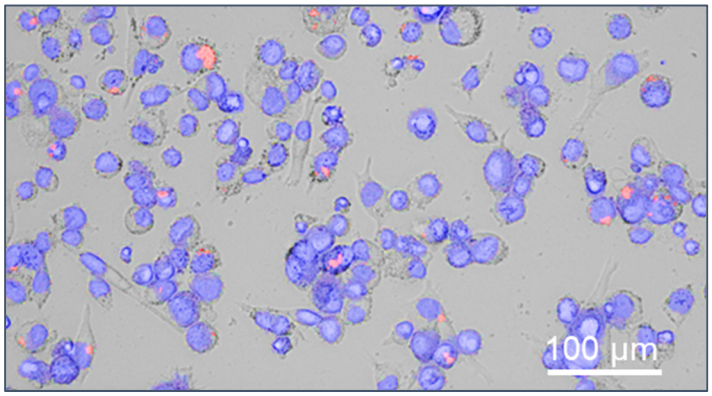


**Figure 4** *THP-1 cell derived macrophages infected with M. abscessus.*
*Overlay of a brightfield image with fluorescence staining*: *Macrophages (DAPI, blue) infected with M. abscessus pTEC27 ATCC 19977 (red fluorescent protein, red). The image was taken 4 days post infection with the CX5 Thermo Fisher fluorescence microscope at 20-fold magnification by Lea Mann, 2023.*

#### 1.1.4.3 Infections with NTM

In addition to lung infections caused by inhaling environmental pathogens, NTM can cause infections in different parts of the body.

The following are some examples of how infections with different types of mycobacteria manifest themselves. Disseminated infections are most common in immunocompromised individuals and are often caused by *M. avium*. Bone and joint infections caused by NTM such as *M. avium* complex or *Mycobacterium kansasii* are usually caused by trauma. Skin and soft tissue infections are caused by mycobacteria such as *M. abscessus, Mycobacterium ulcerans* or *Mycobacterium marinum* and occur after surgery or when the skin barrier is disrupted after contact with contaminated water (Baldwin *et al.*, 2019).

However, lung infections caused by NTM are the most common and the most problematic. Symptoms can be varied and have a significant impact on a person's quality of life. One of the most common symptoms of lung disease caused by NTM is a cough. This can be chronic and may be bloody. The cough may occur at night and be accompanied by the production of mucus. Other symptoms of NTM-PD infection may include loss of appetite, weight loss, fever and night sweats, fatigue, chest pain, shortness of breath and wheezing, or recurrent respiratory infections.

### 1.1.5 Therapy and resistance

An NTM infection is difficult to eradicate. Most of the drugs used to treat *M. tuberculosis* are not effective. A misdiagnosis of an NTM infection as a *M. tuberculosis* infection will, therefore, have a significant impact on treatment success. The reasons for the tolerance of NTM lie in several resistance mechanisms, which are discussed in this section.

Intrinsic resistance

The intrinsic resistance mechanisms of NTM include the cell envelope, a hydrophobic double membrane, which acts as a fundamental and important permeability barrier (Figure 1). In addition, efflux pumps (such as MmpLs, Figure 1) prevent drugs like macrolides and fluoroquinolones from accumulating intracellularly. Genetic polymorphisms occur in some NTM species. Mutation-related changes in the amino acids in the target can prevent the binding of a drug. In the case of *M. abscessus*, for example, this applies to ethambutol or BTZ043. Another important characteristic of NTM is the presence of many enzymes that structurally modify drugs (*e.g.* β-lactamases, acetyltransferases, phosphotransferases and ribosyl transferases), converting them into less effective or inactive derivatives (Wu *et al.*, 2018; Johansen, Herrmann and Kremer, 2020; Holt and Baird, 2023).

Adaptive resistance

An example of adaptive resistance is macrolide resistance in *M. abscessus* mediated by the *erm*(41) gene. The subspecies *abscessus* and *bolletii* have a functional *erm*(41) gene (but not the subsp. *massiliense*) that confers inducible macrolide resistance, whose expression is activated by the transcriptional regulator WhiB7 (Wu *et al.*, 2018). Exposure of the bacterium to clarithromycin or azithromycin dramatically increases the expression of the gene. This leads to increased levels of a methylase that methylates the adenine (A2058) in the peptidyl region of the 23S rRNA, the target of the macrolides, thus preventing binding (Johansen, Herrmann and Kremer, 2020; Victoria *et al.*, 2021; Holt and Baird, 2023).

Acquired resistance

Acquired resistance to aminoglycosides or macrolides can occur in *M. abscessus*. During prolonged use of macrolides, resistance can occur caused by a point mutation at position 2058 or 2059 in the 23S rRNA gene. Mutations (at position 1408 in the 16S rRNA) have been observed to lead to resistance during prolonged therapy with aminoglycosides. As in *M. abscessus*, acquired resistance to macrolides in *M. avium* can be caused by mutations in the 23S rRNA gene. Mutations in the 16S rRNA are also responsible for amikacin resistance in *M. avium* and *Mycobacterium intracellulare* (Wu *et al.*, 2018; Johansen, Herrmann and Kremer, 2020; Abdelaal *et al.*, 2022).

#### 1.1.5.1 Therapy of NTM-pulmonary disease

The diagnosis of NTM-PD is based on clinical, microbiological and radiological criteria (Cowman *et al.*, 2019). As with the facultative pathogen *M. avium* and *M. abscessus*, isolation from the respiratory tract does not necessarily indicate disease, as one positive sputum culture may be a false positive due to environmental contamination. In addition, some patients in whom NTM has been isolated from the respiratory tract show no signs of progressive disease. For *M. avium* and *M. abscessus*, it is recommended that at least two positive sputum cultures be isolated for diagnostic purposes (Daley *et al.*, 2020). Before starting pharmacotherapy for NTM-PD, the sensitivity of the isolate to the antibiotics to be used should be determined. The breakpoints defined by the Clinical and Laboratory Standards Institute (CLSI) provide an indication of the sensitivity of the pathogen to the respective substance. Testing for resistance to macrolides is particularly important for the success of treatment in the presence of an infection with *M. abscessus* (Holt and Baird, 2023).

Treatment of *M. abscessus*-pulmonary disease

The optimal treatment strategies for *M. abscessus*-PD, the choice of drugs, the methods of administration and the duration of treatment are inconsistent. It is generally recommended that at least three effective agents be used in the treatment of *M. abscessus*-PD. Guidelines recommend a two-phase treatment regimen, shown in Table 2. At the start of treatment, intravenous agents such as amikacin and imipenem are recommended for several weeks to months, combined with oral antibiotics. This should be followed by a second phase of oral agents such as macrolides and inhaled amikacin for more than 12 months after sputum culture conversion.

Therapy can be successful with macrolide-susceptible isolates, but permanent culture conversion is rarely achieved with macrolide-resistant organisms. Data from a systematic review and meta-analysis show the proportion of patients who achieve sustained conversion of sputum cultures with macrolide-containing multidrug therapy. In patients infected with an isolate without macrolide resistance, the proportion is 79%. In patients infected with a macrolide-resistant isolate, the proportion is only 35% (Kumar *et al.*, 2022; Holt and Baird, 2023). It is recommended to reconfirm species identity and repeat susceptibility testing after six months of appropriate antimicrobial therapy (CLSI, 2011).

**Table 2** *Treatment regimen for M. abscessus-PD.*

| **Macrolide susceptible** | |
|---|---|
| Initial Phase | **At least 4 of:**<br>**1-2 IV:** amikacin, imipenem (or cefoxitin), tigecycline<br>**2 oral**: macrolide, clofazimine, linezolid |
| Continuation phase | **At least 2 of:**<br>macrolide, clofazimine, linezolid, inhaled amikacin |
| **Inducible macrolide resistance/ Constitutive macrolide resistance (with or without inducible macrolide resistance)** | |
| Initial Phase | **At least 4 of:**<br>**2-3 IV:** amikacin, imipenem (or cefoxitin), tigecycline<br>**2-3 oral:** macrolide, clofazimine, linezolid |
| Continuation phase | **At least 2 of:**<br>macrolide, clofazimine, linezolid, inhaled amikacin |

Frequency: Daily (or 3 times/week for IV aminoglycosides), **IV** = parenteral.
Table adapted from (Kumar *et al.*, 2022).

Treatment of *Mycobacterium avium*-pulmonary disease

The American Thoracic Society 2020 NTM guideline recommends a macrolide-based treatment regimen for *M. avium*-PD (Nguyen and Daley, 2023) that should include a total of three agents. The susceptibility of the isolate to clarithromycin and amikacin should be tested before starting treatment to ensure a response to therapy.

Treatment of *M. avium*-PD, as shown in Table 3, usually includes a macrolide, a rifamycin and ethambutol. For cavitary NTM-PD, intravenous amikacin or intramuscular/intravenous streptomycin may be given. Treatment of refractory *M. avium*-PD includes at least four drugs: a rifamycin, a macrolide, ethambutol and inhaled amikacin (Kumar *et al.*, 2022). Treatment should be continued for up to 12 months after culture conversion. Macrolide-based treatment regimens for *M. avium* show better results than regimens without the administration of a macrolide. However, the success of the combination of a macrolide, rifampicin and ethambutol depends on the macrolide susceptibility of the isolate.

Despite prolonged combination therapy and sometimes a lung resection, relapses are common, often due to reinfection. A meta-analysis of 1,462 patients who were treated for *M. avium*-PD with macrolide-containing regimens showed a success rate of 60% (Kumar *et al.*, 2022; Nguyen and Daley, 2023). Other data show cure rates of 39% to 68% (meta-analyses) (Dartois and Dick, 2024a).

**Table 3** *Treatment regimen for M. avium-PD.*

| | |
|---|---|
| **Nodular-bronchiectatic** | macrolide, rifamycin, ethambutol |
| **Cavitary** | **At least 3 of:**<br>macrolide, rifamycin, ethambutol, systemic aminoglycoside (amikacin (**IV**) or streptomycin) |
| **Refractory** | **At least 4 of:**<br>macrolide, rifamycin, ethambutol, amikacin liposome inhalation suspension or systemic aminoglycoside (amikacin (**IV**) or streptomycin) |

Frequency: Daily (or 3 times/week for IV aminoglycosides), *3 times/week (daily if advanced or severe disease), **IV** = parenteral.
Table adapted from (Kumar *et al.*, 2022).

The long treatment period, the need to take at least three different antibiotics with significant side effects and drug interactions promise to be an unpleasant therapy for the patient together with compliance problems and poor prospects of therapeutic success. In addition, there is evidence in the literature that rifampicin is not effective in the treatment of *M. avium*-PD and a recommendation has been made to find alternative substances for the treatment (van Ingen *et al.*, 2024).

## 1.2 Challenges in NTM drug discovery

As evidenced by the treatment regimen and the low likelihood of treatment success, there are currently no reliable options for treating *M. abscessus* lung infection (Dartois and Dick, 2022). The development and discovery of new drug candidates is necessary but is hampered by the numerous resistance mechanisms of the pathogen. The current NTM-drug pipeline is described as empty and understaffed (Ganapathy and Dick, 2022; Dartois and Dick, 2024a). Only a few new drugs are currently in clinical trials for NTM-PD: omadacycline, epetraborole and SPR720 (NCT04922554, 2021; NCT05327803, 2022; NCT05496374, 2022; Dartois and Dick, 2024a). However, the developing company recently announced that the clinical trials on SPR270 failed as the active ingredient was unable to beat the placebo and showed signs of hepatotoxicity (Spero Therapeutics, 2025).

Therefore, strategies have been published to accelerate the pipeline of new anti-NTM compounds and to advance the development of new compounds as NTM drugs.

One of the strategies is to repurpose known drugs for new indications, *i.e.* to test established drugs against new indications/new diseases such as NTM. An advantage of repurposing would be the shorter time to bring a new drug to the clinic, as many lengthy development processes could be skipped. For example, one successful hit found in a screening of FDA-approved drugs is rifabutin, which belongs to the rifamycin class and has activity against *M. abscessus* (Aziz *et al.*, 2017).

Another approach is repositioning, *i.e.* optimising approved classes of antibiotics for activity (bacteriostatic and bactericidal) and resistance. This involves the chemical optimisation of antibiotic classes developed for other infectious diseases against targets that have already been validated, for example rifamycins, fluoroquinolones and oxazolidinones. The compounds have already been tested in humans for tolerability, efficacy and oral bioavailability, which is an advantage because testing in animal models can be postponed (Dartois and Dick, 2022). One example is the development of rifabutin analogues that overcome bacterial metabolism and are 50 to 100 times more effective against *M. abscessus* (Lan *et al.*, 2022).

The identification of new chemical space is a third approach. However, since whole cell screening against mycobacteria is likely to yield only a small number of hits, it is proposed to use collections containing compounds with known activity against *M. tuberculosis* for screening. The success of this approach has already been confirmed and will be taken up again later (Low *et al.*, 2017; Wu *et al.*, 2018).

Strategies have been published on how to develop a compound against NTM, from whole-cell screening to pre-clinical development, which are shown below in Figure 5.

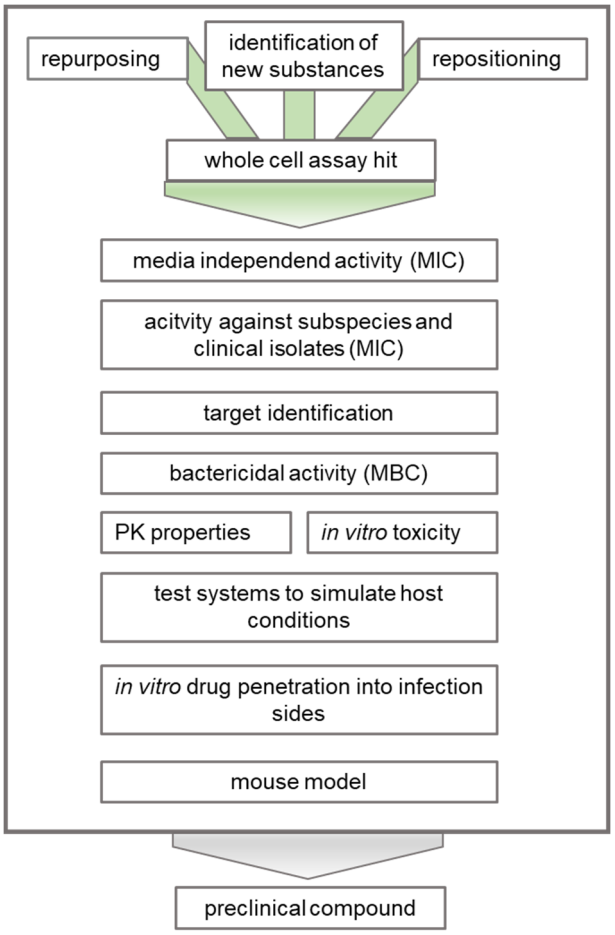


**Figure 5** *NTM drug discovery workflow.*
*Adapted from* (Wu *et al.*, 2018).

After the discovery of an initial hit in the whole cell assay, further testing to determine media-independent activity is suggested. The CLSI recommends the use of Mueller-Hinton broth or Middlebrook 7H9 broth for *in vitro* testing of drugs against NTM. Drugs should show activity in both media to be considered media independent. In the further course of drug development, it is helpful to test a drug with growth inhibitory activity for bacteriostatic activity against reference strains of *M. avium* and *M. abscessus*. This should be followed by a determination of the bactericidal activity. After analysis of pharmacokinetic properties (*e.g.* mouse pharmacokinetics) and toxicity *in vitro*, testing in various assay systems should be performed before testing against clinical isolates in the mouse model prior to preclinical development. The recommendation and need for testing in the various assay-systems mentioned is based on the adaptability of mycobacterial pathogens. Properties such as tendency to form biofilms, growth in macrophages and formation of granulomas lead to different growth conditions in the host. A low *in vitro* minimum inhibitory concentration (MIC) against NTM (with good pharmacokinetic properties) does, therefore, not necessarily mean a positive outcome *in vivo* (Van Ingen *et al.*, 2012). The discrepancy between *in vivo* and *in vitro* results of drug testing against mycobacteria can be explained by the way the MIC

is determined. Within the host, bacteria adapt to survive in different environments. They can adapt to a lipid-rich environment, such as in the case of lung lesions, or to a low-oxygen environment and exist within the host as “persisters”. In contrast, the culture conditions of an MIC assay with an optimal nutrient and oxygen supply provide the opportunity for unrestricted, exponential growth. For the development of drug candidates with *in vivo* activity it is, therefore, advisable to use different test systems that can simulate different conditions in the host.

Persister-specific assays should be emphasised here, as the persistence of bacteria in the host significantly hinders their eradication. Various assay systems have been developed to investigate whether active substances are able to eradicate bacteria in a state of persistence. One of these is the biofilm assay, in which a biofilm is created and the sensitivity of the bacteria to active substances within the mucus layer can be tested (Teng and Dick, 2003; Carter, Young and Bermudez, 2004; Yam *et al.*, 2020).

Another equally relevant assay is the caseum assay. Caseum, the central necrotic material of tuberculous lesions, can be obtained from the lungs of infected rabbits, or artificial caseum can be used. The bacteria living within this environment adapt to hypoxia, nutrient deprivation and altered carbon sources. It is possible to investigate the activity of substances against metabolically adapted bacteria *ex vivo* in caseum by determining minimal bactericidal concentrations (Sarathy and Dartois, 2020; Lanni *et al.*, 2023; Xie *et al.*, 2023).

Various models of macrophage infection assays have been developed to investigate the activity of active substances on phagocytised bacteria. The determination of the minimum inhibitory concentration of a substance within this assay system includes not only the effect on the target but components such as the ability to penetrate the macrophage cell and can differ considerably from the MIC determined in liquid medium (Franzblau *et al.*, 2012; Wu *et al.*, 2018; Richter, Shapira and Av-Gay, 2019).

To evaluate the efficacy of the drug against non-replicating bacilli, a so-called non-replicating assay can be used. Existing models such as the Loebel or Wayne model simulate nutrient or oxygen poverty, so that bacteria in adapted growth states can be examined for their drug sensitivity, which can be quantified by MIC and MBC determination (M. L. Wu, Gengenbacher, and Dick 2016).

Due to the complexity of NTM pathology (vascularisation, occurrence in lung lesions), it is difficult to obtain information about the distribution of the drug at the site of infection, such as within the lesions, in patients. There is a direct correlation between the ability of the drug to penetrate lung lesions and the shortening of a patient's treatment duration. It is recommended that the next step is to use a drug assay that can predict the distribution of the drug within the lesions, such as the caseum binding assay according to Sarathy *et al*. (Sarathy *et al.*, 2016; Wu *et al.*, 2018).

Prior to the preclinical development of a drug, studies in animal models (nonmammalin eg. zebrafish and mammalian eg. mice), are of ultimate importance. However, it is difficult to generate persistent lung infections in animals that are comparable to human pathology (D Chan and Bai, 2016; Abdelaal *et al.*, 2022).

## 1.3 *N*α-aroyl-*N*-aryl-phenylalanine amides

Figure 6 shows the structures of MMV688845 and D-AAP1, which belong to the class of *N*α-aroyl-*N*-aryl-phenylalanine amides (AAPs). The two compounds are shown with an obligatory stereochemical configuration, as only (R)-configured derivatives show activity (Ebright *et al.*, 2015; Lin *et al.*, 2017). This thesis is part of our research towards a drug candidate from this compound class.

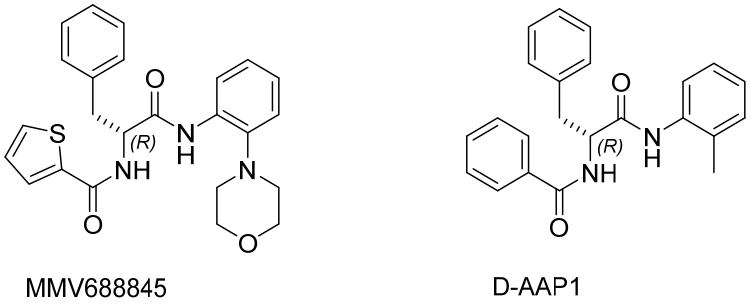


**Figure 6** *Chemical diagrams of MMV688845 and D-AAP1.*

Discovery of compounds in the class

The first compound in the AAP class was discovered in 2013 in a high-throughput screening of a GlaxoSmithKline small-molecule *M. tuberculosis* lead compound library. *N*α-2-thiophenoyl-D-phenylalanine-2-morpholinoanilide (GSK1055950A = MMV688845) showed < 10 μM activity against *Mycobacterium bovis* and an $MIC_{90}$ of 7.6 μM against *M. tuberculosis* H37Rv, with no cytotoxicity against HepG2. However, the compound was not subsequently selected for further investigation (Ballell *et al.*, 2013).

MMV688845 was found to be active against *M. abscessus* in three different drug-discovery screenings, of which a summary of the published MIC values is shown in Table 5. In 2017, Low *et al*. carried out screenings of the Pathogen Box library (provided by Medicines for Malaria Ventures (MMV, Geneva, Switzerland)), in which 129 out of 400 compounds had already shown activity against *M. tuberculosis*. The compound MMV688845 showed activity against *M. tuberculosis* H37Rv $MIC_{90}$ = 1.7 μM, *M. abscessus* Bamboo $MIC_{90}$ = 7 μM and *M. avium* 11 $MIC_{90}$ = 3 μM in 7H9 medium (Low *et al.*, 2017). Subsequently, in 2018, Jeong *et al.* published the results of a screening of the Pathogen Box library against *M. abscessus* ATCC 19977 with an $MIC_{50}$ = 9.3 μM for MMV688845 in a resazurin reduction assay (Jeong *et al.*, 2018) In 2018, Richter *et al.* also published results of the combined screening of the Pathogen Box library and GlaxoSmithKline small-molecule *M. tuberculosis* lead compound set. Here, compound MMV688845 with an activity of $MIC_{90}$ = 7.4 μM in 7H9 medium and $MIC_{90}$ = 1.0 μM in MHII medium was characterised as a media-independent hit against *M. abscessus* ATCC 19977 red fluorescent protein (RFP) expressing strain (Richter *et*

*al.*, 2018). Later, MMV688845 was found to be active in the macrophage infection model (Richter, Shapira and Av-Gay, 2019).

**Table 4** *Published MIC values of MMV688845 against several mycobacterial strains.*

| **Mycobacterial strain** | **Medium** | **$MIC_{90}$ [µM]** | **$MIC_{50}$ [µM]** |
|---|---|---|---|
| **Low *et al.*** | | | |
| *M. tuberculosis* H37Rv | 7H9 | 1.7 | < 0.2 |
| *M. abscessus* Bamboo | 7H9 | 7.0 | 1.5 |
| *M. avium* 11 | 7H9 | 3.0 | 0.6 |
| **Jeong *et al.*** | | | |
| *M. abscessus* ATCC 19977 | 7H9 | - | 9.3 |
| **Richter *et. al*** | | | |
| *M. abscessus* ATCC 19977 | 7H9 | 7.4 | - |
| | MHII | 1.0 | - |

- = Not published.

In 2017, a study by Lin *et al*. was published, which found *in vitro* activity of the substance D-AAP1, the second substance from the class of AAPs shown in Figure 6. It was found that the compound inhibited the growth of *M. tuberculosis* H37Rv (MIC = 3.13 µg/ml, 8.73 µM), *M. smegmatis* $mc^2$ 155 (MIC = 0.78 µg/ml, 2.18 µM) and *M. avium* ATCC 25291 (MIC = 6.25 µg/ml, 17.44 µM) *in vitro* but was not active against *Staphylococcus aureus* or *Escherichia coli* (Lin *et al.*, 2017).

Targeting RNA Polymerase

In the study by Lin *et al*. the active compound D-AAP1 was found by a target-based screening approach using an enzyme inhibition assay against mycobacterial RNA polymerase (RNAP). Specifically, synthetic compounds were screened using an *in vitro* fluorescence assay for promoter-dependent transcription by the *M. tuberculosis* RNAP σA holoenzyme. The substance D-AAP1 showed selective, stereospecific activity against *M. tuberculosis* RNAP ($IC_{50}$ = 0.4 µM), but weak inhibition of other bacterial RNAP such as *Staphylococcus aureus* or *Escherichia coli* and human RNAP I, II and III (all $IC_{50}$ >25 µM).

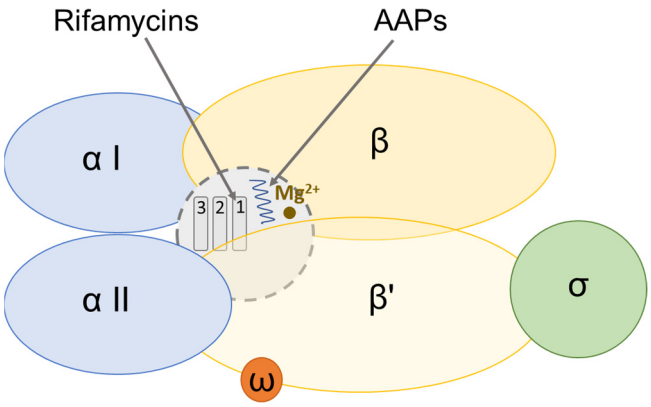


**Figure 7** *Schematic structure of bacterial RNA polymerase.*
*The core enzyme consists of two α subunits (blue), the β and β' subunits (yellow) and the ω subunit (orange). The σ factor is required to initiate transcription (green). The magnesium-containing catalytic site, three channels (primary, secondary and RNA exit channel) and the bridge helix (blue spiral) are located between the β and β' subunits. APPs: Target active site near $Mg^{2+}$, rifamycins: Target primary channel. Figure according to* (Kirsch, Haeckl and Müller, 2022).

Crystal structures of *M. tuberculosis* RNAP alone and together with rifampicin (an RNA-polymerase inhibitor of the rifamycin class) and/or AAPs at 4 Å resolution were published in the study by *Lin et al.* . This revealed the inhibition binding mode of AAPs and elucidated the mechanism of transcription inhibition by this compound class. A schematic representation of bacterial RNA polymerase is shown above in Figure 7. Lin *et al.* showed, that AAPs bind to the *N*-terminus of the RNAP bridge helix (*M. tuberculosis* RNAP β/β'- subunit). Rifampicin, on the other hand, binds to the β-subunit and sterically blocks the elongation of RNA products by 2-3 nucleotides, preventing the formation of further RNA strands. The structure of *M. tuberculosis* open promoter complex co-crystallized with both, D-AAP1 and rifampicin confirms that the AAP binding site is distinct from the rifampicin binding site and does not overlap. Furthermore, AAPs and rifampicin can simultaneously bind RNAP. It was predicted that due to the lack of overlap between the AAP and rifampicin binding sites, AAPs and rifampicin do not exhibit cross-resistance (Ebright *et al.*, 2015; Lin *et al.*, 2017).

# 2 Aim of the dissertation

The development of new drugs against NTM, in particular against *M. abscessus* and *M. avium*, is of great importance to combat infections with these pathogens. Resistance to many common antibiotics, together with the increasing prevalence of NTM infections worldwide and the associated health risks, emphasise the urgency of developing effective drugs. The overall aim of this thesis is to contribute to the development of a drug candidate with activity against NTM. The focus of my work has been on the microbiological characterisation of the drug candidates.

The aim of my research was the establishment and application of different assay methods against the mycobacterial pathogens *M. smegmatis* $mc^2$ 155, *M. intracellulare* ATCC 35761 and *M. abscessus* ATCC 19977 (subsp. *abscessus*) type strain under S2 laboratory conditions. With the overall intention to develop an antimycobacterial drug candidate, new AAPs synthesised within the working group were characterised against the pathogens under different conditions during my work.

Concrete objectives were:

1. In depth characterisation of the assay hit MMV688845 and analogues.
2. Characterisation of AAP derivatives in broth and in the macrophage infection assay.
3. Development of a new fluorescence-based method for MBC determination.

# 3 Collection of articles

## 3.1 Information on publications

**Table 5** *General information on the journals.*

| **General information on the journals** | | | |
|---|---|---|---|
| Title | Microbiology Spectrum | Journal of Medicinal Chemistry | Journal of Microbiological Methods |
| Impact factor | 3.7 (2023) | 7.3 (2022) | 1.7 (2023) |
| 5-Year Impact | - | 7.3 | - |
| Publisher | American Society for Microbiology | American Chemical Society | Elsevier B.V. |

**Table 6** *Overview of the publications discussed in this paper.*

| | |
|---|---|
| **Publication I** | *In Vitro* Profiling of the Synthetic RNA Polymerase Inhibitor MMV688845 against *Mycobacterium abscessus*<br><br>**Lea Mann**, Uday S. Ganapathy, Rana Abdelaziz, Markus Lang, Matthew D. Zimmerman, Véronique Dartois, Thomas Dick, Adrian Richter.<br><br>Microbiology Spectrum 2022 |
| **Publication II** | Synthesis and Characterization of Phenylalanine Amides Active against Mycobacterium abscessus and Other Mycobacteria<br><br>Markus Lang, Uday S. Ganapathy, **Lea Mann**, Rana Abdelaziz, Rüdiger W. Seidel, Richard Goddard, Ilaria Sequenzia, Sophie Hoenke, Philipp Schulze, Wassihun Wedajo Aragaw, René Csuk, Thomas Dick, Adrian Richter.<br><br>Journal of Medicinal Chemistry 2023 |
| **Publication III** | Determination of bactericidal activity against 3HC-2-Tre-labelled *Mycobacterium abscessus* (*Mycobacteroides abscessus*) by automated fluorescence microscopy<br><br>**Lea Mann**, Fabienne Siersleben, Markus Lang, Adrian Richter.<br><br>Journal of Microbiological Methods 2024 |

## 3.2 Publication I

### *In Vitro* Profiling of the Synthetic RNA Polymerase Inhibitor MMV688845 against *Mycobacterium abscessus*

Lea Mann, Uday S. Ganapathy, Rana Abdelaziz, Markus Lang, Matthew D. Zimmerman, Véronique Dartois, Thomas Dick, Adrian Richter.

ASM Journals Microbiology Spectrum, Mann *et al.*, *In Vitro* Profiling of the Synthetic RNA Polymerase Inhibitor MMV688845 against *Mycobacterium abscessu*s. Microbiol Spectr 10,
 DOI: 10.1021/acs.jmedchem.3c00009

**Summary**

In this study, the compound MMV688845 was evaluated in detail for its activity against *M. abscessus*. The activity against different strains of *M. abscessus* as well as against different clinical isolates was characterised and compared with rifabutin. Bactericidal activity, including intracellular activity, was investigated. The combination of the RNA polymerase inhibitor with several different antibiotics was tested for synergistic effects of the combination. This was done using 7H9 and MHII media and the macrophage infection model. In addition, the activity against spontaneously resistant mutants was investigated and first pharmacokinetic data on the metabolism of MMV688845 in mice were published.

**Own contribution:**

Writing, review & editing, writing of the original draft, visualization, software, methodology, investigation and data curation.

The following assays were contributed: MIC tests against *M. abscessus* ATCC 19977 in MHII, 7H9 and in the macrophage infection model (MBC). Including all combination assays.

AMERICAN SOCIETY FOR MICROBIOLOGY | Microbiology Spectrum

RESEARCH ARTICLE

# *In Vitro* Profiling of the Synthetic RNA Polymerase Inhibitor MMV688845 against *Mycobacterium abscessus*

**Lea Mann,[a] Uday S. Ganapathy,[b] Rana Abdelaziz,[a] Markus Lang,[a] Matthew D. Zimmerman,[b] Véronique Dartois,[b,c] Thomas Dick,[b,c,d] Adrian Richter[a]**

[a]Institut für Pharmazie, Martin-Luther-Universität Halle-Wittenberg, Halle (Saale), Germany
[b]Center for Discovery and Innovation, Hackensack Meridian Health, Nutley, New Jersey, USA
[c]Department of Medical Sciences, Hackensack Meridian School of Medicine, Nutley, New Jersey, USA
[d]Department of Microbiology and Immunology, Georgetown University, Washington, DC, USA

**ABSTRACT** In a library screen of tuberculosis-active compounds for anti-*Mycobacterium abscessus* activity, we previously identified the synthetic phenylalanine amide MMV688845. In *Mycobacterium tuberculosis*, this class was shown to target the RpoB subunit of RNA polymerase, engaging a binding site distinct from that of the rifamycins. Due to its bactericidal activity, rifampicin is a key drug for the treatment of tuberculosis (TB). However, this natural product shows poor potency against *M. abscessus* due to enzymatic modification, and its clinical use is limited. Here, we carried out *in vitro* microbiological profiling of MMV688845 to determine its attractiveness as a substrate for a chemistry optimization project. MMV688845 was broadly active against the *M. abscessus* complex, displayed bactericidal against *M. abscessus in vitro*, and in a macrophage infection model showed additivity with commonly used anti-*M. abscessus* antibiotics and synergy with macrolides. Analyses of spontaneous resistant mutants mapped resistance to RpoB, confirming that MMV688845 has retained its target in *M. abscessus*. Together with its chemical tractability, the presented microbiological profiling reveals MMV688845 as an attractive starting point for hit-to-lead development to improve potency and to identify a lead compound with demonstrated oral *in vivo* efficacy.

**IMPORTANCE** Infections with nontuberculous mycobacteria are an increasing health problem, and only a few new drug classes show activity against these multidrug-resistant bacteria. Due to insufficient therapy options, the development of new drug leads is necessary and should be advanced. The lead compound MMV688845, a substance active against *M. abscessus* complex, was characterized in depth. In various assays, it showed activity against *M. abscessus*, synergy with other antibiotics, and bactericidal effects.

**KEYWORDS** *M. abscessus*, MMV688845, RNA polymerase, drug development, nontuberculous mycobacteria

*Mycobacterium abscessus* is a fast-growing *mycobacterium*, classified as a nontuberculous *mycobacterium* (NTM). It is an opportunistic pathogen that causes serious respiratory infections, especially in patients with preexisting health conditions such as immunosuppression or cystic fibrosis (1). However, infections with *M. abscessus* are not limited to the lungs but can also occur in the skin, soft tissues, and central nervous system (2). Diseases caused by *M. abscessus* are difficult to treat because the pathogen is resistant to numerous classes of antibiotics (3). *M. abscessus* infections often require years of treatment, with 12 months of continuation treatment after sputum conversion with a combination of three or more antibiotics (4). Treatment regimens often include clarithromycin, amikacin, and cefoxitin or imipenem. Despite the combination therapy, cure rates are poor. Acquired and intrinsic resistance, including inducible resistance, causes the loss of efficacy of many antibiotics (5, 6). Like *Mycobacterium tuberculosis*, *M. abscessus* can escape host defense mechanisms by infecting human

**Editor** Prabagaran Narayanasamy, UNMC
**Ad Hoc Peer Reviewer** Sangeeta Tiwari

Address correspondence to Adrian Richter, adrian.richter@pharmazie.uni-halle.de.
The authors declare no conflict of interest.
**Received** 19 July 2022
**Accepted** 20 October 2022
**Published** 15 November 2022

macrophages, leading to granuloma formation (7). Due to the poor clinical outcomes and the increase of diagnosed NTM infections, the development of new efficacious antibiotics is urgently needed.

MMV688845 (*Nα*-2-thiophenoyl-*d*-phenylalanine-2 morpholinoanilide), identified by screening of the Pathogen Box library (Medicines for Malaria Ventures [MMV]) against *M. abscessus* (ATCC 19977) (8–10), is a promising hit compound for drug development focused on NTM and *M. abscessus* in particular. Initially, MMV688845 was discovered as an anti-*M. tuberculosis* (11, 12) hit. The compound shows activity *in vitro* against *M. abscessus* ATCC 19977 in 7H9 medium and in cation-adjusted Mueller-Hinton broth (MHII). Recently, an improvement in the synthetic route for the active R enantiomer was achieved (13). In a previous study (13), the cytotoxicity of MMV688845 was investigated. Cytotoxicity was analyzed against five mammalian cell lines, including A375 (melanoma), HT29 (colon adenocarcinoma), MCF-7 (breast adenocarcinoma), A2780 (ovarian carcinoma), and NIH 3T3 (nonmalignant mouse fibroblast). The compound was evaluated using a sulforhodamine B (SRB) (Kiton-Red S; ABCR GmbH, Karlsruhe, Germany) microculture colorimetric assay in which MMV688845 showed no cytotoxicity (13).

In this study, MMV688845 was characterized in depth as a potent inhibitor against *M. abscessus*. MMV688845 was tested against a range of clinical isolates to demonstrate that MMV688845 is not only effective against selected laboratory strains. To evaluate the bactericidal effects of MMV688845, we performed CFU determinations, both *in vitro* and in a macrophage infection model. For target validation in *M. abscessus*, spontaneous resistant mutants were isolated and sequenced.

To study the synergy of MMV688845 with approved antimycobacterial drugs and to assess its suitability for combination therapy, we performed synergy testing against *M. abscessus* (ATCC 19977) by checkerboard assays. In particular, we were interested in the interaction with macrolides, e.g., clarithromycin, as clarithromycin and rifabutin were shown to be synergistic for *erm41*-positive *M. abscessus* strains. Transcriptional inhibition by rifabutin disables inducible macrolide resistance in *M. abscessus*, inhibiting the expression of *erm41*. Therefore, this study investigated the hypothesis that the RNA polymerase inhibitor MMV688845 exhibits synergy with macrolides (14–16).

## RESULTS

**MMV688845 is active against various *M. abscessus* strains *in vitro*.** To fully determine the potential of MMV688845, we investigated its activity against a panel of *M. abscessus* subspecies and clinical isolates (Table 1). MMV688845 is active against all three *M. abscessus* subspecies and a variety of clinical isolates. Based on the activity of MMV688845 against *M. abscessus* Bamboo and *M. abscessus* ATCC 19977 (Table 1), we investigated the effect of the hit compound against the three subspecies of the *M. abscessus* complex (*M. abscessus* subsp. *abscessus*, *M. abscessus* subsp. *massiliense*, and *M. abscessus* subsp. *bolletii*), which are known to have different antibiotic susceptibilities (17, 18). We found that MMV688845, like clarithromycin and rifabutin, is effective against the reference strains of the three subspecies (Table 1). Against 10 clinical *M. abscessus* isolates, MMV688845 showed activity comparable to the reference strains (15).

To further mimic infections in human macrophages, a macrophage infection model based on THP-1 cells was used to determine the effect of MMV688845 on bacteria growing inside cells, as activity of MMV688845 in a macrophage model has been reported previously (19) (Table 2). We found MMV688845 to be active against intracellular *M. abscessus* with an $MIC_{90}$ of 16 $\mu$M (Table 2).

As demonstrated by Lin et al. (12), analogues closely related to MMV688845 bind to the RpoB subunit of the mycobacterial RNA polymerase at a different site than rifamycins, leading to efficient enzyme inhibition (12, 20, 21). To validate the RNA polymerase as the target of MVV688845 in *M. abscessus*, resistant mutants were isolated (Table 1). For MMV688845-resistant *M. abscessus* strains, there is no cross-resistance to rifamycins,

**TABLE 1** *In vitro* activity of MMV688845 against *M. abscessus* reference strains and clinical isolates

| *M. abscessus* strain | *erm41* sequevar | CLR susceptibility | $MIC_{90}$ ($\mu$M) of: | | |
|---|---|---|---|---|---|
| | | | CLR | RFB | MMV688845 |
| Reference strains[a] | | | | | |
| *M. abscessus* subsp. *abscessus* ATCC 19977 | T28 | Resistant | 1.3 | 1.8 | 7.5 |
| *M. abscessus* subsp. *bolletii* CCUG 50184T | T28 | Resistant | 2.6 | 2.1 | 10 |
| *M. abscessus* subsp. *massiliense* CCUG 48898T | Deletion | Sensitive | 0.3 | 0.8 | 10 |
| Clinical isolates[a] | | | | | |
| *M. abscessus* subsp. *abscessus* Bamboo | C28 | Sensitive | 0.3 | 1.3 | 8 |
| *M. abscessus* subsp. *abscessus* K21 | C28 | Sensitive | 0.6 | 2.4 | 6.6 |
| *M. abscessus* subsp. *abscessus* M9 | T28 | Resistant | 1.7 | 2.2 | 8.9 |
| *M. abscessus* subsp. *abscessus* M199 | T28 | Resistant | 3.4 | 1.5 | 8.6 |
| *M. abscessus* subsp. *abscessus* M337 | T28 | Resistant | 1.2 | 1.2 | 5.4 |
| *M. abscessus* subsp. *abscessus* M404 | C28 | Sensitive | 0.3 | 1.1 | 6.6 |
| *M. abscessus* subsp. *abscessus* M422 | T28 | Resistant | 0.8 | 1.1 | 8.4 |
| *M. abscessus* subsp. *bolletii* M232 | T28 | Resistant | 1.7 | 1.2 | 6.9 |
| *M. abscessus* subsp. *bolletii* M506 | C28 | Sensitive | 0.3 | 1.1 | 4.5 |
| *M. abscessus* subsp. *massiliense* M111 | Deletion | Sensitive | 0.3 | 2.3 | 8.4 |
| *M. abscessus* subsp. *abscessus* ATCC 19977 (RFP assay)[b] | | | | | |
| In 7H9 + ADS | T28 | Resistant | 0.4 | 1.2 | 11.9 |
| In MHII | T28 | Resistant | 0.2 | 2.6 | 10.8 |
| In the macrophage infection model | T28 | Resistant | 50 | 5.5 | 15.9 |
| *M. abscessus* subsp. *abscessus* ATCC 19977 RFB-R1[a,c] | T28 | Resistant | 3.5 | >100 | 10 |
| *M. abscessus* subsp. *abscessus* Bamboo 845-2[a,d] | T28 | Resistant | 0.3 | 1.1 | >100 |

[a]MICs were determined in 7H9 via $OD_{600}$ measurement and evaluated via method B.
[b]MICs were determined by RFP measurement and evaluated via method A.
[c]Spontaneous RFB-resistant strain.
[d]Spontaneous MMV688845-resistant strain.

which was investigated by MIC determination of rifabutin (RFB) against *M. abscessus* Bamboo 845-2 (Table 1).

The $MIC_{90}$ values shown in Table 1 were obtained by determining the optical density at 600 nm ($OD_{600}$) or by measuring red fluorescent protein. For the RFP-based method, the *mycobacterium* is transformed with plasmid pTEC27 for RFP tdTomato expression (22). Fluorescence measurement was used for quantification of bacterial growth because this method is sensitive and specific, as has been shown previously (23, 24). Table 1 shows that the results of the fluorescence-based *in vitro* assay are consistent with optical density measurements.

**MMV688845 has bactericidal activity *in vitro* and in a macrophage infection model.** To assess the bactericidal efficacy of MMV688845, CFU counting experiments were conducted, and the results were compared with those for rifabutin as a reference, including the combination of both agents (Table 2).

We found that MMV688845 achieves a significant reduction of colony forming units of *M. abscessus* in vitro. The MBC90 was determined to be 15 $\mu$M (2× MIC90) against the reference strain ATCC 19977. As shown in Fig. 1, a concentration-dependent reduc-

**TABLE 2** MICs and MBCs of MMV688845 and rifabutin against *M. abscessus* subsp. *abscessus* ATCC 19977

| Growth condition | $MIC_{90}$ ($\mu$M) of: | | $MBC_{90}$ ($\mu$M) of: | |
|---|---|---|---|---|
| | RFB | MMV688845 | RFB | MMV688845 |
| 7H9 + ADS | 1.2[a] | 7.5[a] | 2.4 (2 × MIC)[b] | 15 (2 × MIC)[b] |
| Macrophage infection model | 5.5[c] | 15.9[c] | ND[d] | 16 (1 × MIC)[e] |

[a]Determined in 7H9 via $OD_{600}$ measurement and evaluated via method B.
[b]Determined in duplicate via method B.
[c]Determined by fluorescence measurement.
[d]ND, not determined.
[e]Determined in triplicate via method A. For the MBC determination, statistical evaluation was carried out via one-way ANOVA multiple-comparison test, as for Fig. 1.

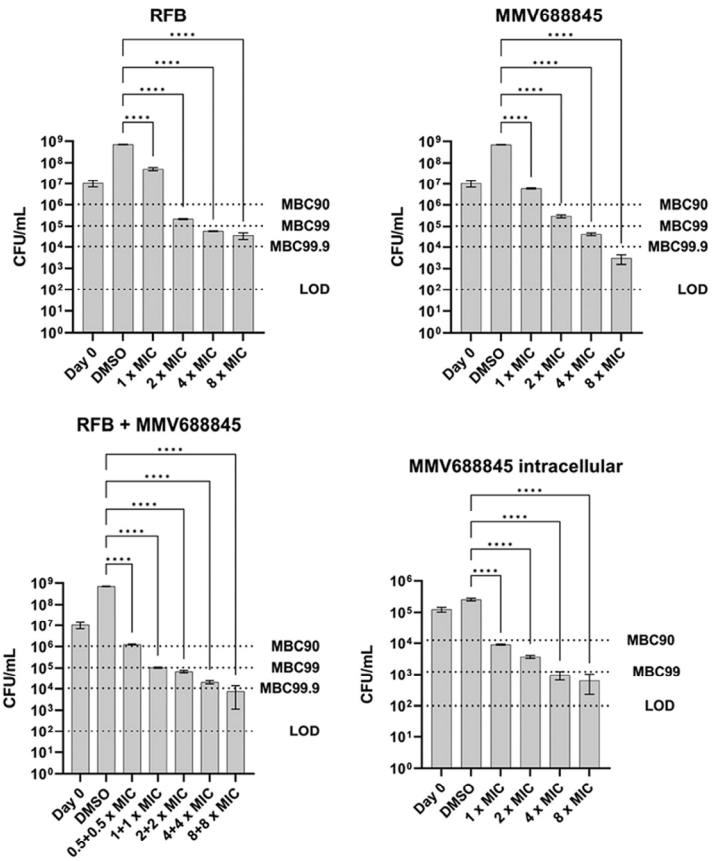


**FIG 1** Bactericidal activity of MMV688845 and rifabutin against *M. abscessus* ATCC 19977. LOD, limit of detection. Experiments were carried out in duplicate or triplicate. Results are means, with the standard deviations displayed as error bars. A one-way analysis of variance (ANOVA) multiple-comparison test was performed using GraphPad Prism 8 software to compare treated groups with the DMSO control. ****, $P \leq 0.0001$.

tion of CFU was observed; however, a reduction of the CFU count by 3 logarithmic units could be achieved only with a concentration of 8 $\times$ MIC (Fig. 1). In parallel, the bactericidal activity of MMV688845 was investigated in the macrophage infection model, where a reduction in the bacterial count was also observed and an $MBC_{90}$ of $\leq$16 $\mu$M (1 $\times$ MIC) was determined. The reference compound rifabutin also showed bactericidal effects with a minimal bactericidal concentration at which 90% of the bacteria are inhibited ($MBC_{90}$) of 2.4 $\mu$M (2 $\times$ MIC) (Table 2).

In combination, a reduction in CFU of about 90% can be achieved with 0.5 $\times$ MIC of each drug (Fig. 1), indicating an additive effect and consistent with the observation that rifabutin and MMV688845 engage different binding sites on the RpoB subunit of RNA polymerase (12).

**MMV688845 targets the RNA polymerase in *M. abscessus*.** Data in the literature show that the structural class of phenylalanine amides are inhibitors of the RpoB subunit of the mycobacterial RNA polymerase (12). However, these studies were performed on the RNA polymerase of *M. tuberculosis* with analogues of MMV688845. To confirm the molecular mechanism of action for MMV688845 in *M. abscessus*, six strains of resistant mutants

**TABLE 3** Characterization of *M. abscessus* MMV688845-resistant mutants

| *M. abscessus* subsp. *abscessus* strain | Batch | $MIC_{90}$ ($\mu$M)[a] of MMV688845 | RpoB mutation(s) |
|---|---|---|---|
| Bamboo | | 8 | |
| Bamboo $845^R$-1.1 | 1 | >100 | P473L |
| Bamboo $845^R$-2.1 | 2 | >100 | P473L |
| Bamboo $845^R$-2.2 | 2 | >100 | G562S |
| Bamboo $845^R$-2.3 | 2 | >100 | L556P, V557P |
| Bamboo $845^R$-2.4 | 2 | >100 | Q581R |
| Bamboo $845^R$-2.5 | 2 | >100 | D576Y |

[a]Determined by measurement of $OD_{600}$ and evaluated via method B. Two batches of spontaneous resistant mutants were generated by selection at 50 $\mu$M MMV688845. The observed frequency of resistance was $6 \times 10^{-8}$ $CFU^{-1}$.

were isolated and characterized. All resistant strains show a significant increase in MIC (>100 $\mu$M) and mutations in the RpoB subunit of the RNA polymerase (Table 3).

In this study, a frequency of resistance of $6 \times 10^{-8}$ $CFU^{-1}$ was determined. The localization of the above-mentioned mutations leading to MMV688845 resistance was visualized in a homology model of the RpoB subunit of *M. abscessus* RNA polymerase (Fig. 2). The basis for the model is an X-ray crystal structure (PDB code 5UHE) of the enzyme from *M. tuberculosis* which was determined by Lin et al. (12) with an *N*$\alpha$-aroyl-*N*-aryl-phenylalaninamide (d-AAP 1). Even though d-AAP 1 has small structural differences from MMV688845, it belongs to the same chemical class, which makes a similar binding mode very likely.

The six mutations described in Table 3 are located near the binding pocket of the inhibitor and are highlighted in red in Fig. 2. The fact that the substitution of individual amino acids leads to a loss of efficacy of MMV688845 suggests that the binding site on the RNA polymerase is relevant for the activity of the compound. Glycine 566 (*M. tuberculosis* numbering) is involved in hydrogen bonding with the inhibitor molecule, highlighting its importance in binding. It is likely that in the *M. abscessus* form of the enzyme, glycine 562 takes part in the formation of this hydrogen bond. One of the observed mutations affects this glycine and leads to MMV688845 resistance of the strain.

**Antibiotics for synergy testing with MMV688845.** As a requirement for the synergy testing described below, the individual $MIC_{90}$ values of each antibiotic for *M. abscessus* ATCC 19977 were determined in a microplate dilution assay. We decided to analyze the activity of antibiotics that are used for the treatment of NTM infections *in vitro* under three different assay conditions against *M. abscessus*. For this purpose, two assay media (7H9 and MHII) were used to identify a possible medium dependency of the results. The intracellular MICs were determined in a fluorescence-based macrophage infection model.

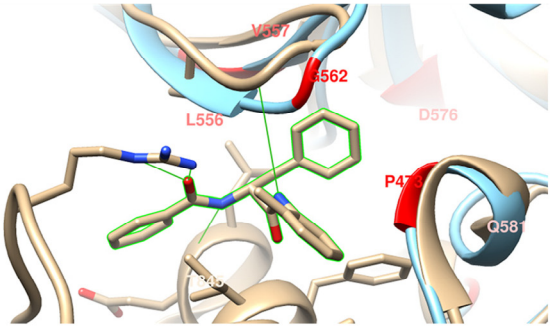


**FIG 2** Visualization of RpoB mutations in an *M. abscessus* homology model. Beige, *M. tuberculosis* RpoB [PDB 5UHE] with d-AAP 1 bound; light blue, *M. abscessus* homology model built using RoseTTAfold; red, *M. abscessus* resistance mutations; green, H bonds. (12, 39).

**TABLE 4** *In vitro* activity of antibiotics against *M. abscessus* ATCC 19977

| | $MIC_{90}$ ($\mu$M)[b] in: | | |
|---|---|---|---|
| Drug[a] | 7H9 | MHII | THP-1 |
| AMK | 1.5 | 2.1 | — |
| BDQ | 0.5 | 1.5 | 0.8 |
| CEF | 36 | 16 | — |
| CLR | 0.4 | 0.2 | 50 |
| AZM | 2.6 | 5.9 | 224[c] |
| EMB | 68 | — | — |
| RMP | 14 | 20 | — |
| TEI | 16[d] | 4.5 | — |
| TIG | 0.8 | 1.7 | 6.1 |
| TLM | 0.8 | 3 | 298[c] |

[a]AMK, amikacin; AZM, azithromycin; BDQ, bedaquiline; CLR, clarithromycin; CEF, cefoxitin; EMB, ethambutol; RFB, rifabutin; RMP, rifampicin; TEI, teicoplanin; TIG, tigecycline; TLM, telithromycin.
[b]Determined by RFP measurement and calculated by method A. —, no growth inhibition was observed.
[c]$MIC_{50}$.
[d]$MIC_{80}$.

For the initial MIC determination, the broth microdilution assay was performed in quadruplicate on each 96-well plate, which was performed in duplicate. The results were averaged and plotted logarithmically with Origin, and the $MIC_{90}$/$MIC_{80}$ and $MIC_{50}$ were determined through graphic evaluation.

The results of the MIC determination of the individual antibiotics are shown in Table 4. We included antibiotics with comparatively high MICs, such as ethambutol and cefoxitin, to analyze potential synergy with MMV688845. The MICs determined in this study do not show a strong dependence on the growth medium used.

Since *M. abscessus* can survive and replicate in macrophages, we were interested in whether it is possible to detect synergy in the macrophage infection model. For this type of *in vitro* assay, bacterial growth is analyzed by high-content microscopy and automated image analysis. For the evaluation of the assay, image data were recorded for the DAPI (4′,6-diamidino-2-phenylindole) channel for cell counting and in the RFP channel for quantification of bacterial growth. Higher MICs in the macrophage assay were expected, as permeability, metabolic (in)stability, and individual properties of the antibiotics might influence the efficacy in macrophages. To analyze synergy with this advanced *in vitro* method, we determined MICs for the antibiotics first in the macrophage infection assay. Amikacin, as an example, shows no efficacy in macrophages due to its polarity and thus low intracellular permeability. Cefoxitin, clarithromycin, rifampicin, and teicoplanin show up to an 10-fold increase in MIC compared to *in vitro* tests in MHII and 7H9 media. In addition, cytotoxic properties of the substances on THP-1 cells are considered by analysis of the cell count after the incubation period. Rifampicin, for example, shows toxic effects on macrophages (cell count reduced by at least 10% compared to the reference according to microscopic evaluation) at concentrations higher than 125 $\mu$M, so the $MIC_{90}$ could not be determined.

**Synergy testing of MMV688845.** The interaction of MMV688845 with the antibiotics mentioned above was analyzed by checkerboard assays and quantified by calculating the fractional inhibitory concentration index (FICI). Synergy testing by checkerboard assays is a method commonly used to test the effectiveness of antibiotic combinations *in vitro* (25, 26).

Within the FICIs obtained from the checkerboard experiments, no antagonism (FICI $>$ 4) of combinations with MMV688845 was observed. Clearly, for all compound combinations, a reduced MIC of both antibiotics was obtained, compared to the original MIC from the single determination (Table 3). In the majority of the combination experiments, an additive effect is observed.

As mentioned above, we did expect synergy of MMV688845 with macrolides. It is known that rifabutin inhibits the transcriptional induction of *erm41* and thereby enhances the effect of macrolides (16). Therefore, a combination with clarithromycin was analyzed, and the effect of the combination with MMV688845 stood out as the most potent

**TABLE 5** FICI values for combinations of MMV688845 with antimycobacterial drugs against *M. abscessus* ATCC 19977[a]

| | 7H9 | | | MHII | | | THP-1 | | |
|---|---|---|---|---|---|---|---|---|---|
| Drug[b] | Conc. ($\mu$M) | Conc. of MMV688845 ($\mu$M) | FICI | Conc. ($\mu$M) | Conc. of MMV688845 ($\mu$M) | FICI | Conc. ($\mu$M) | Conc. of MMV688845 ($\mu$M) | FICI |
| AMK | 0.8 | 1.6 | 0.7 | 1.3 | 6.3 | 1.2 | — | — | — |
| BDQ | 0.3 | 1.6 | 0.8 | 0.2 | 6.3 | 0.7 | 0.1 | 3.1 | 0.6 |
| CEF | 25 | 1.6 | 0.8 | 12.5 | 1.6 | 0.9 | — | — | — |
| CLR | 0.02 | 3.1 | 0.3 | 0.04 | 3.1 | 0.5 | 3.1 | 1.6 | 0.2 |
| AZM | 0.8 | 3.1 | 0.6 | 1.6 | 1.6 | 0.4 | — | — | — |
| TLM | 0.2 | 3.1 | 0.5 | 0.8 | 3.1 | 0.6 | — | — | — |
| EMB | 50 | 1.6 | 0.9 | — | — | — | — | — | — |
| RFB | 0.3 | 6.3 | 0.7 | 1.6 | 3.1 | 0.9 | 5.0 | 0.8 | 1.0 |
| RMP | 7.8 | 0.8 | 0.6 | 4.7 | 3.1 | 0.5 | — | — | — |
| TEI | 3.1 | 1.6 | 0.4 | 1.6 | 6.3 | 0.9 | — | — | — |
| TIG | 0.1 | 6.3 | 0.7 | 0.8 | 0.4 | 0.5 | 3.1 | 0.8 | 0.6 |

[a]All concentrations were determined by RFP signal. —, not determined.
[b]AMK, amikacin; AZM, azithromycin; BDQ, bedaquiline; CEF, cefoxitin; CLR, clarithromycin; EMB, ethambutol; RFB, rifabutin; RMP, rifampicin; TEI, teicoplanin; TIG, tigecycline; TLM, telithromycin.

(FICI $\leq$ 0.5). The lowest FICI was determined in the macrophage infection model, with a value of 0.2 (Table 5), indicating synergism against intracellular *M. abscessus*. A concentration of 3.1 $\mu$M clarithromycin (0.06$\times$MIC) leads to 90% growth inhibition in the presence of 1.6 $\mu$M MMV688845 (10-fold reduced MIC) in the macrophage infection assay (Fig. 3). In 7H9 broth and MHII, FICIs of 0.3 and 0.5 were obtained, confirming that the synergistic effect is independent of the assay medium used.

We corroborated this result by characterization of other macrolide antibiotics in combination. For this experiment, we chose the macrolide azithromycin and the ketolide telithromycin. We maintained our approach and first determined the $MIC_{90}$ of each compound alone, in 7H9, in MHII, and in the macrophage infection model (Table 4). The $MIC_{90}$s obtained for azithromycin and telithromycin in 7H9 and MHII are higher than those of clarithromycin. Our results are consistent with data found by Aziz et al. (21) for the *M. abscessus* strain Bamboo, which confirm the up-to-10-fold-higher inhibitory effect of clarithromycin compared to azithromycin and telithromycin. Growth inhibition of 90% or more by azithromycin and telithromycin was not achieved in the macrophage infection assay (Table 4), and higher concentrations displayed cytotoxicity against the eukaryotic cells. Therefore, we report $MIC_{50}$ values in this study, but for consistency with the previous results, no FICI was calculated. The combination with azithromycin shows additive effects with MMV688845 in 7H9 but a synergistic FICI of 0.4 in MHII media. For the combination assay with telithromycin, comparable results were observed. The ketolide shows synergy with MMV688845 in 7H9 (FICI 0.5) and additive effects in MHII medium (FICI 0.6) (Table 5).

The RNA polymerase inhibitors rifabutin and rifampicin showed predominantly additive effects in combination with MMV688845. For rifampicin, a FICI of 0.5 was obtained in MHII medium, which is indicative for synergy with MMV688845, leading to a 3- to 4-fold dose reduction. Since rifamycins and MMV688845 do not compete for the same binding site, additive effects were expected, underlining the suitability of MMV688845 as a combination partner.

**Pharmacokinetic properties of MMV688845 *in vivo*.** The pharmacokinetic behavior of MMV688845 was investigated in mice to determine whether the plasma concentrations necessary for efficacy are achieved. The results are shown in Fig. 4. Following oral administration, at 25 mg/kg, exposure was very low, in accordance with an earlier study (9). Given the average peak plasma concentration of 0.07 $\mu$M, higher doses are unlikely to achieve the MIC (6.6 $\mu$M) against strain K21, which was used for *in vivo* efficacy studies.

## DISCUSSION

The data obtained in this study underline the suitability of MMV688845 as a lead structure for drug development against *M. abscessus*. MMV688845 is active *in vitro* against all *M. abscessus* subspecies and clinical isolates analyzed in this study. Thus, we conclude that MMV688845 is active against a broad variety of *M. abscessus* strains. The

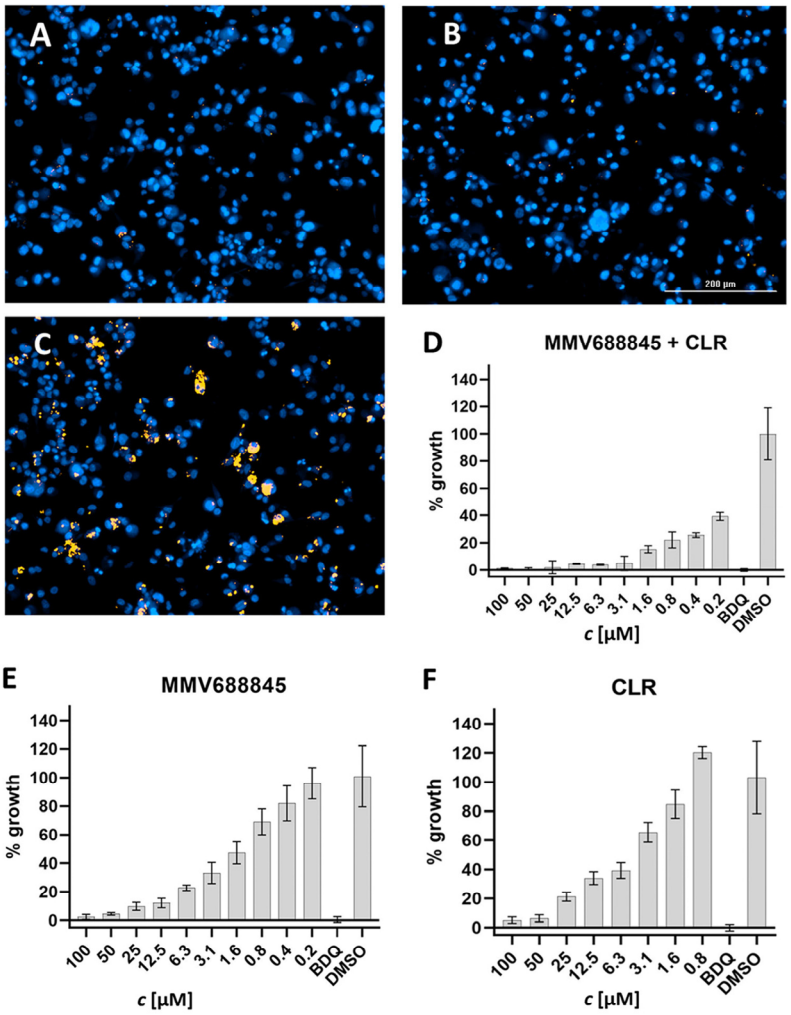


**FIG 3** Intracellular synergy of MMV688845 and clarithromycin (CLR). (A to C) Results of the macrophage infection assay with 1.5 $\mu$M bedaquiline (BDQ) (A), 3.1 $\mu$M CLR plus 1.6 $\mu$M MMV688845 (B), or 1% DMSO (C). Pictures were taken with a Cytation 5 imaging reader fluorescence microscope (BioTek). THP-1 macrophages are shown in blue, and *M. abscessus* (pTEC27) cells are in red. (D to F) growth inhibition of intracellular *M. abscessus* in the presence of 1.6 $\mu$M MMV688845 plus CLR (D), MMV688845 (E), or CLR. Experiments were carried out in duplicate, and the results presented are means, with the standard deviations displayed as error bars.

*in vitro* activity was validated in different media and intracellularly, showing that the lead's structure inhibits the growth of *M. abscessus* independently of the medium composition. By isolation of resistant mutants, MMV688845 was shown to target RNA polymerase in *M. abscessus*. This enzyme is a very well-validated antimycobacterial target and one of the cornerstones of TB therapy and could also be exploited for NTM treatment by using the substance class described here. Particularly noteworthy is that MMV688845 shows pronounced bactericidal activity, which is rare for anti-*M. abscessus* antibiotics (27). The reductions in bacterial counts in broth culture and inside macrophages underscore the idea that MMV688845 or analogues could be an important

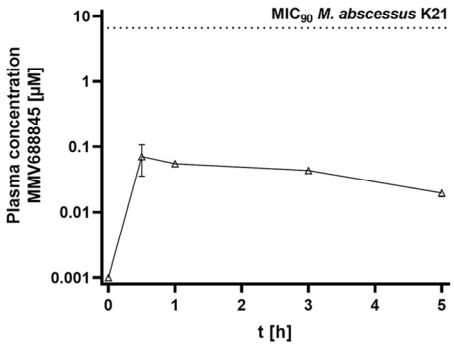


**FIG 4** Plasma concentration-time profile of MMV688845 following a single oral dose of 25 mg/kg in CD-1 mice. The MIC of MMV688845 against *M. abscessus* K21 (Table 1) is indicated by a dotted line. Experiments were carried out in duplicate, and the results presented are as means, with the standard deviations displayed as error bars.

component of a sterilizing *M. abscessus* therapy. The microbiological profile of MMV688845 *in vitro* and in the macrophage infection model has been extended and confirmed as positive in this study. Because mycobacterial infections are treated by combination therapy, the interaction between antibiotics should be analyzed in an early stage of the drug development process. Only a well-tuned combination has the potential to eradicate pathogens like *M. abscessus* while preventing resistance development. Our results show that MMV688845 acts synergistically with the macrolides and ketolides investigated in this study against *M. abscessus* ATCC 19977. The resulting dual inhibition of mRNA biosynthesis and bacterial ribosomal translation is particularly effective. Since *M. abscessus* ATCC 19977 is an *erm41*-positive strain, the results are consistent with the observation of Aziz et al. (16) showing that the RNA polymerase inhibitor rifabutin suppresses inducible macrolide resistance and acts synergistically in *erm41*-positive strains in combination with clarithromycin. We were able to demonstrate synergistic effects of MMV688845 with clarithromycin, in the standard assay in MHII and 7H9 and also in the macrophage infection model. An useful addition in future experiments could be a longer incubation period for MIC determination. This would have the advantage of taking (slowly) inducible resistance into account in the assay, but it would require sufficient stability of the compounds tested.

We observed additive effects for the combinations of MMV688845 with rifabutin and with rifampicin in different assay systems, indicating that the rifamycins do not compete with MMV688845 for one binding site but address different domains in the enzyme, leading to the result mentioned above. X-ray data of the *M. tuberculosis* RNA polymerase/inhibitor complex published by Lin et al. (12) explain this observation, as both binding sites were identified, the observation that the simultaneous administration of MMV688845 and rifamycins, would show an additive effect was expected, because Lin et al. had shown an additive effect for the combination of rifampicin and *N*$\alpha$-aroyl-*N*-aryl-phenylalaninamides before against *M. tuberculosis* (12). For other classes of antibiotics, additive effects were observed and antagonism was not found, indicating that combination therapies with MMV688845 and the clinically used antibiotics are possible. Our data support the further development of synthetic RNA polymerase inhibitors as an antimycobacterial compound class. The effects between MMV688845 and antibiotics observed in this study, especially in the synergistic combinations, suggest that clinically required concentrations can be more easily achieved *in vivo* in such combinations. This can lead to reduced drug doses, which might reduce the adverse effects of antibiotic therapy. The synergy shown with clarithromycin suggests that MMV688845 may maintain the efficacy of macrolides during clinical therapy

by repressing transcription of the *erm41* gene if sufficient exposures of MMV688845 or an analogue could be achieved.

However, an *in vivo* study on the bioavailability of MMV688845 found that the compound did not reach sufficient plasma concentrations after oral administration in mice to investigate efficacy. Because of the promising *in vitro* properties of the compound revealed in this study, chemical derivatization is desirable. Based on the results of this study, efforts to improve bioavailability and profile efficacy are in progress, as the mechanism of action of MMV688845 has the potential to exhibit *in vivo* activity against *M. abscessus*. We assume a low metabolic stability for MMV688845, since the amide bonds in the molecule are prone to enzymatic hydrolysis. In this context, derivatives in which the amide bonds in the molecule are shielded against hydrolytic attack might be an interesting option. We highlight that MMV688845 is a promising substance for the development of new antibiotics targeting *M. abscessus*. In this context, it seems to us to be a meaningful approach to improve antibacterial efficacy and oral bioavailability to identify an oral lead compound with proven *in vivo* efficacy.

## MATERIALS AND METHODS

**$MIC_{90}$ determination in 7H9 and MHII by RFP measurement.** MICs were determined against *M. abscessus* ATCC 19977(pTEC27) by the broth microdilution method in 7H9 containing 10% filter sterilized solution of 0.8% sodium chloride, 5.0% bovine serum albumin, and 2.0% dextrose in purified water (ADS) and 0.05% Tween 80 or MHII containing 0.05% Tween 80. A nine-point 2-fold serial dilution of each compound was prepared in 96-well flat-bottom plates (Sarstedt, 3924500). Column 1 of the 96-well plate included eight negative controls (1% dimethyl sulfoxide [DMSO]), and column 2 contained eight positive controls (100 $\mu$M amikacin). Column 12 contained only medium as sterile control. The concentration of the inoculum was $5 \times 10^5$ cells/mL ($OD_{600}$, 0.1 [$1 \times 10^8$ CFU/mL]). The starting inoculum was diluted from a preculture at the mid-log phase ($OD_{600}$, 0.2 to 0.8). The plates were sealed with Parafilm, placed in a container with moist tissue, and incubated for 3 days at 37°C. After incubation, the plates were monitored by RFP measurement at 590 nm (BMG Labtech Fluostar Optima microplate reader). Growth inhibition of >90% is considered to indicate activity. The assay was performed in quadruplicate on each 96-well plate, which was performed in duplicate (8).

**Checkerboard titration assay in 7H9 or MHII and intracellular checkerboard assay.** For each determination, eight concentrations of MMV688845 (50 $\mu$M to 0.039 $\mu$M) were combined with nine concentrations of another substance. The concentration range of the second substance was selected depending on its MIC alone. In total, each compound pair was tested in 72 different concentration combinations. The assay was carried out using the microdilution method as previously described. The assay was performed in two replicates.

**FICI determination.** The fractional inhibitory concentration index (FICI) was used to analyze the results of the checkerboard assay. The FIC was determined as follows: (concentration of drug A in combination/concentration of drug A when used alone) + (concentration of drug B in combination/concentration of drug B when used alone) (26). The FICI was then calculated using the FICs corresponding to the wells with the lowest concentration resulting in >90% inhibition. The lowest FICI of all the nonturbid wells along the turbidity/nonturbidity interface was used (28). Synergy is defined as a FICI of ≤0.5, additivity is defined as a FICI of >0.5 and ≤4, and antagonism is defined as a FICI of >4 (26).

***M. abscessus* infection assay in human macrophages.** For the infection assay, an *M. abscessus* pTEC27 culture ($OD_{600}$, 0.2 to 0.8; mid-log phase) was centrifuged (4,000 rpm, room temperature [RT], 7 min), washed with 7H9 medium with 0.05% Tween 80 (about 10 mL), and vortexed. After another centrifugation (4,000 rpm, RT, 7 min), 7H9 medium was replaced by RPMI medium (at the same volume or a little less to concentrate the bacteria), and the sample was vortexed and incubated at RT for 5 min. After incubation, the bacterial suspension was filtered through a 5-$\mu$m-pore-size filter to remove the clumps. The $OD_{600}$ was determined after filtration (an $OD_{600}$ of 0.1 is equal to $1 \times 10^8$ CFU/mL). The appropriate number of bacteria was incubated in the presence of 10% human serum at 37°C for 30 min for opsonization. A suspension of THP-1 cells ($1 \times 10^6$ cells/mL) in RPMI incomplete medium was incubated with the opsonized *M. abscessus* single-cell suspension (multiplicity of infection [MOI], 5:1) and phorbol myristate acetate (PMA) (40 ng/mL) for 4 h at 37°C under constant agitation. After infection, the THP-1 cell suspension was centrifuged (750 rpm, RT, 10 min) and washed with RPMI medium. Afterward, the cell suspension was dispensed in 96-well plates (Sarstedt, 3924) with $1 \times 10^5$ THP-1 cells/well. The test compounds at the appropriate concentration were added, and the plates, which were sealed with Parafilm, were incubated for 4 days (37°C, 5% $CO_2$). After incubation, the cells were fixed with paraformaldehyde (PFA; 4% in phosphate-buffered saline buffer) for 30 min. After removal of the PFA the cells were stained with ready-made DAPI solution (Sigma, MBD0015). The plates were washed twice with RPMI medium. Image acquisition (DAPI, 386 to 23 nm; RFP, 560 to 25 nm; bright field) and analysis were done with a Cytation 5 imaging reader fluorescence microscope (BioTek). The sum of the spot area (ObjectSumArea) of the RFP channel was used for the calculation of growth inhibition (19).

**$MIC_{90}$ determination in human macrophages.** MICs for *M. abscessus* ATCC 19977(pTEC27) ($OD_{600}$, 0.2 to 0.8, mid-log phase) were determined by the microdilution method in RPMI incomplete medium (RPMI 1640 medium supplemented with 5% fetal bovine serum [FBS], 2% glutamine, and 1%

nonessential amino acids) with 70 $\mu$M amikacin. A 10-point 2-fold serial dilution of each compound was prepared in tissue culture-treated 96-well flat-bottom plates (Sarstedt, 3924). Column 1 of the 96-well plate included eight negative controls (1% DMSO), and column 2 had eight positive controls (1.5 $\mu$M bedaquiline). The plates inoculated with the infected cells ($1 \times 10^5$ THP-1 cells/well) were incubated for 4 days (37°C, 5% $CO_2$). After incubation, the cells were fixed with paraformaldehyde, stained, and washed with RPMI medium. Image acquisition (DAPI, 386 to 23 nm; RFP, 560 to 25 nm; bright field) and analysis were done with a Cytation 5 imaging reader fluorescence microscope (BioTek). The sum of the spot area (ObjectSumArea) of the RFP channel was used for the calculation of growth inhibition (19). The assay was performed in quadruplicate on each 96-well plate, which was performed in duplicate.

**MIC calculation method A.** MIC calculation method A (for the assay described above, including $MIC_{90}$ determination in 7H9 and MHII by RFP measurement, checkerboard assay, and $MIC_{90}$ determination in human macrophages) was done as follows. Every assay plate contained eight wells with DMSO (1%) as a negative control, which correspond to 100% bacterial growth, and eight wells with amikacin (100 $\mu$M) or bedaquiline (1.5 $\mu$M) as a positive control, in which 100% inhibition of bacterial growth was reached. The controls were used to monitor assay quality through the determination of the *Z* score and for normalizing the data on a plate basis. The *Z* factor was determined using the following formula: $1 - [3(SD_{positive\ control} + SD_{DMSO})/(M_{positive\ control} - M_{DMSO})]$, where SD is the standard deviation and M is the mean. Percent inhibition was calculated as follows: $-100 \times [(signal_{sample} - signal_{DMSO})/(signal_{DMSO} - signal_{positive\ control})]$.

For $MIC_{90}$ determination, growth inhibition curves were calculated with OriginPro 2019 software (OriginLab Corporation). The curves were fitted using the following formula: $y = A2 + \{(A1 - A2)/[1 + (x/x_0)^p]\}$, where *A*1 is the initial value for *y*, *A*2 is the final value for *y*, *x* is the concentration of the test compound, $x_0$ is the concentration of the test compound at the center of the curve, and *p* is the power.

**MBC determination method A.** For MBC determination *M. abscessus* ATCC 19977 was incubated in a microplate macrophage infection dilution assay for 4 days as described below. Subsequently, the MBC was determined by CFU counting. For this purpose, 6-well plates were used, each filled with 4 mL 7H10 agar supplemented with 0.5% glycerol, 10% ADS, and 400 $\mu$g/mL hygromycin. From the wells where growth inhibition was detected in the microplate dilution assay, 10 $\mu$L (undiluted or diluted 1:100) was plated into one well of the 6-well plates. The colonies were counted after 4 days of incubation at 37°C, and the experiment was carried out in triplicate. Based on the result, the concentration of CFUs per milliliter was calculated. The number of CFUs was also determined in the inoculum prior to the 4-day incubation.

**Bacterial cells and culture media.** *M. abscessus* expressing RFP tdTomato was used for the activity assays. Stocks of the bacteria grown in complete 7H9 broth were stored in approximately 15% glycerol at −80°C. Using an inoculation loop, bacteria were spread on 7H10 plates (containing 500 $\mu$g/mL hygromycin) and grown for 5 days in an incubator at 37°C.

Bacteria were grown in complete 7H9 broth supplemented with 10% ADS and 0.05% Tween 80 or in MHII broth supplemented with 0.05% Tween 80. After one colony was scraped off the 7H10 plate, hygromycin (400 $\mu$g/mL) was added for *M. abscessus*(pTEC27) growth. The culture volume was 10 mL in a 50-mL Falcon tube. The tubes were covered to protect the photosensitive hygromycin and shaken in an incubator at 37°C. Solid cultures were grown on 7H10 medium supplemented with 0.5% glycerol and 10% ADS. For *M. abscessus* pTEC27, hygromycin (500 $\mu$g/mL) was added. (ADS supplement is a filter-sterilized solution of 0.8% sodium chloride, 5.0% bovine serum albumin, and 2.0% dextrose in purified water).

**THP-1 cells and culture media.** The THP-1 cells (ATCC TIB-202) used were derived from human monocytes obtained from a 1-year-old male infant with acute monocytic leukemia. The cells were put in 90% FBS–10% DMSO and stored in liquid nitrogen. THP-1 cells were grown in a complete RPMI medium. The cells were grown in a tissue culture flask with a minimum volume of 20 mL and a maximum volume of 50 mL and were incubated in an atmosphere of 95% air and 5% carbon dioxide ($CO_2$) at a temperature of 37°C. The cell density was kept between 0.25 million and 1 million cells/mL. Every 2 or 3 days, the cells were counted and diluted to 0.25 million cells/mL. The cells doubled every 48 h. A culture from nitrogen stock could be subcultured for up to 3 months; after this time, a change in morphology and growth behavior was observed. For culturing of THP-1 cells, RPMI 1640 medium supplemented with 5% FBS, 2% glutamine, and 1% nonessential amino acids.

**Bacterial strains, culture media, and drugs.** *M. abscessus* Bamboo was isolated from the sputum of a patient with amyotrophic lateral sclerosis and bronchiectasis and was provided by Wei Chang Huang, Taichung Veterans General Hospital, Taichung, Taiwan. *M. abscessus* Bamboo whole-genome sequencing showed that the strain belongs to *M. abscessus* subsp. *abscessus* and harbors an inactive clarithromycin-sensitive *erm41* C28 sequevar (29, 30). *Mycobacterium abscessus* subsp. abscessus strain ATCC 19977, harboring the inducible clarithromycin resistance-conferring *erm41* T28 sequevar (31), was purchased from the American Type Culture Collection (ATCC). *Mycobacterium abscessus* subsp. *bolletii* CCUG 50184T, harboring the inducible clarithromycin resistance-conferring *erm41* T28 sequevar (32), and *Mycobacterium abscessus* subsp. *massiliense* CCUG 48898T, harboring the nonfunctional *erm41* deletion sequevar (33), were purchased from the Culture Collection University of Goteborg (CCUG). Clinical isolates covering the *M. abscessus* complex (M9, M199, M337, M404, M422, M232, M506, and M111) were provided by Jeanette W. P. Teo (Department of Laboratory Medicine, National University Hospital, Singapore). For information on the origin of the isolates, see reference 21. The subspecies and *erm41* sequevars of these isolates were determined previously (21). *M. abscessus* subsp. *abscessus* K21 was isolated from a patient and provided by Sung Jae Shin (Department of Microbiology, Yonsei University College of Medicine, Seoul, South Korea) and Won-Jung Koh (Division of Pulmonary and Critical Care Medicine, Samsung Medical Center, Seoul, South Korea) (34). This strain harbors the inactive, clarithromycin-sensitive *erm41* C28 sequevar as determined previously (34). For general bacteria culturing and certain MIC experiments, Middlebrook 7H9 broth (BD Difco) was supplemented with 0.5% albumin, 0.2% glucose, 0.085% sodium

chloride, 0.0003% catalase, 0.2% glycerol, and 0.05% Tween 80. Unless otherwise stated, solid cultures were grown on Middlebrook 7H10 agar (BD Difco) supplemented with 0.5% albumin, 0.2% glucose, 0.085% sodium chloride, 0.5% glycerol, 0.0003% catalase, and 0.006% oleic acid. All drugs were prepared as 10 mM stocks in 100% DMSO.

**Selection of spontaneous resistant mutants.** Spontaneous resistant mutants were selected as described previously (35). Exponentially growing *M. abscessus* Bamboo culture ($10^7$ to $10^9$ CFU) was plated on 7H10 agar containing 50 $\mu$M MMV688845. The plates were incubated for 7 days at 37°C. Apparently resistant colonies were purified and confirmed by restreaking on agar containing the same drug concentration. Two independent batches of resistant mutants were generated in this manner. Genomic DNA was extracted as described previously using the phenol-chloroform method (36). Sanger sequencing of the RpoB (MAB_3869c) genomic region was performed by Genewiz (Genewiz, Inc., South Plainfield, NJ, USA) using 14 primers as previously described (37).

**MIC assay in 7H9 by OD measurement.** MIC determination by $OD_{600}$ was carried out in 96-well plate format as previously described (9, 21). Ninety-six-well plates were initially set up with 100 $\mu$L of 7H9 per well. For each compound, a 10-point 2-fold dilution series starting at twice the desired highest concentration was dispensed into the 96-well plates using a Tecan D300e digital dispenser, with the DMSO concentration normalized to 2%. A bacterial culture grown to mid-log phase ($OD_{600}$, 0.4 to 0.6) was diluted to an $OD_{600}$ of 0.1 ($1 \times 10^7$ CFU/mL). One hundred microliters of the resulting bacteria suspension was dispensed into the 96-well plates containing compounds to give a final volume of 200 $\mu$L per well with an initial $OD_{600}$ of 0.05 ($5 \times 10^6$ CFU/mL) and a final DMSO concentration of 1%. Final compound concentration ranges were typically 50 to 0.098 $\mu$M or 6.25 to 0.012 $\mu$M but were adjusted to 100 to 0.195 $\mu$M for testing of MMV688845-resistant mutant strains. Untreated control wells were included on each plate that contained a bacterial suspension and 1% DMSO. Plates were sealed with Parafilm, stored in boxes with wet paper towels, and incubated at 37°C with shaking (110 rpm). Plates were incubated for 3 days.

**MIC calculation method B.** To determine growth, $OD_{600}$ was measured using a Tecan Infinite M200 plate reader on day 0 and day 3. Two biological replicates were performed. Clarithromycin was included in each experiment as a positive control. For each well in the 96-well plate, bacterial growth was calculated by subtracting the day 0 $OD_{600}$ value from the day 3 $OD_{600}$ value. For each compound series, the bacterial growth values for the untreated control wells were averaged to give the average drug-free bacterial growth. For compound-containing wells, percent growth was calculated by dividing growth values by the average bacterial growth in drug-free wells for the compound series and multiplying by 100. For each compound series, we plotted percentage growth versus compound concentration. By visual inspection of the dose-response curve, we determined the MIC of a compound as the compound concentrations that would result in 90% growth inhibition. The MIC determination was performed twice with different starter cultures. The MICs shown here are the averaged results of the two biological replicates.

**MBC determination method B.** To determine the MBC, CFU measurement was done for the bacteria suspension at an $OD_{600}$ of 0.1 on day 0 and for each well on day 3. Specifically, serial 10-fold dilutions were prepared in phosphate-buffered saline (Thermo Fisher, 10010023) containing 0.05% Tween 80 (PBS-Tween 80) and plated on 7H10 agar. The $MBC_{90}$, $MBC_{99}$, and $MBC_{99.9}$ were defined as the lowest concentrations of drug that reduced the number of CFUs per milliliter by 10-fold, 100-fold, and 1,000-fold, respectively, relative to the day 0 value.

***M. abscessus* homology model.** The built model was then compared to the model for *M. tuberculosis* RpoB (PDB 5UHE) bound to d-AAP 1 in UCSF Chimera (38, 39), and the mutations observed in the *M. abscessus* model were highlighted.

***In vivo* mouse pharmacokinetics.** All animal experiments were approved by the Center for Discovery and Innovation, Institutional Animal Care and Use Committee, and were conducted in compliance with their guidelines. Female CD-1 mice ($n = 2$) were weighed and received a single dose of MMV688845 orally (p.o.) (25 mg/kg of body weight). The compound was formulated in 5% *N*,*N*-dimethylacetamide, 60% polyethylene glycol 300, and 35% D5W (5% dextrose in water). Blood samples were serially collected via tail snip from each individual mouse at 0.5, 1, 3, and 5 h postdose. Blood (50 $\mu$L) was collected in capillary Microvette K2EDTA tubes (16.444.100; Sarstedt, Inc.) and kept on ice prior to centrifugation at 1,500 $\times$ *g* for 5 min. The supernatant (plasma) was transferred into a 96-well plate and stored at −80°C.

**HPLC-MS analysis.** Liquid chromatography-tandem mass spectrometry (LC-MS/MS) analysis was performed on a Sciex Applied Biosystems Qtrap 6500+ triple-quadrupole mass spectrometer coupled to a Shimadzu Nexera 2 high-pressure liquid chromatography (HPLC) system to quantify each drug in plasma. Neat 1-mg/mL DMSO stocks for MMV688845 were serially diluted in 50:50 acetonitrile (ACN)/water to create standard curves and quality control (QC) spiking solutions. Standards and QCs were created by adding 10 $\mu$L of spiking solutions to 90 $\mu$L of drug-free plasma (CD-1 K2EDTA Mouse; Bioreclamation IVT). Twenty microliters of control, standard, QC, or study sample was added to 200 $\mu$L of ACN-methanol (MeOH; 50:50) protein precipitation solvent containing an internal standard (10 ng/mL verapamil). Extracts were vortexed for 5 min and centrifuged at 4,000 rpm for 5 min. One hundred microliters of supernatant was transferred for HPLC-MS/MS analysis and diluted with 100 $\mu$L of Milli-Q deionized water.

Chromatography was performed on an Agilent Zorbax SB-$C_8$ column (2.1 $\times$ 30 mm; particle size, 3.5 $\mu$m) using a reverse-phase gradient. Milli-Q deionized water with 0.1% formic acid was used for the aqueous mobile phase and 0.1% formic acid in ACN for the organic mobile phase. Multiple-reaction monitoring of precursor/product transitions in electrospray positive-ionization mode was used to quantify the analytes. Data processing was performed using Analyst software (version 1.6.2; Applied Biosystems Sciex).

## ACKNOWLEDGMENTS

We thank Nadine Taudte and Jens-Ulrich Rahfeld for providing and maintaining the biosafety 2 facility. We are grateful to Wei Chang Huang (Taichung Veterans General Hospital, Taichung, Taiwan) for providing *M. abscessus* Bamboo, to Jeanette W. P. Teo (Department of Laboratory Medicine, National University Hospital, Singapore) for providing the collection of *M. abscessus* clinical isolates, to Sung Jae Shin (Department of Microbiology, Yonsei University College of Medicine, Seoul, South Korea), to Won-Jung Koh (Division of Pulmonary and Critical Care Medicine, Samsung Medical Center, Seoul, South Korea) for providing *M. abscessus* K21, and to Chao Chen for generating the *M. abscessus* MMV688845-resistant mutants.

This work was funded by the Deutsche Forschungsgemeinschaft (DFG, German Research Foundation), no. 432291016, and by the National Institute of Allergy and Infectious Diseases of the National Institutes of Health under award number R01AI132374.

## REFERENCES

1. Baldwin SL, Larsen SE, Ordway D, Cassell G, Coler RN. 2019. The complexities and challenges of preventing and treating nontuberculous mycobacterial diseases. PLoS Negl Trop Dis 13:e0007083. https://doi.org/10.1371/journal.pntd.0007083.
2. Ahmed I, Tiberi S, Farooqi J, Jabeen K, Yeboah-Manu D, Migliori GB, Hasan R. 2020. Non-tuberculous mycobacterial infections—a neglected and emerging problem. Int J Infect Dis 92:S46–S50. https://doi.org/10.1016/j.ijid.2020.02.022.
3. Boudehen YM, Kremer L. 2021. Mycobacterium abscessus. Trends Microbiol 29:951–952. https://doi.org/10.1016/j.tim.2021.06.006.
4. Novosad SA, Beekmann SE, Polgreen PM, Mackey K, Winthrop KL, M. abscessus Study Team. 2016. Treatment of mycobacterium abscessus infection. Emerg Infect Dis 22:511–514. https://doi.org/10.3201/eid2203.150828.
5. Aksamit TR, Philley JV, Griffith DE. 2014. Nontuberculous mycobacterial (NTM) lung disease: the top ten essentials. Respir Med 108:417–425. https://doi.org/10.1016/j.rmed.2013.09.014.
6. Daley CL, Iaccarino JM, Lange C, Cambau E, Wallace RJ, Andrejak C, Böttger EC, Brozek J, Griffith DE, Guglielmetti L, Huitt GA, Knight SL, Leitman P, Marras TK, Olivier KN, Santin M, Stout JE, Tortoli E, Van Ingen J, Wagner D, Winthrop KL. 2020. Treatment of nontuberculous mycobacterial pulmonary disease: an official ATS/ERS/ESCMID/IDSA clinical practice guideline. Clin Infect Dis 71:E1–E36. https://doi.org/10.1093/cid/ciaa241.
7. Johansen MD, Herrmann JL, Kremer L. 2020. Non-tuberculous mycobacteria and the rise of Mycobacterium abscessus. Nat Rev Microbiol 18:392–407. https://doi.org/10.1038/s41579-020-0331-1.
8. Richter A, Strauch A, Chao J, Ko M, Av-Gay Y. 2018. Screening of preselected libraries targeting mycobacterium abscessus for drug discovery. Antimicrob Agents Chemother 62:e00828-18. https://doi.org/10.1128/AAC.00828-18.
9. Low JL, Wu ML, Aziz DB, Laleu B, Dick T. 2017. Screening of TB actives for activity against nontuberculous mycobacteria delivers high hit rates. Front Microbiol 8:1539. https://doi.org/10.3389/fmicb.2017.01539.
10. Jeong J, Kim G, Moon C, Kim HJ, Kim TH, Jang J. 2018. Pathogen Box screening for hit identification against Mycobacterium abscessus. PLoS One 13:e0195595. https://doi.org/10.1371/journal.pone.0195595.
11. Ballell L, Bates RH, Young RJ, Alvarez-Gomez D, Alvarez-Ruiz E, Barroso V, Blanco D, Crespo B, Escribano J, González R, Lozano S, Huss S, Santos-Villarejo A, Martín-Plaza JJ, Mendoza A, Rebollo-Lopez MJ, Remuiñan-Blanco M, Lavandera JL, Pérez-Herran E, Gamo-Benito FJ, García-Bustos JF, Barros D, Castro JP, Cammack N. 2013. Fueling open-source drug discovery: 177 small-molecule leads against tuberculosis. ChemMedChem 8:313–321. https://doi.org/10.1002/cmdc.201200428.
12. Lin W, Mandal S, Degen D, Liu Y, Ebright YW, Li S, Feng Y, Zhang Y, Mandal S, Jiang Y, Liu S, Gigliotti M, Talaue M, Connell N, Das K, Arnold E, Ebright RH. 2017. Structural basis of Mycobacterium tuberculosis transcription and transcription inhibition. Mol Cell 66:169–179.E8. https://doi.org/10.1016/j.molcel.2017.03.001.
13. Mann L, Lang M, Schulze P, Halz JH, Csuk R, Hoenke S, Seidel RW, Richter A. 2021. Racemization-free synthesis of N$\alpha$-2-thiophenoyl-phenylalanine-2-morpholinoanilide enantiomers and their antimycobacterial activity. Amino Acids 53:1187–1196. https://doi.org/10.1007/s00726-021-03044-1.
14. Richard M, Gutiérrez AV, Kremer L. 2020. Dissecting erm(41)-mediated macrolide-inducible resistance in mycobacterium abscessus. Antimicrob Agents Chemother 64:e01879-19. https://doi.org/10.1128/AAC.01879-19.
15. Maurer FP, Castelberg C, Quiblier C, Böttger EC, Somoskövi A. 2014. Erm(41)-dependent inducible resistance to azithromycin and clarithromycin in clinical isolates of mycobacterium abscessus. J Antimicrob Chemother 69:1559–1563. https://doi.org/10.1093/jac/dku007.
16. Aziz DB, Go ML, Dick T. 2020. Rifabutin suppresses inducible clarithromycin resistance in mycobacterium abscessus by blocking induction of whiB7 and erm41. Antibiotics 9:72. https://doi.org/10.3390/antibiotics9020072.
17. Strnad L, Winthrop KL. 2018. Treatment of Mycobacterium abscessus complex. Semin Respir Crit Care Med 39:362–376. https://doi.org/10.1055/s-0038-1651494.
18. Lee MR, Sheng WH, Hung CC, Yu CJ, Lee LN, Hsueh PR. 2015. Mycobacterium abscessus complex infections in humans. Emerg Infect Dis 21:1638–1646. https://doi.org/10.3201/2109.141634.
19. Richter A, Shapira T, Av-Gay Y. 2019. THP-1 and Dictyostelium infection models for screening and characterization of anti-Mycobacterium abscessus hit compounds. Antimicrob Agents Chemother 64:e01601-19. https://doi.org/10.1128/AAC.01601-19.
20. Ganapathy US, Dartois V, Dick T. 2019. Repositioning rifamycins for Mycobacterium abscessus lung disease. Expert Opin Drug Discov 14:867–878. https://doi.org/10.1080/17460441.2019.1629414.
21. Aziz DB, Low JL, Wu M-L, Gengenbacher M, Teo JWP, Dartois V, Dick T. 2017. Rifabutin is active against Mycobacterium abscessus complex. Antimicrob Agents Chemother 61:e00155-17. https://doi.org/10.1128/AAC.00155-17.
22. Takaki K, Davis JM, Winglee K, Ramakrishnan L. 2013. Evaluation of the pathogenesis and treatment of Mycobacterium marinum infection in zebrafish. Nat Protoc 8:1114–1124. https://doi.org/10.1038/nprot.2013.068.
23. Ollinger J, Bailey MA, Moraski GC, Casey A, Florio S, Alling T, Miller MJ, Parish T. 2013. A dual read-out assay to evaluate the potency of compounds active against Mycobacterium tuberculosis. PLoS One 8:e60531. https://doi.org/10.1371/journal.pone.0060531.
24. Sorrentino F, del Rio RG, Zheng X, Matilla JP, Gomez PT, Hoyos MM, Herran MEP, Losana AM, Av-Gay Y. 2016. Development of an intracellular screen for new compounds able to inhibit Mycobacterium tuberculosis growth in human macrophages. Antimicrob Agents Chemother 60:640–645. https://doi.org/10.1128/AAC.01920-15.
25. Pryjma M, Burian J, Thompson CJ. 2018. Rifabutin acts in synergy and is bactericidal with frontline mycobacterium abscessus antibiotics clarithromycin and tigecycline, suggesting a potent treatment combination. Antimicrob Agents Chemother 62:e00283-18. https://doi.org/10.1128/AAC.00283-18.
26. Hsieh MH, Yu CM, Yu VL, Chow JW. 1993. Synergy assessed by checkerboard. Diagn Microbiol Infect Dis 16:343–349. https://doi.org/10.1016/0732-8893(93)90087-n.
27. Yam YK, Alvarez N, Go ML, Dick T. 2020. Extreme drug tolerance of Mycobacterium abscessus "persisters." Front Microbiol 11:359. https://doi.org/10.3389/fmicb.2020.00359.
28. Bonapace CR, Bosso JA, Friedrich LV, White RL. 2002. Comparison of methods of interpretation of checkerboard synergy testing. Diagn Microbiol Infect Dis 44:363–366. https://doi.org/10.1016/s0732-8893(02)00473-x.

29. Yee M, Klinzing D, Wei JR, Gengenbacher M, Rubin EJ, Dick T. 2017. Draft genome sequence of Mycobacterium abscessus Bamboo. Genome Announc 5:e00388-17. https://doi.org/10.1128/genomeA.00388-17.
30. Bastian S, Veziris N, Roux AL, Brossier F, Gaillard JL, Jarlier V, Cambau E. 2011. Assessment of clarithromycin susceptibility in strains belonging to the Mycobacterium abscessus group by erm(41) and rrl sequencing. Antimicrob Agents Chemother 55:775–781. https://doi.org/10.1128/AAC.00861-10.
31. Ripoll F, Pasek S, Schenowitz C, Dossat C, Barbe V, Rottman M, Macheras E, Heym B, Herrmann J-L, Daffé M, Brosch R, Risler J-L, Gaillard J-L. 2009. Non mycobacterial virulence genes in the genome of the emerging pathogen Mycobacterium abscessus. PLoS One 4:e5660. https://doi.org/10.1371/journal.pone.0005660.
32. Choi GE, Cho YJ, Koh WJ, Chun J, Cho SN, Shin SJ. 2012. Draft genome sequence of Mycobacterium abscessus subsp. bolletii BDT. J Bacteriol 194:2756–2757. https://doi.org/10.1128/JB.00354-12.
33. Cho YJ, Yi H, Chun J, Cho SN, Daley CL, Koh WJ, Shin SJ. 2013. The genome sequence of "Mycobacterium massiliense" strain CIP 108297 suggests the independent taxonomic status of the Mycobacterium abscessus complex at the subspecies level. PLoS One 8:e81560. https://doi.org/10.1371/journal.pone.0081560.
34. Dick T, Shin SJ, Koh WJ, Dartois V, Gengenbacher M. 2020. Rifabutin is active against mycobacterium abscessus in mice. Antimicrob Agents Chemother 64:e01943-19. https://doi.org/10.1128/AAC.01943-19.
35. Yang T, Moreira W, Nyantakyi SA, Chen H, Binte Aziz D, Go ML, Dick T. 2017. Amphiphilic indole derivatives as antimycobacterial agents: structure-activity relationships and membrane targeting properties. J Med Chem 60:2745–2763. https://doi.org/10.1021/acs.jmedchem.6b01530.
36. Negatu DA, Yamada Y, Xi Y, Go ML, Zimmerman M, Ganapathy US, Dartois V, Gengenbacher M, Dick T. 2019. Gut microbiota metabolite indole propionic acid targets tryptophan biosynthesis in Mycobacterium tuberculosis. mBio 10:e02781-18. https://doi.org/10.1128/mBio.02781-18.
37. Ganapathy US, Lan T, Krastel P, Lindman M, Zimmerman MD, Ho HP, Sarathy JP, Evans JC, Dartois V, Aldrich CC, Dick T. 2021. Blocking bacterial naphthohydroquinone oxidation and ADP ribosylation improves activity of rifamycins against mycobacterium abscessus. Antimicrob Agents Chemother 65:e00978-21. https://doi.org/10.1128/AAC.00978-21.
38. Pettersen EF, Goddard TD, Huang CC, Couch GS, Greenblatt DM, Meng EC, Ferrin TE. 2004. UCSF Chimera—a visualization system for exploratory research and analysis. J Comput Chem 25:1605–1612. https://doi.org/10.1002/jcc.20084.
39. Baek M, DiMaio F, Anishchenko I, Dauparas J, Ovchinnikov S, Lee GR, Wang J, Cong Q, Kinch LN, Schaeffer RD, Millán C, Park H, Adams C, Glassman CR, DeGiovanni A, Pereira JH, Rodrigues AV, van Dijk AA, Ebrecht AC, Opperman DJ, Sagmeister T, Buhlheller C, Pavkov-Keller T, Rathinaswamy MK, Dalwadi U, Yip CK, Burke JE, Garcia KC, Grishin NV, Adams PD, Read RJ, Baker D. 2021. Accurate prediction of protein structures and interactions using a three-track neural network. Science 373:871–876. https://doi.org/10.1126/science.abj8754.

## 3.3 Publication II

### Synthesis and Characterization of Phenylalanine Amides Active against *Mycobacterium abscessus* and Other Mycobacteria

Markus Lang, Uday S. Ganapathy, Lea Mann, Rana Abdelaziz, Rüdiger W. Seidel, Richard Goddard, Ilaria Sequenzia, Sophie Hoenke, Philipp Schulze, Wassihun Wedajo Aragaw, René Csuk, Thomas Dick, Adrian Richter.

Reprinted with permission from ACS Journal of Medicinal Chemistry, Lang *et al.*, Synthesis and Characterization of Phenylalanine Amides Active against *Mycobacterium abscessus* and Other Mycobacteria, J Med Chem 66:5079–5098,
 DOI: 10.1021/acs.jmedchem.3c00009

**Summary**

This paper describes the synthesis and characterisation of derivatives of the hit substance MMV688845. Within the synthetic part of the publication, X-ray crystallographic molecular structures are presented. In addition, the synthesis and docking pose of the structures on the RNAP of *M. tuberculosis* are discussed. The water solubility (kinetic solubility) and lipophilicity (LogP values) of the derivatives were determined. All 25 derivatives were characterised in the MIC assay against *M. abscessus*, *M. intracellulare*, *M. smegmatis* and *M. tuberculosis* using different media and the macrophage infection assay (for *M. abscessus*). The MBC against *M. abscessus* was determined for selected derivatives. The minimum inhibitory concentration against *M. abscessus* was improved to 0.78 µM, the MBC values of the selected derivatives were improved compared to the lead compound. The compounds were further tested for cytotoxicity against various mammalian cell lines. In addition, pharmacokinetic studies in the form of *in vitro* plasma and microsomal stability are presented for the derivatives.

**Own contribution:**

Writing, review & editing, visualization, methodology, investigation and data curation.

This paper was chosen as the second publication to contribute to this work. This was on the grounds that the microbiological work on which the paper is based was done by myself. The experimental contributions were as follows: Characterisation of the compounds against *M. abscessus* ATCC 19977, *M. smegmatis*, *M. intracellulare*, against *M. abscessus* in the macrophage infection model and determination of the MBC against *M. abscessus.*

Journal of Medicinal Chemistry

pubs.acs.org/jmc Article

# Synthesis and Characterization of Phenylalanine Amides Active against *Mycobacterium abscessus* and Other Mycobacteria

Markus Lang, Uday S. Ganapathy, Lea Mann, Rana Abdelaziz, Rüdiger W. Seidel, Richard Goddard, Ilaria Sequenzia, Sophie Hoenke, Philipp Schulze, Wassihun Wedajo Aragaw, René Csuk, Thomas Dick, and Adrian Richter*

Cite This: *J. Med. Chem.* 2023, 66, 5079−5098 Read Online

ACCESS | Metrics & More | Article Recommendations | Supporting Information

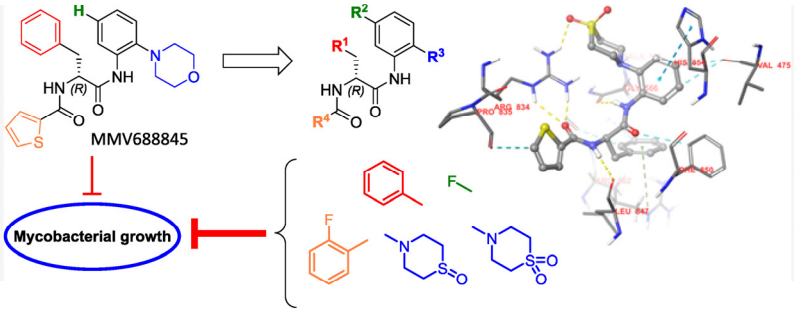


**ABSTRACT:** *Nα*-2-thiophenoyl-D-phenylalanine-2-morpholinoanilide [MMV688845, Pathogen Box; Medicines for Malaria Venture; IUPAC: (2*R*)-*N*-(1-((2-morpholinophenyl)amino)-1-oxo-3-phenylpropan-2-yl)thiophene-2-carboxamide)] is a hit compound, which shows activity against *Mycobacterium abscessus* ($MIC_{90}$ 6.25−12.5 μM) and other mycobacteria. This work describes derivatization of MMV688845 by introducing a thiomorpholine moiety and the preparation of the corresponding sulfones and sulfoxides. The molecular structures of three analogs are confirmed by X-ray crystallography. Conservation of the essential *R* configuration during synthesis is proven by chiral HPLC for an exemplary compound. All analogs were characterized in a MIC assay against *M. abscessus*, *Mycobacterium intracellulare*, *Mycobacterium smegmatis*, and *Mycobacterium tuberculosis*. The sulfone derivatives exhibit lower $MIC_{90}$ values (*M. abscessus*: 0.78 μM), and the sulfoxides show higher aqueous solubility than the hit compound. The most potent derivatives possess bactericidal activity (99% inactivation of *M. abscessus* at 12.5 μM), while they are not cytotoxic against mammalian cell lines.

## 1. INTRODUCTION

Infections with mycobacteria are difficult to treat, as they often require prolonged antibiotic therapy, which can be accompanied by severe side effects. Whereas drug-susceptible tuberculosis can usually be treated successfully within six months,[1−4] the therapy of infections with multidrug-resistant (MDR) *Mycobacterium tuberculosis* (*Mtb*) strains and nontuberculous mycobacteria (NTM)[5,6] is protracted and cure rates are often low (25−58% for *Mycobacterium abscessus*[7,8] (*Mabs*) infections[9−11]). For infections with MDR *Mtb*, progress has already been made in recent years. Research efforts have led to the approval of two new drugs: bedaquiline and pretomanid.[12−14] Bedaquiline acts by inhibiting mycobacterial ATP synthase, while pretomanid has a rather complex mechanism of action. Under normoxic conditions, pretomanid is converted into reactive intermediates that interfere with mycolic acid synthesis, while in anaerobic environments, it acts as an NO donor that effectively poisons the respiration of mycobacteria.[15,16] By combining bedaquiline, pretomanid, and linezolid, a new therapeutic regimen for treatment of MDR tuberculosis has been established.[17]

NTM have come into scientific focus in recent years, owing to the fast-growing, multidrug-resistant *Mabs* and the *Mycobacterium avium* complex (MAC), which have emerged as problematic opportunistic pathogens.[18−21] They possess numerous intrinsic resistance mechanisms, which render classical antitubercular drugs and many other common antibiotics ineffective.

Currently, the RNA polymerase (RNAP) inhibitor rifampicin (RIF) is a cornerstone of antimycobacterial therapy. As a result,

Received: January 2, 2023
Published: March 31, 2023





https://doi.org/10.1021/acs.jmedchem.3c00009
*J. Med. Chem.* 2023, 66, 5079−5098

mycobacteria with acquired or intrinsic resistance to rifamycins, e.g., MDR *Mtb* or *Mabs*, are a particular threat. Mycobacteria use different mechanisms to counteract the effect of RIF. In *Mtb*, 95% of the resistant strains possess acquired mutations in the target of RIF, the $\beta'$ subunit of the RNAP. Less frequently, the expression of efflux pumps influences RIF resistance.[22] In contrast, RIF resistance in *Mabs* is caused by other mechanisms. *Mabs* has the ability to covalently modify RIF through the enzyme ADP ribosylase[23] and thereby inactivate it. In addition, naphthohydroquinone oxidation increases resistance.[24] Certain rifamycins, such as rifabutin, are less susceptible to these mechanisms of resistance, which is reflected in improved efficacy *in vitro* and *in vivo*.[25,26] Recent advances in rifamycin research made it possible to completely block ADP-ribosylation while retaining its antimycobacterial activity. The redesign of the C25-*O*-acyl position was crucial for these improvements of the rifamycin structures.[27,28]

Despite the promising attributes of rifabutin, a synthetic RNAP inhibitor that exhibits no cross-resistance with rifamycins is of interest for antimycobacterial drug development. The *Nα*-aroyl-*N*-aryl-phenylalanine amide (AAP) MMV688845 (*Nα*-2-thiophenoyl-D-phenylalanine-2-morpholinoanilide), discovered as an anti-*Mtb* hit,[29] has been shown to be active against *Mabs* (ATCC19977) by screening of the Pathogen Box library[30] (Medicines for Malaria Ventures, MMV). Analogs of MMV688845 have been shown to be inhibitors of *Mtb* RNAP that bind to the $\beta$ and $\beta'$ subunits but address a different binding site than rifamycins.[31] In addition, derivatives of MMV688845 are described in a patent,[32] although these were not investigated against NTM including *Mabs*. Based on the promising screening experiments, we have developed a synthesis for MMV688845, yielding the active enantiomer with *ee*-values of >99% and investigated its stereospecific activity against *Mabs*, as well as its cytotoxicity.[33] In parallel, the RNAP was validated as target in *Mabs*, and a detailed *in vitro* profiling of the hit compound was performed.[34] Motivated by these encouraging results, a series of MMV688845 derivatives was synthesized with the aim of increasing *in vitro* activity against NTM, improving physicochemical properties such as solubility and getting a first insight into *in vitro* metabolism properties of this compound class.

## 2. RESULTS AND DISCUSSION

**2.1. Docking Studies.** To explore which structural alternations of the hit molecule MMV688845 may be favourable for target binding, a molecular docking was conducted based on the published crystallographic structure of *Mtb* RNAP (PDB code: 5UHE). We used the X-ray structure of the crystallized protein with the model compound D-AAP1 as a reference for our modeling approaches.[31] The chemical diagrams of both substances are given in Scheme 1.

**Scheme 1. Structures of the Hit Compound MMV688845 and D-AAP1**

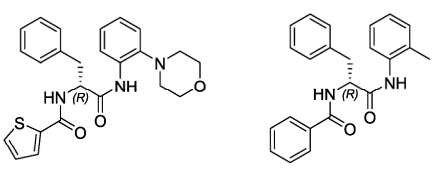


MMV688845 D-AAP1

According to Lin et al., D-AAP1 offers space for six additional nonhydrogen atoms at the position of the methyl group, while it is coordinated to its target enzyme, offering potential for structure-based hit to lead optimization.[31] In MMV688845, the methyl group is replaced by a morpholine ring, introducing five additional nonhydrogen atoms while retaining activity.[30] The docking study of MMV688845 and $RNAP_{Mtb}$ (Figure 1A) indicates a hydrogen bond between the morpholine oxygen atom and arginine residue R834 of the $\beta'$ subunit. Motivated by this finding, we were eager to find other hydrogen bond acceptor groups, which exploit the potential additional hydrogen bond for drug−target interactions and possibly lead to different physiochemical properties.

As the results of Lin et al. suggest only limited space for derivatization (five of the six proposed nonhydrogen atoms are already part of MMV688845), we chose to investigate structures that offer the desired properties while keeping the size of the relevant part of the molecule almost unchanged with only one or two additional atom(s). Our docking studies indicate that substitution of the morpholine part with a thiomorpholine and its respective oxidation products (sulfoxide and sulfone) will lead to a similar binding mode as observed for MMV688845. Figure 1B,C depicts the modeled complexes with MMV688845 derivatives containing sulfone and sulfoxide groups. The modeling data suggest that the oxygen atom(s) of the sulfone or sulfoxide can act as hydrogen bond acceptors for R834, whereas clashes with the target protein could not be observed. A superimposed visualization of D-AAP1 and substance **20** can be found in the Supporting Information (Figure S1).

In addition, our docking experiments revealed that a *p*-hydroxy group of a tyrosine analog of MMV688845 is positioned to form an additional hydrogen bond to the backbone of the target protein at P477 (Figure 1D) without any calculated clashes.

To check whether the proposed binding modes also have relevance in the RNAP of *Mabs*, a protein−protein BLAST (Basic Local Alignment Search Tool) was used to align and compare the *Mtb* $\beta$ and $\beta'$ RNAP subunits with their respective relatives in *Mabs*. The sequence homology was found to be 90.4% for the $\beta$ subunits and 89.9% for the $\beta'$ subunits, while the amino acids that are relevant for drug−target interaction in *Mtb* RNAP are highly conserved (only exception: A563 in *Mtb* to G512 in *Mabs*, a list of the relevant amino acids can be found in the Supporting Information, Table S1), making a similar binding mode in *Mabs* RNAP probable.

**2.2. Synthesis.** The objective of the synthetic work described in this study is the derivatization of MMV688845. For this purpose, a synthetic route based on a published synthesis of the hit compound[33] was designed. Starting from Boc-protected amino acids, the preparation of analogs is possible in three steps, as shown in Scheme 2. This modified synthetic route allows targeted derivatization of MMV688845 without racemization of the amino acid stereocenter.

In the first step (general procedure A), an amide bond is synthesized using the phosphonic acid anhydride T3P in a mixture of EtOAc and pyridine,[35] followed by removal of the Boc-protecting group using TFA. The second amide bond in the molecule is formed using the coupling reagent DEPBT,[36] for which the amine is reacted with an aromatic carboxylic acid.

The synthesis and modification of aniline building blocks were crucial for the desired derivatization, for which the 2-morpholinoaniline in MMV688845 was the starting point. Using the syntheses shown in Scheme 3, thiomorpholine and its



https://doi.org/10.1021/acs.jmedchem.3c00009
J. Med. Chem. 2023, 66, 5079−5098

Journal of Medicinal Chemistry pubs.acs.org/jmc Article

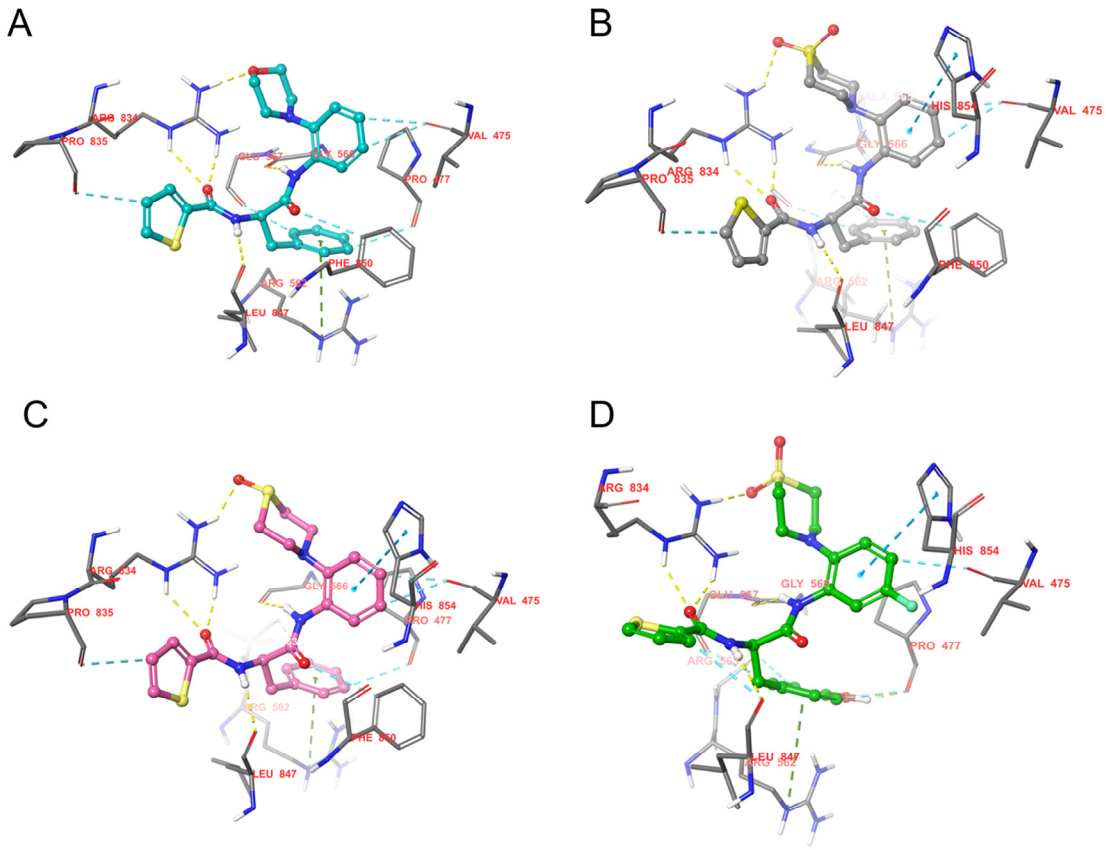


**Figure 1.** Docking poses of MMV688845 (A), compound **20** (B), compound **14** (C) and the $\beta$ and $\beta'$ subunits of $RNAP_{Mtb}$, and compound **39** after exchange of phenylalanine for tyrosine (D). Hydrogen bonds are displayed as yellow dashed lines. 2D visualizations of the shown interactions can be found in the Supporting Information (Figure S2). Visualization generated with the Maestro graphical interface (Schrödinger Release 2022-3: Maestro, Schrödinger, LLC, New York, NY, 2021).

**Scheme 2. Synthetic Pathway for Derivatization of MMV688845 Analogues (T3P: Propanephosphonic Acid Anhydride, TFA: Trifluoroacetic Acid, DEPBT: 3-(Diethoxyphosphoryloxy)-1,2,3-benzotriazin-4(3*H*)-one, DIPEA: *N*,*N*-Diisopropylethylamine)**

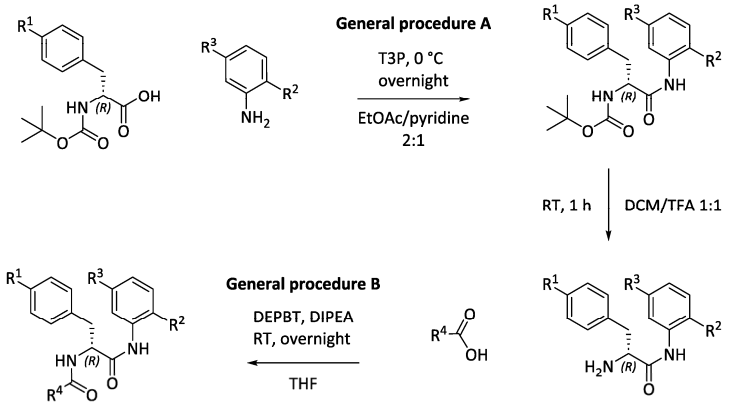


oxidation products, i.e., sulfone and sulfoxide, were introduced as substituents for derivatization. The introduction of thiomorpholine was achieved by a nucleophilic substitution on 2-bromonitrobenzene (general procedure C) and subsequent reduction of the nitro group by hydrazine (general procedure D). In the case of **21**, we tried to couple commercially available thiomorpholine dioxide to 1-bromo-2-nitrobenzene to avoid the use of oxidizing agents completely, because oxidization could



https://doi.org/10.1021/acs.jmedchem.3c00009
J. Med. Chem. 2023, 66, 5079−5098

Scheme 3. Preparation of the Aniline Building Block (BINAP: 2,2′-Bis(diphenylphosphino)-1,1′-binaphthyl; TFA: Trifluoroacetic Acid)

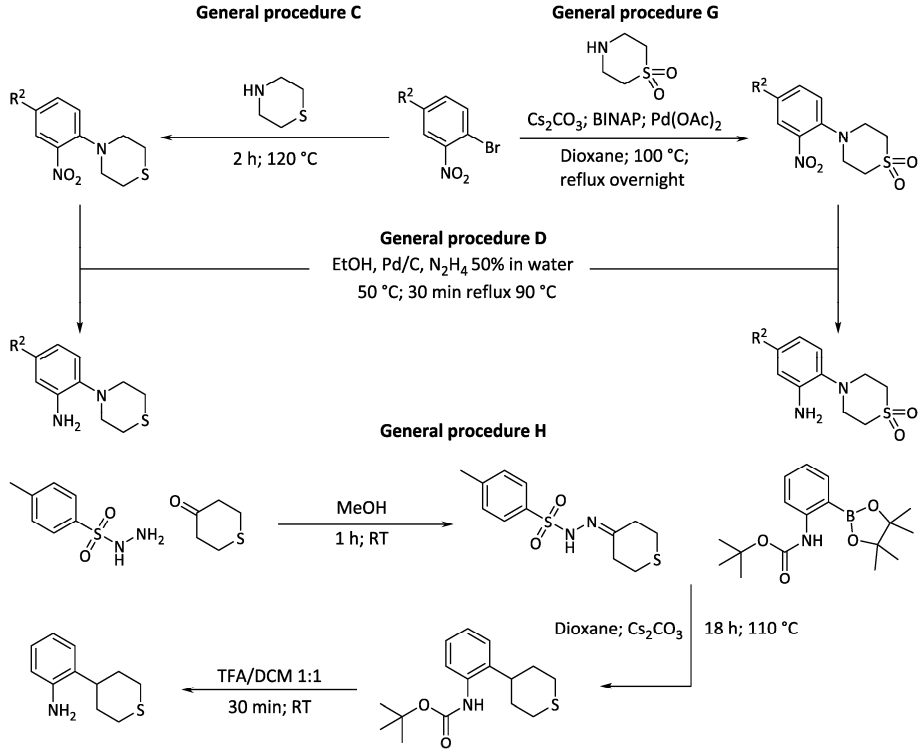


Scheme 4. Synthesis of Thiomorpholine Sulfoxides and Sulfones (m-CPBA: *meta*-Chloroperoxybenzoic Acid)

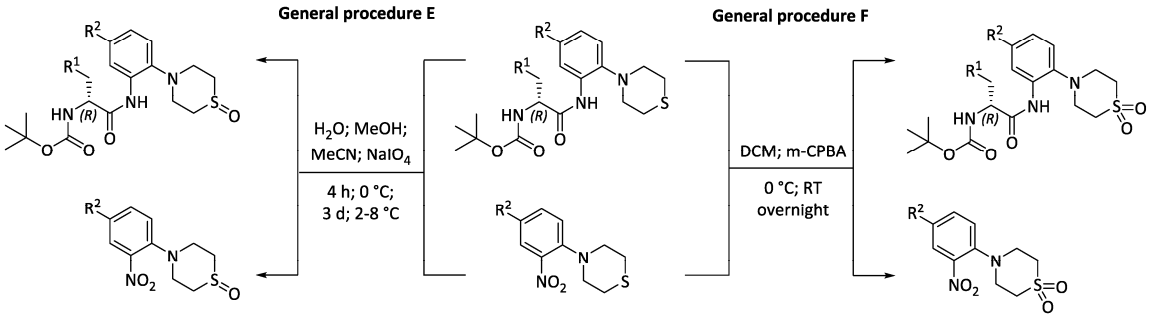


also occur at the aniline nitrogen atom to form its *N*-oxide. General procedure C did not yield the desired product in this case. A reason for this could be the electron-withdrawing effect of the two oxygen atoms, which makes the nitrogen of thiomorpholine dioxide less nucleophilic preventing the substitution. A BINAP and transition metal-aided coupling was investigated, which produced the desired aniline in a yield of 32%. Thus, we eventually decided against this latter approach as it is more expensive and less efficient than the nucleophilic substitution approach.[37]

For the synthesis of 2-(tetrahydro-2*H*-thiopyran-4-yl) anilines, a different synthetic strategy was necessary (general procedure H in Scheme 3). The desired derivatives were prepared by C-C coupling of 4-oxothiane and Boc-2-amino-phenylboronic acid pinacol ester.[38] For this synthetic method, 4-oxothiane was transformed to a sulfonylhydrazone using tosylhydrazide. In the subsequent step, the C-C coupling was carried out by reaction of the sulfonylhydrazone with the boronic acid pinacol ester in the presence of $Cs_2CO_3$. The final Boc cleavage was performed in TFA/DCM. Barluenga et al. postulated that the tosylhydrazones formed like that decompose thermally forming a diazo intermediate (Bamford−Stevens reaction), which reacts with the boronic acid or its ester.[39]

The oxidation of the thioether moiety was carried out according to general procedures E and F as shown in Scheme 4. By using different oxidizing agents, sulfone and sulfoxides were selectively obtained. The oxidation was conducted on the products of general procedure A or on the substituted nitro



https://doi.org/10.1021/acs.jmedchem.3c00009
J. Med. Chem. 2023, 66, 5079−5098

building blocks. Starting from the thiomorpholine derivatives, sulfoxides were prepared using $NaIO_4$, while the analogous sulfones were obtained by oxidation with *m*-CPBA. The molecular structures of the oxidation products were unambiguously determined by X-ray crystallography, as described below. Oxidizing the sulfur in the 4-(4-$R^2$-2-nitro-phenyl)-thiomorpholine intermediates is an alternative way to achieve oxidation (for example, see synthesis of **47** (sulfoxide) or **25** (sulfone)). S-Oxidation of the nitro building block has the disadvantage that the more polar groups (especially the sulfoxides) are present in subsequent synthetic steps, which complicates purification of the products by normal phase column chromatography. S-Oxidation after the final coupling step has not been investigated since the thiophene groups are also prone to oxidation.[40]

*2.2.2. Stereochemical Evaluation of the Synthetic Pathway.* It is known that only the *R* enantiomer of MMV688845 shows activity against *Mabs*, whereas the *S* enantiomer is inactive.[31,33] The synthetic procedure described by Ebright et al.[32] required preparative chiral HPLC separation of the enantiomers in the racemic mixture of the final compounds. To avoid the necessity of enantiomer separation, an important goal in the design of the synthesis was to start with reactants containing the required *R* configuration and preserve that configuration throughout the synthesis. Boc-protected (*R*)-phenylalanine is a readily available and inexpensive starting material for most compounds. In our previous study, we made important steps toward the realization of this goal.[33] To determine the stereochemistry of the reactions, (*R*)-MMV688845, (*S*)-MMV688845, and (*rac*)-MMV688845 were synthesized starting from the (*R*)-, (*S*)-, or (*rac*)-phenylalanine using the new synthetic procedure.

Although phenylalanine is not known for its susceptibility to racemization, like e.g., phenylglycine containing peptides,[41] literature shows that phenylalanine racemization can occur even in relatively mild amidation procedures.[33,42−45] To achieve mild reaction conditions, we adapted the T3P (*n*-propanephosphonic acid anhydride[46]) coupling method published by Dunetz et al.[35] The authors showed that a mixture of EtOAc and pyridine at 0 °C yielded the lowest degree of racemization. Another advantage of T3P is that the side products formed in the coupling reactions are water-soluble and hence can be readily separated by extraction during work up. The intermediate and final compounds were analyzed by chiral HPLC (see the Supporting Information). The *ee*-values are listed in Table 1.

All products that were synthesized from enantiopure Boc-phenylalanine derivatives showed *ee*-values higher than 99% indicating that virtually no racemization occurs under the reaction conditions used. Specific optical rotations have been determined for the compounds in Table 1 and can be found in the Supporting Information.

**Table 1. *ee*-Values of the Starting Materials (Boc-Protected Amino Acids), the Intermediates 1-(*R*), 1-(*S*), and 1-(*rac*) Being the Intermediates after Anilide Formation; 2A-(*R*), 2A-(*S*), and 2A-(*rac*) Being the Boc-Deprotected Intermediate and Final Compounds 2B-(*R*), 2B-(*S*), and 2B-(*rac*) during a Synthetic Route**

| | *ee*-value [%] | | | |
|---|---|---|---|---|
| substance | Boc-Phe- | 1- | 2A- | 2B- |
| (*R*) | 99.82 | 99.80 | 99.92 | 99.70 |
| (*S*) | 100.00 | 99.34 | 99.84 | 99.79 |
| (*rac*) | 0.24 | 0.64 | 0.47 | 0.06 |

*2.2.3. Structural Elucidation.* To prove that oxidation indeed occurred at the *S* atom of the thiomorpholine moiety only, an X-ray crystal structure analysis was conducted on a selection of compounds, viz. **6**, **14**, and **20**, because the formation of thiomorpholine *N*-oxide is also conceivable under the conditions used.[47] We recently described the crystal and molecular structure of racemic MMV688845 (CSD refcode: BALNUB),[33] while the investigated compound set for this study represents the direct thiomorpholine analog of MMV688845 **6**, its sulfoxide derivative **14** and its sulfone derivative **20**.

We obtained colorless crystals of enantiopure **6** and **20** suitable for X-ray diffraction from a chloroform/heptane solvent system. Interestingly, two crystallographically independent homochiral molecules of **6** (Figure 2A) form a hydrogen-bonded dimer about a *pseudo* center of symmetry in the reported crystal structure (triclinic system, space group *P*1) analogous to the crystallographic center of symmetry observed for racemic MMV688845 (monoclinic system, space group $P2_1/n$). The crystal structure of **20** is isomorphous with that of **6**.

The corresponding sulfoxide **14** crystallized as a sesquihydrate from aqueous methanol. The homochiral molecules likewise constitute a hydrogen-bonded dimer through N−H···O hydrogen bonds formed between the phenylalanine amide moieties. The dimer is, however, not *pseudo* centrosymmetric as in **6** and **20** but exhibits a crystallographic 2-fold rotation axis (monoclinic system, space group *I*2). N−H···O hydrogen bond parameters within dimers in are essentially comparable in **6**, **20**, and **14** (see the Supporting Information).

Bearing in mind that single-crystal X-ray diffraction does not prove the homogeneity of the bulk material, the molecular structures and absolute configurations of the sulfone **20** (Figure 2B) and the sulfoxide **14** (Figure 2C) were also confirmed by X-ray crystallography, indicating oxidation of the sulfur atom in the isolated products without formation of thiomorpholine *N*-oxides.

**2.3. Microbiology.** *2.3.1. In Vitro Activity Determination against NTM and Mtb.* The *in vitro* activity of MMV688845 analogs described in this study was determined as $MIC_{90}$ against a panel of NTM (*Mabs*, *Mycobacterium intracellulare* and *Mycobacterium smegmatis*) and *Mtb*—the most prevalent mycobacterial pathogen worldwide. The mycobacteria were selected to ensure comparability of our data (where applicable) to other publications,[31,33,50,51] for their clinical relevance[52] in both pulmonary[53] and extrapulmonary[54] clinical presentations, and in view of the severity and treatability[55] of the infections.

Since *Mabs* has become a serious problem in the clinic,[19] we particularly focused on this species. The activity was therefore analyzed against two different *Mabs* strains, namely, the reference strain ATCC 19977 and clinical isolate *Mabs* Bamboo. To assess possible effects of the growth medium on the *in vitro* activity, the assays were performed in both Middlebrook 7H9 and cation-adjusted Mueller-Hinton II broth medium (MHII).

As *Mabs* is capable of infecting human macrophages and actively proliferates intracellularly by evading certain immune defense mechanisms,[55] activity was also determined in a fluorescence based macrophage infection assay[59] (for detailed method description, see the Supporting Information).

*M. intracellulare* ATCC 35761 (*Mintra*) was chosen to represent the clinically relevant *M. avium* complex (MAC).[56] Studies in the United States have shown that MAC is the most



https://doi.org/10.1021/acs.jmedchem.3c00009
J. Med. Chem. 2023, 66, 5079−5098

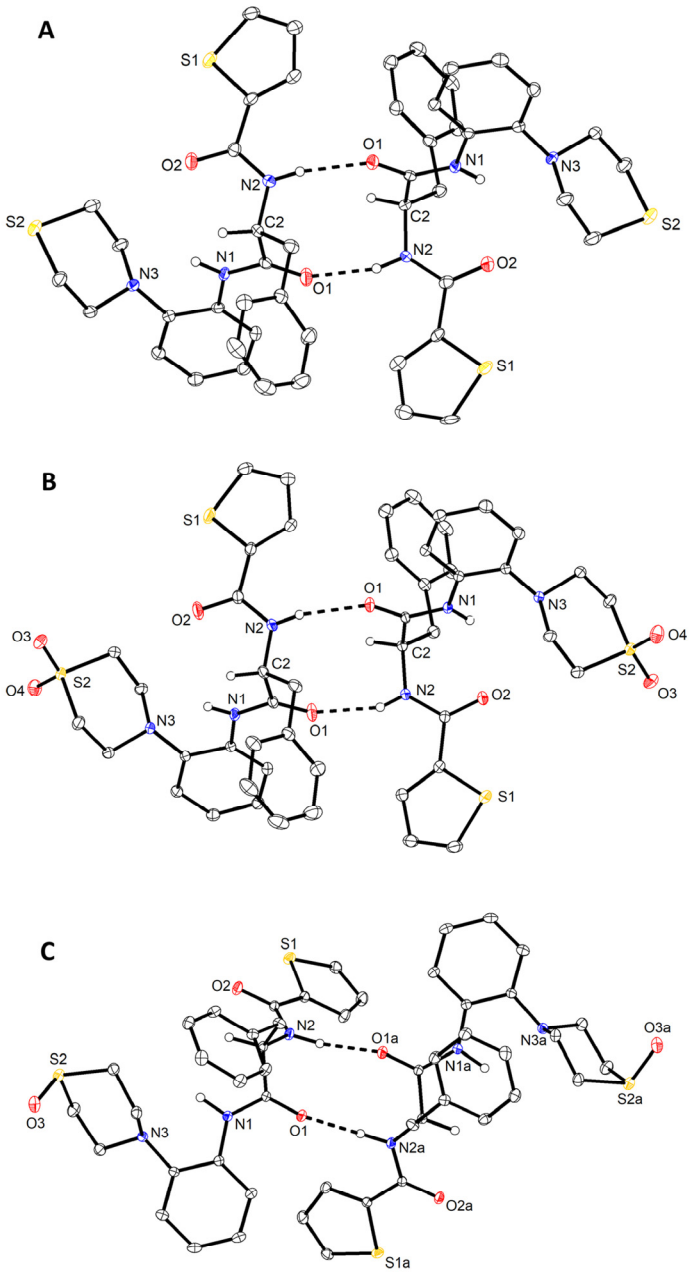


**Figure 2.** Molecular structures of **6** (A), **20** (B), and **14** (C), as determined by X-ray crystallography. Displacement ellipsoids are drawn at the 50% probability level. Hydrogen atoms on nitrogen and the chirality center are represented by small spheres of arbitrary radius otherwise omitted for clarity. Dashed lines represent N−H···O hydrogen bonds. Minor positional disorder of thiophene rings (ca. 6%) in **6** (A) and **20** (B) is also not shown for the sake of clarity. Solvent water in the crystal structure of **14** (C)· 1.5 $H_2O$ is not shown (suffix a denotes symmetry-related atoms). The structure of **14** (C) was refined with aspherical atomic scattering factors using NoSpherA2.[48,49]

frequently isolated NTM in both pulmonary lung disease[53] and extrapulmonary infections.[57]

*M. smegmatis* (*Msmeg*) is a fast-growing mycobacterium generally considered nonpathogenic and often used as a surrogate organism for *Mtb*.[50,51] To demonstrate a broad spectrum of activity against fast-growing mycobacteria and to analyze species-dependent differences in efficacy, *M. smegmatis* $mc^2$ 155 was included in the selection of mycobacteria. We report the results of broth microdilution $MIC_{90}$ assays for each substance in Table 2.

Optical density-derived and RFP-fluorescence-derived $MIC_{90}$ values were similar. Although OD measurement is a well-



https://doi.org/10.1021/acs.jmedchem.3c00009
J. Med. Chem. 2023, 66, 5079−5098

**Table 2. Antimycobacterial Activity of MMV688845 (abbr. MMV845) Derivatives[a]**

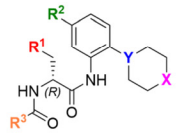

| | | | | | MIC$_{90}$ | | | | | MIC$_{50}$ | MIC$_{90}$ | MIC$_{50}$ | MIC$_{90}$ |
|---|---|---|---|---|---|---|---|---|---|---|---|---|---|
| | | | | | *Msmeg* mc$^2$ 155[B] | *Mtb* H37Rv[C] | *Mabs ATCC19977*[B] | *Mabs* ATCC19977[B] | *Mintra* ATCC 35761[B] | *Mabs* Bamboo[D] | | *Mabs* ATCC 19977 + THP1[E] | |
| | | | | | 7H9 | 7H9 | 7H9 | MHII | 7H9 | 7H9 | | RPMI | |
| | R$^1$ | R$^2$ | X, Y | R$^3$ | RFP | OD | RFP | RFP | RFP | OD | OD | RFP | RFP |
| **MMV845** | Phenyl | H | O, N | 2-Thiophenyl | 0.78 | 0.78 | 6.25 | 12.5 | 0.78 | 1.7 | 4.4 | 1.56 | 12.5 |
| **6** | Phenyl | H | S, N | 2-Thiophenyl | 3.13 | 6.25 | 12.5 | 50 | 0.78 | 2.5 | 14 | 12.5 | > 100 |
| **7** | Phenyl | H | S, N | 2-Fluorophenyl | 3.13 | 6.25 | 12.5 | 50 | 0.78 | 3 | 18 | 12.5 | > 100 |
| **11** | Phenyl | F | S, N | 2-Thiophenyl | 3.13 | 1.56 | 25 | 50 | 0.78 | 1.4 | 14 | 3.13 | > 100 |
| **12** | Phenyl | F | S, N | 2-Fluorophenyl | 6.25 | 1.56 | 25 | 25 | 0.78 | 1.15 | 12 | 3.13 | 100 |
| **14** | Phenyl | H | S=O, N | 2-Thiophenyl | 1.56 | 0.4 | 3.13 | 6.25 | 0.1 | 0.33 | 2 | 3.13 | 25 |
| **15** | Phenyl | H | S=O, N | 2-Fluorophenyl | 0.78 | 0.78 | 6.25 | 3.13 | 0.1 | 0.4 | 2.1 | 0.78 | 12.5 |
| **17** | Phenyl | F | S=O, N | 2-Thiophenyl | 1.56 | 0.4 | 1.56 | 3.13 | 0.05 | 0.28 | 1.9 | 0.78 | 25 |
| **18** | Phenyl | F | S=O, N | 2-Fluorophenyl | 1.56 | 0.78 | 3.31 | 3.13 | 0.2 | 0.52 | 2 | 0.39 | 12.5 |
| **20** | Phenyl | H | O=S=O, N | 2-Thiophenyl | 1.56 | 0.2 | 3.13 | 3.13 | 0.1 | 0.24 | 1.7 | 0.78 | 6.25 |
| **24** | Phenyl | H | O=S=O, N | 2-Fluorophenyl | 0.78 | 0.2 | 0.78 | 1.56 | 0.05 | 0.23 | 4.3 | 0.39 | 6.25 |
| **28** | Phenyl | F | O=S=O, N | 2-Thiophenyl | 1.56 | 0.78 | 6.25 | 3.13 | 0.2 | 0.43 | 6.5 | 0.39 | 3.13 |
| **29** | Phenyl | F | O=S=O, N | 2-Fluorophenyl | 1.56 | 0.78 | 3.13 | 3.13 | 0.1 | 0.4 | 4.5 | 0.39 | 3.13 |
| **32** | Phenyl | H | S, CH | 2-Thiophenyl | 6.25 | > 25 | 50 | 100 | 6.25 | 21 | 44 | > 100 | > 100 |
| **34** | Phenyl | H | S=O, CH | 2-Thiophenyl | 6.25 | > 25 | 25 | 50 | 3.13 | 6 | 20 | > 100 | > 100 |
| **36** | *p*-Hydroxyphenyl | F | S, N | 2-Thiophenyl | 12.5 | 0.78 | 12.5 | 50 | 0.1 | 1.6 | 15 | 12.5 | 50 |
| **37** | *p*-Hydroxyphenyl | F | S, N | 2-Fluorophenyl | 6.25 | 1.56 | 25 | 50 | 0.2 | 1.7 | 15 | 6.25 | 25 |
| **39** | *p*-Hydroxyphenyl | F | O=S=O, N | 2-Thiophenyl | 6.25 | 0.78 | 6.25 | 3.13 | 0.05 | 0.4 | 9 | 6.25 | 25 |
| **40** | *p*-Hydroxyphenyl | F | O=S=O, N | 2-Fluorophenyl | 6.25 | 0.78 | 6.25 | 6.25 | 0.2 | 1.1 | 13 | 3.13 | 25 |
| **42** | 3-Thiophenyl | H | O, N | 2-Thiophenyl | 1.56 | 3.13 | 12.5 | 12.5 | 1.56 | 2.3 | 7 | 12.5 | 50 |
| **43** | 3-Thiophenyl | H | O, N | 2-Fluorophenyl | 1.56 | 3.13 | 12.5 | 12.5 | 0.78 | 1.9 | 7 | 6.25 | 25 |
| **45** | 2-Thiophenyl | H | O, N | 2-Thiophenyl | 1.56 | 6.25 | 12.5 | 12.5 | 1.56 | 2.4 | 9 | 12.5 | > 100 |
| **46** | 2-Thiophenyl | H | O, N | 2-Fluorophenyl | 1.56 | 3.13 | 6.25 | 12.5 | 0.78 | 2 | 7 | 6.25 | 25 |
| **50** | 3-Thiophenyl | H | S=O, N | 2-Thiophenyl | 3.13 | 6.25 | 6.25 | 12.5 | 0.2 | 3.4 | 15 | 12.5 | 100 |
| **51** | 3-Thiophenyl | H | S=O, N | 2-Fluorophenyl | 1.56 | 3.13 | 6.25 | 12.5 | 0.2 | 1.5 | 4.4 | 6.25 | 50 |
| **53** | 2-Thiophenyl | H | S=O, N | 2-Thiophenyl | 3.13 | 3.13 | 12.5 | 12.5 | 0.2 | 1.3 | 5.8 | 12.5 | 100 |
| **54** | 2-Thiophenyl | H | S=O, N | 2-Fluorophenyl | 1.56 | 1.56 | 6.25 | 12.5 | 0.2 | 1.8 | 6.5 | 6.25 | 50 |

[a]Color coding: For each tested mycobacterial strain, the colors show the difference to the average activity value, dark green: lowest MIC value; light green: below average; white: closest to average; light red: above average, dark red: highest MIC value. For detailed information on the methodology of the assays, see the Supporting Information. [b]Incubated for three days at 37 °C (*Msmeg* and *Mabs*) or five days (*Mintra*). Performed in duplicate, results were averaged. Data were obtained via RFP measurement (shown here) or OD measurement (see the Supporting Information). [c]Incubated for seven days at 37 °C. Data were obtained via OD measurement. Performed in duplicate, results were averaged. [d]Incubated for three days at 37 °C. Data were obtained via OD measurement. Performed in duplicate, results were averaged. [e]Infected cells were incubated for four days (37 °C, 5% $CO_2$). Performed in duplicate, results were averaged.

established method to analyze bacterial growth, RFP assay data often offer higher sensitivity and specificity.[58,59] Nevertheless, in our case, the OD and RFP values correlate well and the MIC$_{90}$ values of the reference compound do not differ substantially.

The MIC$_{90}$ values for MMV688845 determined in this study are consistent with values found in the literature. Low et al. determined a MIC$_{90}$ value against *Mabs* of 7 $\mu$M, and we found 6.25 $\mu$M in Middlebrook 7H9 medium. To investigate culture media independency, the growth inhibitory effect was analyzed in MHII and a MIC$_{90}$ value of 12.5 $\mu$M was determined indicating culture medium independency. The MIC$_{90}$ value we determined against *Mtb* is slightly lower (0.78 $\mu$M) than that of Low et al. (1.2 $\mu$M).

Derivatization of the parent compound MMV688845 was performed at the residues R$^1$−R$^4$ as shown in Scheme 5.

**Scheme 5. AAP Base Scaffold and Derivatized Residues**

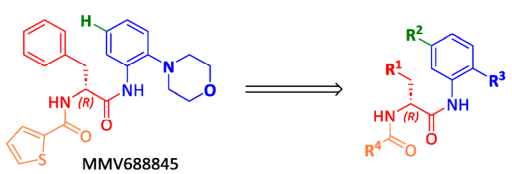


First, we compared analogs that only differ at the R$^1$ substitution site. Figure 3 gives an overview. Four different moieties for R$^1$ (phenyl, *p*-hydroxyphenyl, 2-thiophenyl, 3-thiophenyl) were included in our study. As a patent by Ebright et al. reveals,[32] MIC$_{90}$ values are particularly sensitive to changes at the R$^1$ position. The most active compounds against *Mtb* and *M. avium* that were synthetized have a phenyl group in position R$^1$. *p*-Hydroxyphenyl groups and their respective acetyl or benzoic acid esters substitutions at R$^1$ were also investigated in this patent and resulted in a loss in activity against both *Mtb* and *M. avium*. The other variations in R$^1$ that are shown (e.g., *m*-hydroxyphenyl) resulted in severe activity loss.[32] Bearing this in mind, we decided to include both phenyl and *p*-hydroxyphenyl substituents for derivatization and screening. Despite knowing that even minor changes result in activity loss, 2- and 3-thiophenyl substituents were included because these structures are bioisosteric to phenyl[60] and therefore offer a hopefully tolerable change to the molecule without activity loss.

For *Mabs*, no differences in activities can be seen, but there is a trend that phenyl groups perform better than *p*-Hydroxyphenyl, e.g., **29** has a 2-fold increased activity compared to **40**. The same trend can also be seen in *Mabs* Bamboo. It is remarkable that the difference becomes more pronounced when looking at the MIC$_{90}$ values determined in the macrophage infection model assay. In this case, the compounds suffer from a 4-to-8-fold



https://doi.org/10.1021/acs.jmedchem.3c00009
J. Med. Chem. 2023, 66, 5079−5098

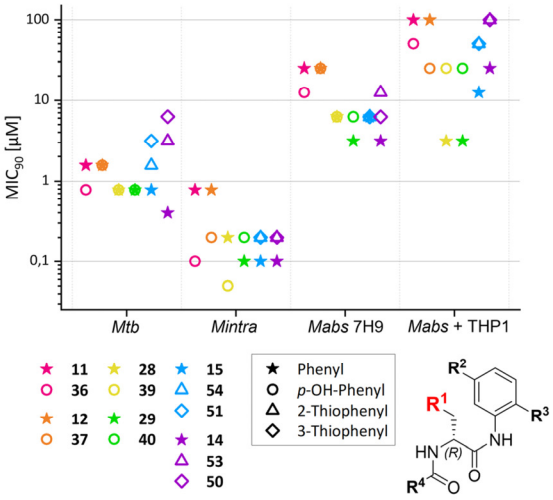


**Figure 3.** Comparison of $MIC_{90}$ values of compounds that only differ in $R^1$. Compounds that only differ in $R^1$ are shown in the same color; the symbols represent the respective $R^1$ substituent. Displayed values were generated by RFP measurement. Only *Mtb* $MIC_{90}$ values were generated by OD measurement. Compounds that only differ in $R^1$ are displayed in the same color.

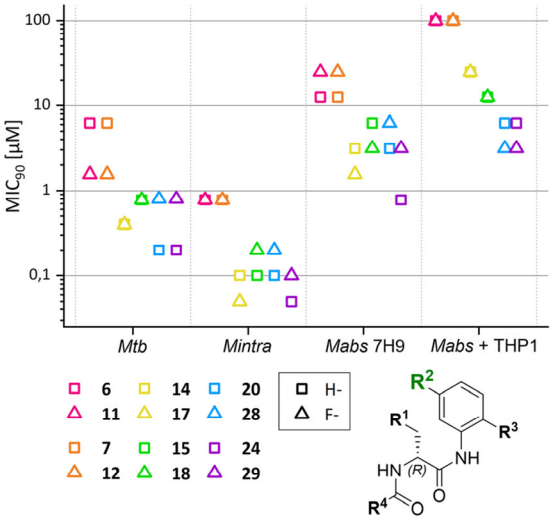


**Figure 4.** Comparison of $MIC_{90}$ values of compounds that only differ in $R^2$. Compounds that only differ in $R^2$ are shown in the same color; the symbols represent the respective $R^2$ substituent. Displayed values were generated by RFP measurement. Only *Mtb* $MIC_{90}$ values were generated by OD measurement.

decrease in activity when a *p*-Hydroxyphenyl group is present. Possibly, these results are based on the higher polarity of the *p*-Hydroxyphenyl group leading to lower permeability through the membranes of both the macrophages and bacteria.

In *Msmeg*, $MIC_{90}$ values show a 4-fold increase when a *p*-Hydroxyphenyl group is introduced into the molecule.

Interestingly, the $MIC_{90}$ values against *Mintra* show an opposite trend. A comparison of **28** and **39** shows that the *p*-Hydroxyphenyl group has a positive effect on the $MIC_{90}$ values with a 2-to-4-fold increase in activity. Currently, we have no well-founded explanation for this result, although structural differences between the RNAPs of *Mabs* and *Mintra* and the interaction of $R^1$ with the target may play a role.

The $MIC_{90}$ values determined against *Mtb* show that *p*-Hydroxyphenyl as a substituent is never inferior to phenyl. In the case of compounds **11** and **36**, *p*-Hydroxyphenyl substitution shows a better activity against *Mtb*.

Although the change from phenyl to 2- or 3-thiophenyl is very small regarding the chemical and electronic properties of the molecule, it leads to activity loss in every single species investigated, showing that $R^1$ is indeed sensitive to even minor changes in the substituent $R^1$.

The primary intent of derivatizing $R^2$ was to sterically shield the anilide to prevent hydrolysis and to slow down or prevent metabolism of the morpholino-anilide moiety of the molecule. To this end, we introduced a fluorine atom in the *para* position to the morpholine moiety and determined whether this resulted in lower $MIC_{90}$ values. An overview of compounds only different at $R^2$ is given in Figure 4.

The introduction of the fluorine atom results in a tendency for higher $MIC_{90}$ values. It is worth noting that, for *Mabs*, a 2-to-4-fold increase in $MIC_{90}$ values was observed (e.g., **6**/**11** or **24**/**29**). Interestingly, this behavior is reversed when $R^3$ contains a thiomorpholine sulfoxide group. Both thiomorpholine sulfoxide structures (**14**/**17**, **15**/**18**) show 2-fold increased $MIC_{90}$ values against *Mabs*. This effect is not observed for the respective sulfones. For example, the *Mabs* and *Mtb* $MIC_{90}$ values of the most active compound **24** are increased 4-fold on addition of the fluorine substituent. A similar effect was observed in the other sulfones, **20**/**28**.

The $MIC_{90}$ values determined for *Mabs* in the macrophage infection model decreased upon introduction of the fluorine substituent. The effect is more pronounced in the $MIC_{50}$ values. Here, a 2-to-4-fold decrease for all substances with the fluorine substituent was found.

The main $R^3$ variation of the compound set presented here is the exchange of the morpholine group of MMV688845 by a thiomorpholine group and the respective oxides $1\lambda^4$-thiomorpholin-1-one (thiomorpholine-sulfoxide) and $1\lambda^6$-thiomorpholine-1,1-dione (thiomorpholine-sulfone). Tetrahydrothiopyran and its sulfone were included to check on the necessity of an aromatic amine structure within $R^3$. An overview of the MIC values is given in Figure 5.

$MIC_{90}$ determination against *Msmeg* revealed a decrease (4-fold) in activity when morpholine was exchanged for thiomorpholine in MMV688845. An increase of activity was seen for the respective oxides (2-fold increase). For all other comparison groups, S-oxidation had no strong effect on the $MIC_{90}$ values.

In *Mtb*, however, oxidation to the sulfone in **20** resulted in a 4-fold decrease in the $MIC_{90}$ values (**20**, $MIC_{90}$ down to 200 nM) in comparison to MMV688845. The respective sulfoxide also showed better activity than the hit compound (2-fold decrease in the $MIC_{90}$ values).

For *Mabs*, a similar behavior was observed: in comparison to MMV688845, a 2-to-4-fold increase in activity was observed, the sulfone leading to lower MIC values. The same is true for all other compared groups that contain either phenyl or *p*-hydroxyphenyl as $R^1$. In these groups, improvements of $MIC_{90}$ values of down to 0.78 $\mu$M (**24**) were achieved. Groups that contain 2- or 3-thiophenyl as $R^1$ did not benefit from the oxidation. The same effects are seen with the clinical isolate



https://doi.org/10.1021/acs.jmedchem.3c00009
J. Med. Chem. 2023, 66, 5079−5098

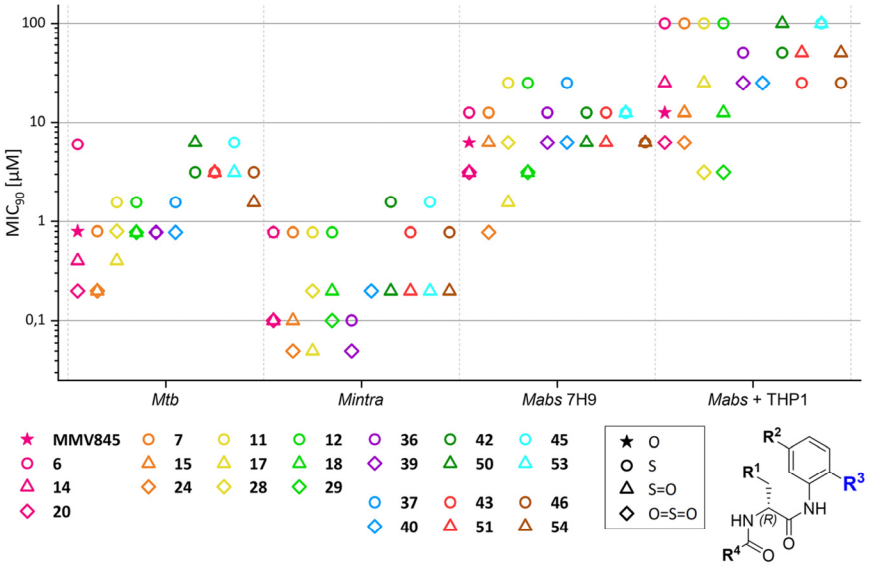


**Figure 5.** Comparison of $MIC_{90}$ values of compounds that only differ in $R^3$. Compounds that only differ in $R^3$ are shown in the same color; the symbols represent the respective $R^3$ substituent. Displayed values were generated by RFP measurement. Only *Mtb* values were generated by OD measurement. Compounds **32** and **34** were excluded in this figure. MMV845 abbr. MMV688845.

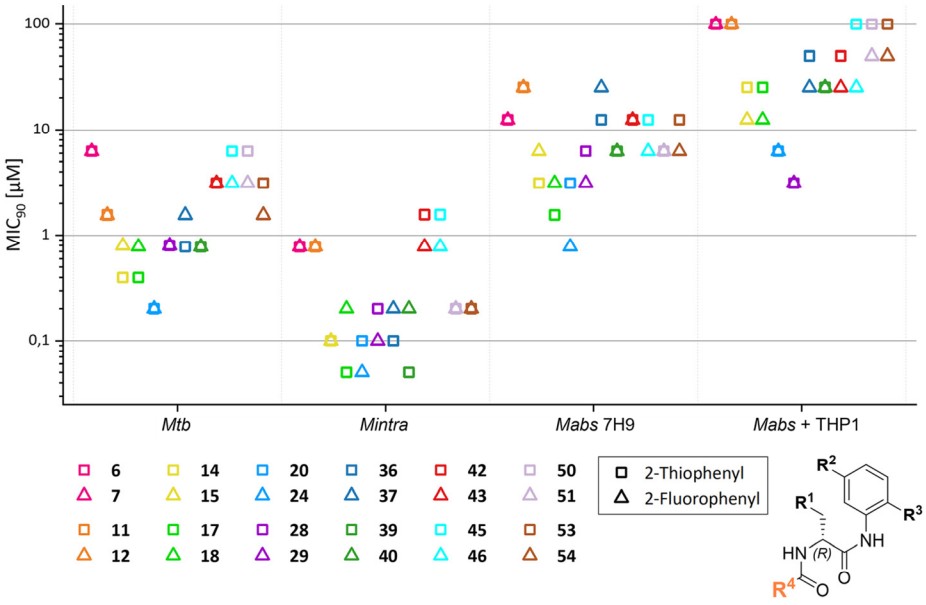


**Figure 6.** Comparison of $MIC_{90}$ values of compounds that only differ in $R^4$. Compounds that only differ in $R^4$ are shown in the same color; the symbols represent the respective $R^4$ substituent. Displayed values were generated by RFP measurement. Only *Mtb* values were generated by OD measurement.

*Mabs* Bamboo, even though the most active substances do not reach as low $MIC_{90}$ values as those that we observed with the *Mabs* ATCC 19977 strain. Nevertheless, the respective sulfones and sulfoxides offer submicromolar $MIC_{50}$ values and low-micromolar $MIC_{90}$ values. Within the macrophage infection model, we noted that the oxides are still more potent than MMV688845 but with less of a difference. The difference between the sulfoxides used and their respective sulfones is remarkable: sulfoxides show a strong decrease in activity when tested in the macrophage infection model. This could be due to their high polarity, which could negatively affect their ability to cross biological bilayer membranes. The need to pass two membranes (macrophage and bacterium) rather than one may have magnified this effect.

Against *Mintra*, thiomorpholine oxidation also increases activity. $MIC_{90}$ values are decreased by a factor of 4 in



https://doi.org/10.1021/acs.jmedchem.3c00009
J. Med. Chem. 2023, 66, 5079−5098

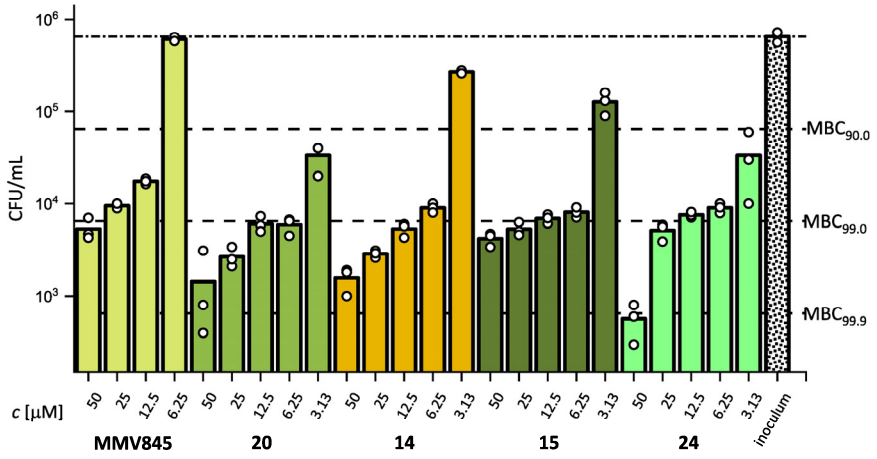


**Figure 7.** MBC determination against *Mabs* ATCC19977 of MMV688845 (abbr. MMV845) and a selection of AAP derivatives. Bacteria reduction levels are displayed as dashed horizontal lines. Substances were analyzed in triplicates as indicated by the white dots.

comparison to MMV688845. In other groups, oxidation resulted in compounds that have $MIC_{90}$ values down to 50 nM (**24** and **39**), which is equivalent to an 8-fold increase in activity.

For varying $R^4$, we considered the thiophene-2-carboxamide (same as in the hit compound MMV688845) and the 2-fluorobenzoic acid amide for initial testing, since Ebright et al. had demonstrated that both these residues are present in the most active compounds.[32]

Figure 6 shows the comparison of $MIC_{90}$ values against the different mycobacterial strains of compounds that differ only in $R^4$. $MIC_{90}$ values of the displayed compounds do not differ substantially depending on the $R^4$ substituent. In most of the cases, 2-fluorophenyl and 2-thiophenyl demonstrate similar activity levels within a maximum 2-fold difference with the tendency that the 2-fluorobenzoic acid compounds achieve slightly lower $MIC_{90}$ values. Only in 17 of 84 direct comparisons (throughout all bacterial species tested), 2-thiophenyl compounds exhibit lower values than their respective 2-fluorophenyl compounds. In the macrophage infection assay, the 2-thiophenyl compounds were always inferior to the 2-fluorophenyl compounds.

*2.3.2. Bactericidality.* The ability to kill mycobacteria instead of forcing them into a dormant or quiescent state is a crucial property of effective antimycobacterial treatments, in particular for the therapy of *Mabs* infections.[61] To find out whether the AAP derivatives kill *Mabs*, a minimum bactericidal concentration (MBC) evaluation was conducted. Typically, an MBC is defined as the concentration at which the level of colony forming units in an inoculum is reduced by three logarithmic units, or in other words, a killing rate of 99.9% of the bacteria that was present at the start of the experiment. In mycobacteriology, this threshold was redefined for reasons of reproducibility and accuracy and is currently set at 99.0% as mycobacteria need inconveniently longer incubation times for high killing rates of 99.9%.[62]

MBC testing against *Mabs* ATCC19977 was conducted for a selection of the most active compounds as well as MMV688845, Figure 7. MMV688845 did not reduce viable bacteria at a concentration below 12.5 $\mu$M. At its $MIC_{90}$ value of 6.25 $\mu$M, no reduction of viable bacteria was observed. It achieves its $MBC_{99}$ at a concentration of 50 $\mu$M ($MBC_{99}$ at 8X $MIC_{90}$). In contrast, the new derivatives reported here show a higher reduction of viable bacteria at lower concentration levels. **14** and **15** (both including a sulfoxide moiety) show a reduction at 3.13 $\mu$M but stay below 90% reduction (58 and 81% respectively), while the sulfones **20** and **24** both reach a reduction of 95% at the same concentration levels. For all tested derivatives, concentration levels of 6.25 $\mu$M and higher result in a reduction of 99% or only slightly above that threshold making them about 4 times more bactericidal than the hit compound. Compounds **20** and **15** achieved their respective $MBC_{99}$ at 2X $MIC_{90}$. This is a significant improvement in cidal activity over MMV688845.

*2.3.3. Testing against MMV688845-Resistent Mutants.* To verify on-target the activity of the analogs described in this study, compounds **14**, **15**, and **24** were tested against the MMV688845-resistant strain *Mabs* Bamboo $845^R$-2.1. The strain and its resistance to MMV688845 were previously described.[34] The data presented in Table 3 show evidence that the target is the $\beta$ subunit of the bacterial RNAP, because *Mabs* Bamboo $845^R$-2.1. harbors a P473L mutation of the $\beta$ subunit, which is located directly at the binding site of the phenylalanine amides that was proposed by Lin et al.[31] and used for the herein described modeling study (2.1).

**Table 3. Activity Data against the MMV688845-Resistant Strain *Mabs* Bamboo $845^R$-2.1**[a]

| | $MIC_{90}$ ($\mu$M) |
|---|---|
| | *Mabs* Bamboo $845^R$-2.1 |
| compound | 7H9 |
| CLR | 0.27 |
| RFB | 1.1 |
| MMV688845 | >100 |
| 24 | 42 |
| 14 | >100 |
| 15 | 100 |

[a]Generated by selecting at 50 $\mu$M MMV688845 using *Mabs* Bamboo. This strain is resistant to MMV688845 and has a rpoB/$\beta$ subunit P473L mutation.[34] The observed frequency of resistance (FoR) was $5.83 \times 10^{-8}$ $CFU^{-1}$. CLR: clarithromycin; RFB: rifabutin.



https://doi.org/10.1021/acs.jmedchem.3c00009
J. Med. Chem. 2023, 66, 5079−5098

Similar to MMV688845, the three tested analogs suffered from a severe activity loss by at least factor 10 indicating the bacterial RNAP is involved in the molecular activity of the newly synthesized phenylalanine amides. Rifabutin, a RNAP inhibitor with a different binding site, achieved a $MIC_{90}$ value of 3 $\mu$M in a former activity determination against the MMV688845-sensitive *Mabs* Bamboo.[25] The results of the present study show no decline in activity against the resistant strain, which indicates that the probability of cross resistance between the two RNAP inhibitors is low.

**2.4. *In Vitro* Plasma and Microsomal Stability.** Former investigations on MMV688845 revealed low drug plasma levels after oral administration in Sprague Dawley male rats[30] and CD 1 mice,[34] which could be due to low metabolic stability. To narrow down the reasons why MMV688845 seems to exhibit low plasma levels, we conducted plasma stability and microsomal stability assays on the hit compound and the most active derivative, compound **24**. The substances were tested in both human and murine plasma and microsomes. The plasma stability is given as a %-remaining concentration versus time plot in Figure 8. Microsomal stability is displayed in Table 4.

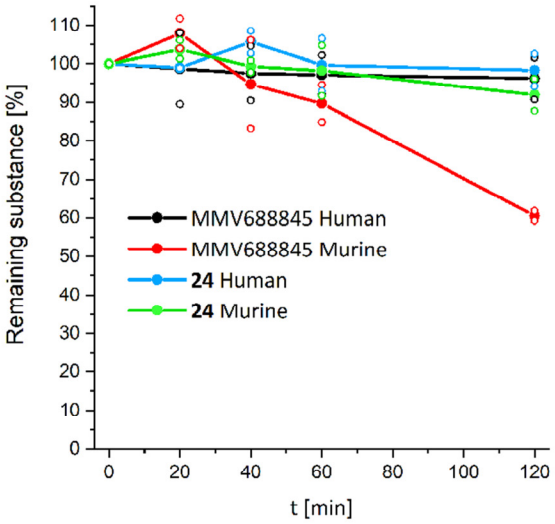


**Figure 8.** Plasma stability of MMV688845 (abbr. MMV845) and compound **24** in human and murine plasma over five different time points. Substances were analyzed in duplicates. Empty circles depict the measured values, filled circles show the respective mean.

The results show that both tested substances are stable in human plasma throughout the tested time frame. In murine plasma, MMV688845 shows a stronger decline in concentration than compound **24**. A possible explanation for this behavior is that the fluorine atom in the phenyl moiety of **24** sterically shields the amide bond of compound **24** from being a target for murine carboxyesterases (CES), leaving it uncleaved. As CES do not seem to be abundant in human plasma,[63] the stability of both substances in human plasma could be higher.

The determined half-lives show that both substances suffer from severe instability in a liver microsome assay, which is probably the reason for the low bioavailability *in vivo* described above. A rapid degradation of the phenylalanine amides by oxidation (e.g., hydroxylation) or hydrolytic activity of the microsomes seems to us a probable explanation for this observation.[64−66]

**2.5. Cytotoxicity.** MMV688845 was tested for cytotoxicity using the HEP 93 liver cancer cell line and found to be noncytotoxic.[29,33] In our study, we extended cytotoxicity testing of MMV688845 and all synthesized compounds to seven mammalian cell lines using a colorimetric microculture assay that utilized sulforhodamine-B as a staining agent. The methodology of this assay is described in various references.[67−69]

The $EC_{50}$ values are listed in Table 5. We confirmed the noncytotoxic properties of MMV688845, which was not cytotoxic for all tested cell lines at concentrations of up to 30 $\mu$M. The same was true for most variants of MMV688845. Only a few of the analogs showed very weak cytotoxicity against the tested cell lines. Most potent compounds can be considered as unproblematic since the MIC values are far below the $EC_{50}$ cytotoxicity values.

**2.6. Determination of Kinetic Solubilities and cLogP Values.** Solubility is a crucial parameter for the development of new drug candidates and their *in vivo* efficacy, especially for oral administration.[70] The calculated LogP value is considered as a predictive parameter to estimate compound solubility and/or permeability(cLogP values between 2 and 3 are desirable for pharmaceutical compounds).[71]

The kinetic solubilities of the new MMV688845 derivatives in PBS were experimentally determined by a nephelometric method described by Bevan and Lloyd.[72] (see the Supporting Information).

Figure 9A shows the relation between the calculated LogP values and measured solubilities of the synthesized compounds. Compounds with cLogP values higher than 3.5 usually have solubilities lower than 50 $\mu$M, making them hard to handle in biological assays and giving them undesirable biopharmaceutical properties. At cLogP values below 3, the solubilities show a much higher variability. In this region, six compounds show high aqueous solubilities of up to 431 $\mu$M.

Figure 9B,C shows the $MIC_{90}$ values determined against *Mabs* in the standard microdilution assay as well as in the macrophage infection model. Compounds with a cLogP between 2 and 3 achieve the lowest $MIC_{90}$ values. Within the macrophage infection model, a general increase in $MIC_{90}$ values is observed as described above. Nevertheless, the most active compounds possess a cLogP value between 2 and 3, verifying a desirable LogP range of 2−3 for the development of the AAP compound class.

**Table 4. Half-Times and Intrinsic Clearance Values after Incubation of MMV688845 (abbr. MMV845) and Compound 24 with Human and Murine Liver Microsomes over 40 min[a]**

| substance | $t_{1/2}$ [min] *human* microsomes | $Cl_{int}$ [$\mu$L/min × mg] *human* microsomes | $t_{1/2}$ [min] *murine* microsomes | $Cl_{int}$ [$\mu$L/min × mg] *murine* microsomes |
|---|---|---|---|---|
| **MMV845** | 1.7 | 1366 | 0.9 | 1837 |
| **24** | 1.5 | 1113 | 1.8 | 1562 |

[a]Experiment has been performed in duplicate.



https://doi.org/10.1021/acs.jmedchem.3c00009
J. Med. Chem. 2023, 66, 5079−5098

Table 5. $EC_{50}$ Values [$\mu$M] of AAP Analogs against Seven Different Mammalian Cell Lines[h]

| compound | A375[a] | HT29[b] | MCF7[c] | A2780[d] | NIH 2T3[e] | HeLa[f] | HEK293[g] |
|---|---|---|---|---|---|---|---|
| MMV688845 | >30 | >30 | >30 | >30 | >30 | >30 | n.d. |
| **6** | >30 | >30 | 16.4 ± 1.7 | 19.8 ± 2.0 | >30 | >30 | 19.1 ± 2.4 |
| **7** | 18.6 ± 4.2 | >30 | 13.6 ± 1.4 | 14.9 ± 1.6 | >30 | >30 | 6.3 ± 1.2 |
| **11** | >30 | >30 | >30 | >30 | >30 | >30 | n.d. |
| **12** | 29.4 ± 1.4 | >30 | >30 | 28.3 ± 1.4 | 28.5 ± 2.0 | 28.3 ± 1.5 | n.d. |
| **14** | >30 | >30 | >30 | >30 | >30 | >30 | >30 |
| **15** | >30 | >30 | >30 | >30 | >30 | >30 | >30 |
| **17** | >30 | >30 | >30 | >30 | >30 | >30 | n.d. |
| **18** | >30 | >30 | >30 | >30 | >30 | >30 | n.d. |
| **20** | >30 | >30 | >30 | 23.6 ± 2.2 | >30 | >30 | >30 |
| **24** | >30 | >30 | >30 | >30 | >30 | >30 | n.d. |
| **28** | >30 | >30 | 23.2 ± 2.8 | 24.0 ± 5.2 | 26.9 ± 5.0 | >30 | >30 |
| **29** | >30 | >30 | 25.9 ± 2.7 | 23.2 ± 4.4 | 24.2 ± 4.2 | >30 | >30 |
| **32** | >30 | >30 | >30 | >30 | >30 | >30 | n.d. |
| **34** | >30 | >30 | >30 | >30 | >30 | 29.8 ± 1.3 | n.d. |
| **36** | >30 | >30 | >30 | >30 | >30 | >30 | n.d. |
| **37** | >30 | >30 | >30 | >30 | >30 | >30 | n.d. |
| **39** | >30 | 29.8 ± 1.7 | >30 | 29.7 ± 1.2 | >30 | >30 | n.d. |
| **40** | >30 | >30 | >30 | >30 | >30 | >30 | >30 |
| **42** | >30 | >30 | >30 | >30 | >30 | >30 | n.d. |
| **43** | >30 | >30 | >30 | >30 | >30 | >30 | n.d. |
| **45** | >30 | 29.8 ± 1.9 | >30 | 29.5 ± 2.0 | 29.0 ± 1.3 | >30 | n.d. |
| **46** | >30 | >30 | >30 | >30 | >30 | >30 | n.d. |
| **50** | >30 | >30 | >30 | >30 | >30 | >30 | n.d. |
| **51** | >30 | >30 | >30 | >30 | >30 | >30 | n.d. |
| **53** | >30 | >30 | >30 | >30 | >30 | >30 | n.d. |
| **54** | 29.3 ± 1.5 | >30 | 28.9 ± 1.8 | 29.0 ± 1.7 | >30 | >30 | n.d. |

[a]Melanoma. [b]Colon cancer. [c]Breast cancer. [d]Ovarian cancer [e]Mouse fibroblasts [f]Cervical cancer. [g]Human embryonic kidney cancer. [h]The assay was performed in triplicate. Standard deviations are displayed if applicable.

Table 6 summarizes the solubilities and cLogP values for the compounds synthesized. Introduction of thiomorpholine lowers the solubility of the compounds in PBS buffer by factor 2 to 3. This may be attributed to the lower electronegativity of the sulfur atom in comparison to oxygen, which reduces the polarity within the molecule. A strong improvement in solubility is observed when thiomorpholine sulfoxides are present. For instance, the solubility of **15** is approximately 5 times higher than the solubility of the hit compound MMV688845. The improvement is not as prominent when thiomorpholine is oxidized to the respective sulfone (e.g., **20**, **24**, **28**). In this case, a 2-fold increase in solubility was observed in comparison to their respective thioethers. The difference in solubility between sulfoxides and sulfones can be explained by the fact that sulfoxide itself is asymmetric since the free electron pair of the sulfur atom is still present. This provides a strong dipole moment to the molecule and increases its polarity. It should be noted that cLogP values are not a good predictor for the high difference in solubility of sulfones and sulfoxides since the cLogP values only differ by a value of 0.05. The results show that the highest increase in solubility is achieved by introduction of the sulfoxide group.

The aqueous solubility can otherwise be increased when $R^1$ is exchanged for a polar *p*-hydroxyphenyl group. This resulted in a doubling of the solubility of thiomorpholine containing compounds (**11**/37 $\mu$M to **36**/78 $\mu$M; **12**/31 $\mu$M to **37**/58 $\mu$M). This is also the case for their respective sulfone derivatives (**36**/78 $\mu$M to **39**/170 $\mu$M; **37**/58 $\mu$M to **40**/158 $\mu$M).

In summary, based on a straightforward synthetic route, systematic derivatization made it possible to obtain an overview of the influence of the different substituents on the antimycobacterial activity of AAPs and hence important structure–activity relationship information as summarized in Scheme 6.

## 3. CONCLUSIONS

We have shown that synthetic RNAP inhibitors derived from MMV688845 have the potential to reach *in vitro* $MIC_{90}$ values of below 1 $\mu$M against pathogenic mycobacteria, e.g., *Mtb* and *Mabs*. In addition to the improved activity against mycobacteria and the absence of cytotoxicity, the new analogs display bactericidal activity (99% CFU reduction) against *Mabs* at concentrations below 10 $\mu$M. Compounds **20** and **15** achieved $MBC_{99}$ at 2X $MIC_{90}$, giving them higher cidality than MMV688845 ($MBC_{99}$ at 8X $MIC_{90}$). Systematic derivatization based on a straightforward synthetic route made it possible to obtain important structure–activity relationship information. It is worth noting that the oxidized thiomorpholine derivatives, sulfoxide and sulfone, result in an increase in activity in comparison to MMV688845 reaching submicromolar activities against *Msmeg*, *Mintra*, and even *Mabs*. Sulfones show higher activities than sulfoxides across the board. Sulfoxides are interesting for further research because of their higher aqueous solubility. The data show that anti-*Mabs* targeting of MMV688845 is possible and that attractive MIC values can be achieved with this compound class, warranting further preclinical investigation. Since MMV688845 analogs do not exhibit cross-resistance with rifamycin-resistant mycobacteria, further investigation is of scientific interest to develop an RNAP inhibitor that is effective against these resistant pathogens.



https://doi.org/10.1021/acs.jmedchem.3c00009
J. Med. Chem. 2023, 66, 5079−5098

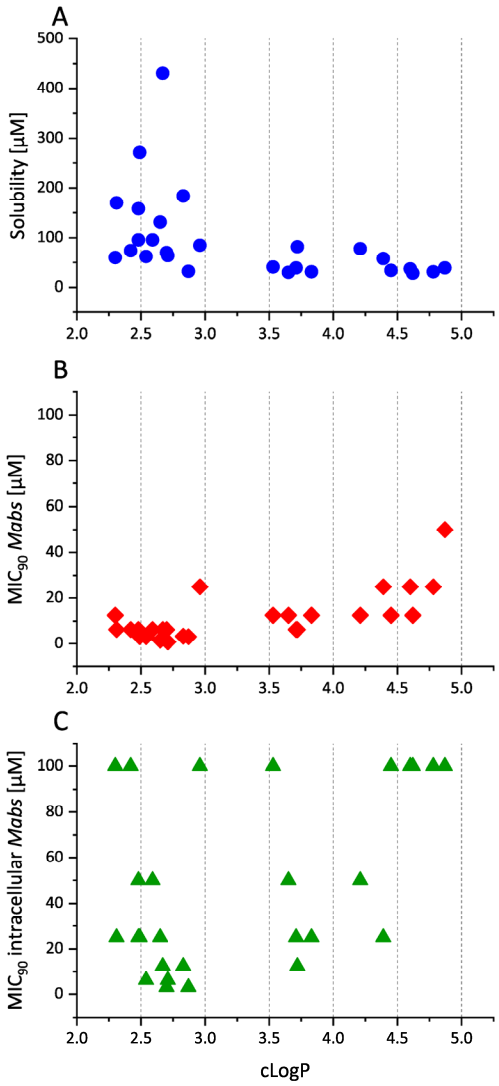


**Figure 9.** Relationship of cLogP values and their corresponding kinetic solubilities of all the synthesized AAP analogs (A). Relationship of cLogP values and their corresponding $MIC_{90}$ values against *Mabs* of all the synthesized AAP analogs (B). Relationship of cLogP values and their corresponding $MIC_{90}$ values against *Mabs* within the macrophage infection model of all the synthesized AAP analogs (C). The cLogP values were calculated with ChemDraw (Perkin Elmer Informatics Inc.).

Particular attention should be paid to NTM, such as *Mabs*, as there are species-dependent differences in the structure−activity relationships, as shown in this study. In addition to further derivatization with the aim of increasing activity, the investigation of hepatic metabolism, pharmacokinetics, and activity of MMV688845 derivatives *in vitro* and *in vivo* should be addressed. In this study, it was possible to show that compound **24** has an improved stability against mouse plasma *in vitro* than the hit compound MMV688845, but the very rapid degradation by liver microsomes is a drawback of the compound class. Elucidation of the hepatic metabolism of phenylalanine amides is desirable in future research, as this should help developing analogs with improved hepatic stability.

## 4. MATERIALS AND METHODS

**4.1. General.** Starting materials were purchased and used as received. Solvents used for either synthetical or purification purposes were distilled and stored over 4 Å molecular sieves. Glassware was oven-dried at 110 °C prior to use. For the determination of $R_f$ values and other analytical purposes such as qualitative chromatography, Merck TLC silica gel 60 on aluminum sheets with fluorescent indicator F254 were used. Flash chromatography was performed with a puriFlash 430 instrument (Interchim, Montluçon, France). Columns were packed in either 8 g ($v$ = 10 mL/min), 45 g ($v$ = 30 mL/min), or 90 g ($v$ = 40 mL/min) cartridges with 40−63 $\mu$m normal phase silica gel produced by Carl Roth. Column loading was performed with the dry load method. NMR spectra were recorded on an Agilent Technologies VNMRS 400 MHz spectrometer. Chemical shifts are reported relative to the residual solvent signal ($CDCl_3$: $\delta_H$ = 7.26 ppm; $\delta_C$ = 77.36 ppm; $CD_3OD$ $\delta_H$ = 3.31 ppm). $^{13}C$ NMR spectral data were generally determined as attached-proton-test spectra (APT). Spectra have been cut, baseline and phase corrected, and analyzed utilizing MestreNova 11.0 software (Mestrelab Research, S.L., Spain). APCI-MS (atmospheric pressure chemical ionization) was performed using an expression CMS mass spectrometer (Advion Inc., Ithaca, NY, USA), with both ASAP (atmospheric solids analysis probe) sampling and with the help of the Plate Express TLC-plate extractor. ESI measurements have been conducted on the same expression CMS mass spectrometer with an ESI ionization module and direct injection sampling. HRMS was carried out using an LTQ Orbitrap XL mass spectrometer (Thermo Fisher Scientific Inc., Waltham, MA, USA).

**4.2. HPLC.** All described final compounds were confirmed to be of >95% purity. Purity was measured by UV absorbance at 254 nm. The HPLC apparatus consists of an XTerra RP18 column (3.5 $\mu$m, 3.9 mm × 100 mm) from the manufacturer Waters (Milford, MA, USA) and two LC-10 AD pumps, a SPD-M10A VP PDA detector, and a SIL-HT autosampler, all from the manufacturer Shimadzu (Kyoto, Japan).

Compounds used for stereochemical analyses (Boc-Phe-(R); **1**-(***R***), **2A**-(***R***), and **2B**-(***R***); Boc-Phe-(S); **1**-(***S***), **2A**-(***S***), and **2B**-(***S***); Boc-Phe-(*rac*); **1**-(*rac*), **2A**-(*rac*), and **2B**-(*rac*)) were checked for purity using an Agilent 1260 HPLC instrument equipped with UV diode array detector (50 mm Eclipse Plus C18 1.8 $\mu$m, i.d. 4.6 mm, $v$ = 1.0 mL $min^{-1}$, $\lambda_{used}$ = 220 nm). Elution systems: [Boc-Phe-(*R*); Boc-Phe-(*S*); Boc-Phe-(*rac*): acetonitrile/water 35:65; 0.1% v/v TFA]; [**1**-(***R***); **1**-(***S***); **1**-(*rac*): acetonitrile/water 55:45]; [**2A**-(***R***); **2A**-(***S***); **2A**-(*rac*): methanol/water 20 mM $NH_4HCO_3$ pH 9 55:45]; [**2B**-(***R***); **2B**-(***S***); **2B**-(*rac*): acetonitrile/water 45:55].

For preparative tasks, an XTerra RP18 column (7 $\mu$m, 19 mm × 150 mm) manufactured by Waters (Milford, MA, USA) and two LC-20 AD pumps (Shimadzu, Kyoto, Japan) were used. The mobile phase was in all cases a gradient of methanol/water (starting at 95% v/v water to 5% v/v water) with 0.05% v/v TFA added.

The determination of *ee*-values was conducted using a Shimadzu Prominence LC-20A HPLC instrument with diode array detection ($v$ = 1.0 mL $min^{-1}$, $\lambda_{used}$ = 220 nm). The utilized elution systems and chiral columns differ according to the structure that had to be analyzed: [Boc-Phe-(*R*); Boc-Phe-(*S*); Boc-Phe-(*rac*): 150 mm Chiralpak IA-3, 4.6 mm i.d.; acetonitrile/water 30:70; 0.1% v/v TFA]; [**1**-(***R***); **1**-(***S***); **1**-(*rac*): 150 mm Chiralpak IB N-3, 4.6 mm i.d.; acetonitrile/water 55:45]; [**2A**-(***R***); **2A**-(***S***); **2A**-(*rac*): 150 mm Chiralpak IG-3, 4.6 mm i.d.; *n*-heptane/*iso*-propanol 90:10]; [**2B**-(***R***); **2B**-(***S***); **2B**-(*rac*): 150 mm Chiralcel OJ-3R, 4.6 mm i.d.; acetonitrile/water 40:60].

**4.3. X-ray Crystallography.** Details of the X-ray intensity data collections, structure solutions and refinements, and hydrogen bond parameters can be found in the Supporting Information. X-ray crystallography structures have been determined for compounds **6**, **14**, and **20**. CCDC 2231845-2231847 contains the supplementary crystallographic data for this paper. The data can be obtained free of



https://doi.org/10.1021/acs.jmedchem.3c00009
J. Med. Chem. 2023, 66, 5079−5098

**Table 6. Kinetic Solubilities and cLogP Values of MMV688845 (abbr. MMV845) and All Synthesized AAP Derivatives**[a]

| | MMV845 | 6 | 7 | 11 | 12 | 14 | 15 |
|---|---|---|---|---|---|---|---|
| Solubility [μM] | 82 | 34 | 28 | 37 | 31 | 271 | 431 |
| cLogP | 3.72 | 4.45 | 4.62 | 4.6 | 4.78 | 2.49 | 2.67 |

| | 17 | 18 | 20 | 24 | 28 | 29 | 32 |
|---|---|---|---|---|---|---|---|
| Solubility [μM] | 131 | 184 | 62 | 64 | 70 | 32 | 39 |
| cLogP | 2.65 | 2.83 | 2.54 | 2.71 | 2.7 | 2.87 | 4.87 |

| | 34 | 36 | 37 | 39 | 40 | 42 | 43 |
|---|---|---|---|---|---|---|---|
| Solubility [μM] | 85 | 78 | 58 | 170 | 158 | 30 | 31 |
| cLogP | 2.96 | 4.21 | 4.39 | 2.31 | 2.48 | 3.65 | 3.83 |

| | 45 | 46 | 50 | 51 | 53 | 54 |
|---|---|---|---|---|---|---|
| Solubility [μM] | 41 | 39 | 74 | 96 | 60 | 96 |
| cLogP | 3.53 | 3.71 | 2.42 | 2.59 | 2.3 | 2.48 |

[a]Color coding: the colors show the difference to the average kinetic solubility of all tested compounds, dark blue: highest solubility, light blue: above average, white: closest to average, light red: below average, dark red: lowest kinetic solubilities of the tested compound set.

**Scheme 6. Overview of the Influence of the Different Substituents on the Antimycobacterial Activity of AAPs**[a]

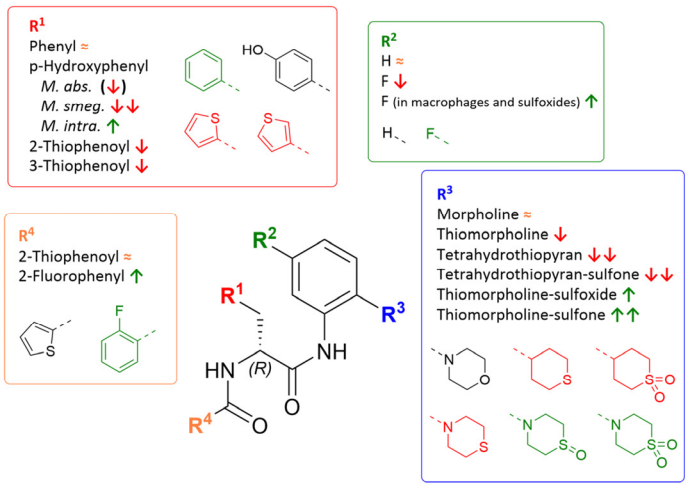


[a]Red arrows indicate a loss in activity; green arrows indicate an increased activity caused by the respective residues.

charge from the Cambridge Crystallographic Data Centre via www.ccdc.cam.ac.uk/structures.

**4.4. General Procedure A—Amide Coupling T3P.** A solution of the Boc-protected α-amino acid (1.1 equiv) and the aniline (1 equiv) in a 1:2 mixture of pyridine (distilled) and EtOAc (distilled) was cooled to −20 °C with an isopropanol/dry ice bath. If the compounds did not dissolve completely at −20 °C, additional pyridine/EtOAc mixture was added until complete dissolution. A 50% m/v solution of T3P in EtOAc (2 equiv) was added to the mixture subsequently. After 10 min, the dry ice bath was removed and replaced by an ice/water bath to keep the temperature at 0 °C overnight.[46] Afterward, a reasonable amount of EtOAc was added to the reaction mixture to wash it with 0.25 M $KH_2PO_4$ solution three times in a separation funnel. The organic phase was collected and dried with $Na_2SO_4$, and the solvent was removed under reduced pressure. As a general purification procedure, flash chromatography was performed with varying gradient eluting systems on 40−63 μm normal phase silica gel (see respective synthesis documentation in the Supporting Information).

**4.5. General Procedure B—Amide Coupling DEPBT.** The formation of the anilide bond (general procedure A) was followed by the cleavage of the Boc-protecting group using TFA. For this purpose, the purified Boc-α-amino anilides were dissolved in DCM and an equal volume of TFA was added under stirring. The solution was stirred for 30 min at room temperature and checked for the complete Boc-cleavage using thin-layer chromatography (TLC). The DCM/TFA mixture was removed under reduced pressure after complete conversion. The crude product was redissolved in EtOAc and washed with saturated $NaHCO_3$ solution three times. The organic phase was collected, and the solvents were evaporated under reduced pressure.

The formation of the second amide bond was achieved with the coupling reagent DEPBT. For this synthetic step, the Boc-deprotected amino acid was dissolved in THF with the respective aromatic carboxylic acid and DEPBT. After complete dissolution, DIPEA was added, and the solution was stirred overnight at room temperature. Afterward, the reaction mixture was washed successively once with 0.25 M $KH_2PO_4$, water, saturated $NaHCO_3$, water, and brine. The organic phase was dried with $Na_2SO_4$, and the solvents were removed under reduced pressure. For purification, a flash chromatography was performed with varying gradient eluting systems on 40−63 μm normal phase silica gel (see respective synthesis documentation in the Supporting Information).

**4.6. General Procedure C—Nucleophilic Substitution of Thiomorpholine.** 1-Bromo-2-nitrobenzene or the respective deriva-



https://doi.org/10.1021/acs.jmedchem.3c00009
J. Med. Chem. 2023, 66, 5079−5098

tives were dissolved in thiomorpholine without addition of solvents in a small glass flask. The mixture was heated to 120 °C and stirred for 2 h. After cooling down to room temperature, the precipitated solid was filtered out, the filter was washed thoroughly with DCM, and the solid was discarded. DCM was evaporated under reduced pressure to obtain the bright-orange oily crude products. For purification, flash chromatography was performed with varying gradient eluting systems on 40−63 μm normal phase silica gel (see respective synthesis documentation in the Supporting Information).

**4.7. General Procedure D—Reduction of 4-(2-Nitrophenyl)-thiomorpholines.** 4-(4-$R^2$-2-Nitro-phenyl)thiomorpholines were dissolved in ethanol. One third of the total amount of palladium 10% m/m on active charcoal was added, and the mixture was then heated to 50 °C and stirred vigorously. A 50% v/v solution of hydrazine in water was added very slowly. The remaining amount of catalyst was added to the mixture in portions. Afterward, the temperature was increased to 90 °C and the mixture was refluxed for 30 min. The bright orange-yellow solution turned to a clear and colorless solution. The mixture was cooled down to room temperature and filtered to remove the catalyst. The filter was washed thoroughly with ethanol to extract residual product. Completion of the reaction and purity were checked with TLC. Solvents were then removed under reduced pressure. The crude product was used for the next synthesis without further purification when applicable (for exceptions see respective synthesis documentation in the Supporting Information).

**4.8. General Procedure E—Oxidation of Thiomorpholines to Sulfoxides.** Sodium periodate was dissolved in water and cooled to 0 °C. 4-(4-$R^2$-2-Nitro-phenyl)thiomorpholines or their respective Boc-amino acid coupled derivatives were dissolved in methanol. This solution was then added to sodium periodate solution under stirring. If a precipitate formed, acetonitrile was added until full dissolution occurred. The mixture was then stirred at 0 °C for 4 h, before it was stored in the fridge for three days. Subsequently, the mixture was extracted with DCM three times. The organic phases were collected, and the solvents were evaporated under reduced pressure. For purification, flash chromatography was performed with varying gradient eluting systems on 40−63 μm normal phase silica gel (see respective synthesis documentation).

**4.9. General Procedure F—Oxidation of Thiomorpholines to Sulfones.** 4-(4-$R^2$-2-Nitro-phenyl)thiomorpholines or their respective Boc-amino acid coupled derivatives were dissolved in DCM. The mixture was cooled to 0 °C before a solution of *m*-chloroperbenzoic acid in DCM was added over 30 min with a syringe. The reaction mixture was stirred overnight at room temperature. After completion of the reaction, the mixture was washed three times with saturated $NaHCO_3$ solution. The organic phase was collected, the solvent was evaporated under reduced pressure, and a dryload was prepared for purification with flash chromatography (see respective synthesis documentation).

**4.10. General Procedure G—Nucleophilic Substitution of Thiomorpholinedioxides.** 1-Bromo-2-nitrobenzene and thiomorpholinedioxide were dissolved in dioxane. Then, palladium(II) acetate, BINAP, and $Cs_2CO_3$ were added. The mixture was then ultrasonically degassed; the flask was flushed with argon and then refluxed at 100 °C overnight. After the reaction mixture had cooled down to room temperature, it was filtered through Celite and the filter was washed thoroughly with EtOAc. The solvents were evaporated under reduced pressure. For purification, flash chromatography utilizing an EtOAc/heptane gradient was used (see respective synthesis documentation).

**4.11. General Procedure H—C-C Coupling of 4-Oxothiane and Boc-2-aminophenylboronic Acid Pinacol Ester.** 4-Oxothiane was added to a solution of *p*-toluenesulfonylhydrazide in methanol. The reaction mixture was stirred at room temperature for 1 h and was then monitored until full conversion using TLC. The solvent was removed under reduced pressure, and the crude product was used in the next step without further purification.

The sulfonylhydrazone formed in the first step, Boc-2-amino-phenylboronic acid pinacol ester, and cesium carbonate were added to a three-necked Schlenk flask attached to a condenser. The apparatus was put under vacuum and backfilled with argon three times, while the mixture of solids was stirred with a magnetic stirrer. Dry and ultrasonic-degassed dioxane was added through a septum with a syringe before the reaction was heated to 110 °C for 18 h. After cooling to room temperature, the reaction was quenched with saturated $NaHCO_3$ solution. The mixture was then extracted with DCM three times. Solvents were removed under reduced pressure, and the crude product was prepared for purification with flash chromatography.

The purified product was then dissolved in DCM, and an equal volume of TFA was added under stirring. The solution was stirred for 30 min at room temperature and checked for the complete Boc-cleavage by TLC. The DCM/TFA mixture was removed under reduced pressure after complete conversion. The crude product was reconstituted in EtOAc and washed with saturated $NaHCO_3$ solution three times. The organic phase was collected, and solvents were evaporated under reduced pressure. The crude product was used for the subsequent reactions without further purification.

**4.12. Microbiological Assays.** *4.12.1. Bacteria and Culture Media.* *M. smegmatis* $mc^2$ 155 pTEC27, *M. intracellulare* ATCC 35761 pTEC27, and *M. abscessus* ATCC 19977 pTEC27 expressing tomato RFP were used for the activity assays. Stocks of the bacteria grown in Middlebrook 7H9 medium +10% v/v ADS +0,05% v/v polysorbate 80 + 400 μg/mL hygromycin were stored in approximately 15% v/v glycerol at −80 °C. Using an inoculation loop, bacteria were streaked on 7H10 agar plates (containing hygromycin 400 μg/mL) and grown for five days in an incubator at 37 °C.

Bacteria were grown in complete 7H9 broth supplemented with 10% v/v ADS and 0.05% v/v polysorbate 80, respectively, in MHII broth supplemented with 0.05% v/v polysorbate 80. The culture volume was 10 mL in a 50 mL Falcon tube. The tubes were covered to protect the photosensitive hygromycin and shaken in an incubator at 37 °C. Solid cultures were grown on a 7H10 medium supplemented with 0.5% v/v glycerol and 10% v/v ADS containing 400 μg/mL hygromycin.

*M. abscessus* Bamboo was isolated from the sputum of a patient with amyotrophic lateral sclerosis and bronchiectasis and was provided by Wei Chang Huang, Taichung Veterans General Hospital, Taichung, Taiwan. *M. abscessus* Bamboo whole-genome sequencing showed that the strain belongs to *M. abscessus subsp. abscessus* and harbors an inactive clarithromycin-sensitive erm41 C28 sequevar. *M. tuberculosis* H37Rv (ATCC 27294) was obtained from the American Type Culture Collection.

For general bacteria culturing and certain MIC experiments, Middlebrook 7H9 broth (BD Difco) was supplemented with 0.5% m/v albumin, 0.2% m/v glucose, 0.085% m/v sodium chloride, 0.0003% m/v catalase, 0.2% v/v glycerol, and 0.05% v/v polysorbate 80. Unless otherwise stated, solid cultures were grown on Middlebrook 7H10 agar (BD Difco) supplemented with 0.5% m/v albumin, 0.2% m/v glucose, 0.085% m/v sodium chloride, 0.5% v/v glycerol, 0.0003% m/v catalase, and 0.006% v/v oleic acid. All drugs were prepared as 10 mM stocks in dimethyl sulfoxide (DMSO).

*4.12.2. THP-1 Cells and Culture Media.* THP-1 cells were put in 90% v/v FBS + 10% v/v DMSO and stored in liquid nitrogen. THP-1 cells were grown in a complete RPMI medium. The cells were grown in a tissue culture flask with a minimum volume of 30 mL and a maximum volume of 40 mL and were incubated in an atmosphere of 95% air and 5% carbon dioxide ($CO_2$) at a temperature of 37 °C. The cell density was kept between 0.25 million and 1 million cells/mL. Every two or three days, the cells were counted and diluted to 0.25 million cells/mL. The cells doubled every 48 h. A culture from nitrogen stock could be subcultured for up to three months; after this time, a change in morphology and growth behavior was observed. For culturing of THP-1 cells, the RPMI 1640 medium supplemented with 5% v/v fetal bovine serum (FBS), 2% m/v glutamine, and 1% v/v nonessential amino acids.

*4.12.3. MIC Determination against M. smegmatis $mc^2$ 155 pTEC27, M. intracellulare ATCC 35761 pTEC27, and M. abscessus ATCC 19977 pTEC27.* MIC values were determined by the broth microdilution method. 96-well flat bottom tissue culture plates (Sarstedt, 83.3924.500) were used.[73] In the third well of each column two times the desired highest concentration of each compound was added in the respective assay medium. Each compound was diluted 2-fold in a nine-point serial dilution. The concentration of the starting



https://doi.org/10.1021/acs.jmedchem.3c00009
J. Med. Chem. 2023, 66, 5079−5098

inoculum was $5 \times 10^5$ cells/mL. The starting inoculum was diluted from a preculture at the mid-log phase ($OD_{600}$, 0.3 to 0.7), and an $OD_{600}$ of 0.1 was correlated to $1 \times 10^8$ CFU/mL. The plates were sealed with Parafilm, placed in a container with moist tissue, and incubated for three days at 37 °C (*M. smegmatis* and *M. abscessus*) or five days (*M. intracellulare*). Each plate had eight negative controls (1% v/v dimethyl sulfoxide) and eight positive controls (100 $\mu$M amikacin). After incubation, the plates were monitored by OD measurement at 550 nm (BMG labtech Fluostar Optima) and by measurement of fluorescence ($\lambda_{ex}$ = 544 nm, $\lambda_{em}$ = 590 nm). The assay was performed in duplicate, and the results were averaged.

*4.12.3.1. Data Analysis.* Every assay plate contained eight wells with dimethyl sulfoxide (1% v/v) as a negative control, which corresponds to 100% bacterial growth and eight wells with amikacin (100 $\mu$M) as a positive control in which 100% inhibition of bacterial growth was reached. Controls were used to monitor the assay quality through determination of the $Z'$ score. The $Z'$ factor was calculated as follows:

$$Z' = 1 - \frac{3(SD_{amikacin} + SD_{DMSO})}{|M_{amikacin} - M_{DMSO}|}$$

where SD is standard deviation and $M$ is mean.

The percentage of growth inhibition was calculated by the equation:

$$\%\text{growth inhibition} = -100\% \times \frac{signal_{sample} - signal_{DMSO}}{signal_{DMSO} - signal_{amikacin}}$$

*4.12.4. MIC Determination against M. abscessus Bamboo.* MIC value determination by optical density at 600 nm [$OD_{600}$] was carried out in 96-well plate format. 96-well plates were initially set up with 100 $\mu$L of 7H9 per well. For each compound, a 10-point 2-fold dilution series starting at twice the desired highest concentration was dispensed onto the 96-well plates using a Tecan D300e Digital Dispenser, with the DMSO concentration normalized to 2% v/v. A bacteria culture grown to mid-log-phase ($OD_{600}$, 0.4 to 0.6) was diluted to $OD_{600}$ = 0.1 ($1 \times 10^7$ CFU/mL). The resulting bacteria suspension (100 $\mu$L) was dispensed onto the 96-well plates containing the sample compounds to give a final volume of 200 $\mu$L per well with an initial $OD_{600}$ = 0.05 ($5 \times 10^6$ CFU/mL) and a final DMSO concentration of 1% v/v. Final compound concentration ranges were typically 50−0.098 $\mu$M or 6.25−0.012 $\mu$M. Untreated control wells, which contained bacteria suspension and 1% v/v DMSO, were included on each plate. Plates were sealed with Parafilm, stored in boxes with wet paper towels, and incubated at 37 °C with shaking (110 rpm) for three days.

To determine growth, $OD_{600}$ was measured using a Tecan Infinite M200 plate reader on day 0 and day 3. Two biological replicates were performed. Clarithromycin was included in each experiment as a positive control. For each well on the 96-well plate, bacterial growth was calculated by subtracting the day 0 $OD_{600}$ value from the day 3 $OD_{600}$ value. For each compound series, the bacterial growth values for the untreated control wells were averaged to give the average drug-free bacterial growth. For compound-containing wells, percentage growth was calculated by dividing their growth values by the average drug-free bacterial growth for the compound series and multiplying by 100. For each compound series, we plotted percentage growth versus compound concentration. By visual inspection of the dose−response curve, we determined the MIC of a compound as the compound concentrations that would result in 90% growth inhibition. The MIC determination was performed two times with different starter cultures. The MIC values shown in this article are the averaged results of biological duplicates.

*4.12.5. MIC Determination against M. tuberculosis H37Rv.* MICs were determined as described previously with slight modifications.[74] Briefly, compounds were serially diluted in flat-bottom 96-well plates, and a mid-log-phase culture was mixed with the compound-containing broth (final $OD_{600}$ = 0.05). Plates were sealed with a Breathe-Easy sealing membrane (Sigma), placed in humidified plastic boxes, and incubated at 37 °C for seven days, shaking at 80 rpm. Growth was monitored by measuring turbidity at 600 nm using a Tecan Infinite 200 Pro microplate reader (Tecan). $MIC_{90}$ values were deduced from the generated dose−response curves. The MIC values shown in the script are the averaged results of the two biological replicates.

*4.12.6. MIC Determination in the Macrophage Infection Model.* For the infection assay, an *M. abscessus* pTEC27 culture (OD, 0.2−0.8, mid-log phase) was centrifuged (4000 rpm, RT, 10 min), washed with 7H9 medium with 0.05% v/v polysorbate 80 (about 10 mL), and vortexed. After a second centrifugation (4000 rpm, RT, 10 min), the 7H9 medium was replaced by the RPMI medium (the same volume or a little less to concentrate the bacteria), vortexed, and incubated at RT for 5 min. After incubation, the bacterial suspension was filtered through a 5 $\mu$M pore-size filter to remove the clumps. The $OD_{600}$ was determined after filtration (OD = 0.1 corresponds to $1 \times 10^8$ CFU/mL). The appropriate number of bacteria was incubated in the presence of 10% v/v human serum at 37 °C for 30 min for opsonization. A cell suspension of THP-1 cells ($1 \times 10^6$ cells/mL) in the RPMI incomplete medium was incubated with the opsonized *M. abscessus* single-cell suspension (MOI, 5:1) and PMA (40 ng/mL) for 4 h at 37 °C under constant agitation. After infection, the THP-1 cell suspension was centrifuged (750 rpm, RT, 10 min) and washed with the RPMI medium. A 10-point 2-fold serial dilution of each compound was then prepared in 96-well flat bottom plates that had been tissue culture treated (Sarstedt, 3924). Column one of the 96-well plate included eight negative controls (1% v/v DMSO) and column two eight positive controls (1.5 $\mu$M bedaquiline). The plates were then inoculated with the infected cells ($1 \times 10^5$ THP-1 cells/well), sealed with Parafilm, and incubated for four days (37 °C, 5% $CO_2$)). After incubation, the cells were fixed with paraformaldehyde (PFA; 4% m/v in PBS) for 30 min. After removal of the PFA, the cells were stained with DAPI readymade solution (Sigma, MBD0015). The plates were washed twice with the RPMI medium. Image acquisition (DAPI 386-23 nm, RFP 560-25 nm, brightfield) and analysis were done with a CellInsight CX5 (Thermofisher). The mean CircSpotAvgArea of the RFP channel was used for calculations of growth inhibition.

MIC values were determined against *M. abscessus* ATCC 19977 pTEC27 by the microdilution method in RPMI incomplete media (RPMI 1640 medium supplemented with 5% v/v FBS, 1% m/v glutamine, and 1% v/v nonessential amino acids) with 70 $\mu$M amikacin in the assay medium. A 10-point 2-fold serial dilution of each compound was prepared in 96-well flat bottom plates that had been tissue culture treated (Sarstedt, 3924). Column one of the 96-well plate included eight negative controls (1% v/v DMSO) and column two eight positive controls (1.5 $\mu$M bedaquiline).

*4.12.6.1. Data Analysis.* Every assay plate contained eight wells with DMSO (1% v/v) as a negative control, which correspond to 100% bacterial growth, and eight wells with bedaquiline (1.5 $\mu$M) as a positive control, in which 100% inhibition of bacterial growth was reached. The controls were used to monitor assay quality through determination of the $Z$-score and for normalizing the data on a plate basis. The $Z$-factor was determined using the following equation:

$$Z' = 1 - \frac{3(SD_{bedaquiline} + SD_{DMSO})}{|M_{bedaquiline} - M_{DMSO}|}$$

where SD is standard deviation and $M$ is mean.

Percent inhibition was calculated as follows:

$$\%\text{growth inhibition} = -100\% \times \frac{signal_{sample} - signal_{DMSO}}{signal_{DMSO} - signal_{bedaquiline}}$$

*4.12.7. MBC Determination against M. abscessus ATCC 19977 pTEC27.* For MBC determination, *M. abscessus* ATCC19977 was incubated in a microplate dilution assay for four days as described above. Subsequently, the MBC was determined by CFU counting: for this purpose, 6-well plates were used, each filled with 4 mL 7H10 agar supplemented with 0.5% v/v glycerol, 10% v/v ADS, and 400 $\mu$g/mL hygromycin. From the drug concentrations where growth inhibition was detected in the microplate dilution assay, 10 $\mu$L (undiluted or diluted 1:100) were plated into one well of the 6-well plates. The colonies were counted after four days of incubation at 37 °C, and the experiment was carried out in triplicate. Based on the result, the



https://doi.org/10.1021/acs.jmedchem.3c00009
J. Med. Chem. 2023, 66, 5079−5098

concentration of CFUs per mL was calculated. The number of CFUs was also determined in the inoculum prior to the four-day incubation.

**4.13. Plasma Stability.** Plasma stability in human and murine plasma was determined at five different time points over 120 min using HPLC-MS/MS analytic. Pooled human plasma, anticoagulated with trisodium citrate, and nonsterile murine plasma, anticoagulated with Li-heparin, were used. The plasma stability is given as the percentage of substance remaining in plasma over time. All measurements were performed using the Shimadzu Prominence HPLC system including a vacuum degasser, gradient pumps, reverse phase column (ZORBAX Extend-C18 column, 2.1x50 mm, 5 $\mu$m), column oven, and autosampler. The HPLC system was coupled with tandem mass API 3000 (AB Sciex). Both positive and negative ion modes of the TurboIonSpray ion source were used. Acquisition and analysis of the data were performed using Analyst 1.6.3 software (PE Sciex).

Incubations of every compound + references (verapamil and propantheline bromide) were carried out in five aliquots of 60 $\mu$L each (one for each time point), in duplicates. Plasma was spiked with test compounds from a 10 mM DMSO stock solution to yield a test concentration of 1 $\mu$M, final DMSO concentration 1% v/v. The aliquots were incubated at 37 °C with shaking at 100 rpm. Five time points over 120 min were analyzed. The reactions were stopped by adding 300 $\mu$L of methanol containing the internal standard with subsequent plasma proteins sedimentation by centrifuging at 6000 rpm for 4 min. Supernatants were analyzed by the HPLC system that was coupled with a tandem mass spectrometer. The percentage of the test compounds remaining after incubation in plasma and their half-lives ($t_{1/2}$) were calculated.

**4.14. Microsomal Stability.** Microsomal stability was determined at five different time points over 40 min using HPLC-MS/MS analytic. Pooled, mixed gender human liver microsomes (XenoTech, H0630/lot N#2010065) and murine liver microsomes (pooled, male BALB/c mice, XenoTech, M3000/lot #1810163) were used.

Microsomal incubations were carried out in 96-well plates in five aliquots of 30 $\mu$L each (one for each time point). The liver microsomal incubation medium composed of phosphate buffer (100 mM, pH 7.4), MgCl2 (3.3 mM), NADPH (3 mM), glucose-6-phosphate (5.3 mM), and glucose-6-phosphate dehydrogenase (0.67 units/mL) with 0.42 mg of liver microsomal protein per mL. In the control reactions, the NADPH-cofactor system was substituted with phosphate buffer. Test compounds (2 $\mu$M, final solvent concentration 1.6% v/v) were incubated with microsomes at 37 °C, shaking at 100 rpm. Five time points over 40 min were analyzed. The reactions were stopped by adding five volumes of 90% v/v acetonitrile with the internal standard to incubation aliquots, followed by protein sedimentation by centrifuging at 5500 rpm for 3 min. Each reaction was performed in duplicates.

Analysis of supernatants was performed using a Shimadzu HPLC system including a vacuum degasser, gradient pumps, reverse phase HPLC column, column oven, and autosampler. Mass spectrometric analysis was performed using an API 3000 mass spectrometer from Applied Biosystems/MDS Sciex (AB Sciex) with a Turbo V ion source and TurboIonspray interface. The TurboIonSpray ion source was used in both positive and negative ion modes. The data acquisition and system control were performed using Analyst 1.6.3 software from AB Sciex.

The microsomal stability is presented as the substances half-life times and intrinsic clearance calculated from their respective elimination constants with the following formula:

$$k_{el} = -\text{slope}$$

$$t_{1/2} = \frac{0.693}{k_{el}}$$

$$\text{Cl}_{int} = \frac{0.693}{t_{1/2}} \times \frac{\mu\text{L}_{incubation}}{\text{mg}_{microsomes}}$$

Eliminations constants were determined in an ln(AUC) versus time plot using linear regression analysis.

**4.15. Determination of Cytotoxicity.** Cytotoxicity was determined using a colorimetric microculture test with sulforhodamine-B (Kiton-Red S, ABCR) as the staining agent. Cells were transferred to a 96-well plate to treat them with increasing compound concentrations (1, 3, 7, 12, 20, and 30 $\mu$M) after 24 h. DMSO/DMF concentrations never exceeded 0.5% v/v, which is nontoxic for the cells. The supernatant was discarded after 72 h; the cells were fixed with 10% v/v TFA and left to rest for 24 h at 4 °C. After washing the cells with a strip, washed cells were stained with a 10 $\mu$M sulforhodamine-B solution (200 $\mu$L) for 20 min before they were washed again with 1% v/v acetic acid solution to remove excess dye. Cells were air-dried overnight. Absorption was determined using a 96-well plate reader (Tecan spectra). Three-independent experiments in triplicate for each were conducted for the given compounds. The averaged data resulted in semilogarithmic dose−effect curves, which were fitted with the Hill equation (GraphPad Prism 5).

**4.16. Nephelometry Solubility Screen.** The solubilities of the final compounds were determined nephelometrically using a NEPHELOstar Plus (BMG Labtech GmbH, GER) device. Stock solutions (25 mM) in DMSO of the compounds were prediluted in pure DMSO. Then, 5 $\mu$L of the predilutions were furtherly diluted in flat-bottom 96-well plates in 245 $\mu$L of phosphate buffered saline (PBS) and mixed and measured immediately (2% v/v DMSO in measured sample). In this way, concentrations of 0.78, 1.56, 3.13, 6.25, 12.5, 25, 50, 100, 150, 200, 250, 300, 350, 400, 450, and 500 $\mu$M were measured. The blank corrected raw data were interpreted with a segmental regression fit utilizing the Omega software (BMG Labtech GmbH, GER). Each compound was analyzed as a quadruplet prepared from the same stock solution.

## ■ ASSOCIATED CONTENT

### Supporting Information

The Supporting Information is available free of charge at https://pubs.acs.org/doi/10.1021/acs.jmedchem.3c00009.

Additional information on the molecular docking studies; 2D visualizations of 3D structures; experimental details of X-ray crystallography; sequence alignment details for *Mtb* and *Mabs* RNAP; antimycobacterial activity of all MMV688845 derivatives derived from OD measurements (not RFP measurements); chemical structures; synthetic protocols, molar equivalents of all reactants, purification procedures, and percentage yields for each synthetic experiment; TLC $R_f$ values for all synthesized compounds, $^1$H-NMR spectra for all synthesized compounds, and respective written documentation; APT-NMR spectra for all *in vitro* tested compounds and respective written documentation; HPLC-purity and respective HPLC traces for all *in vitro* tested; atmospheric pressure chemical ionization mass spectrometry data for all synthesized compounds; high-resolution mass spectrometry data for all *in vitro* tested compounds; molecular formula strings for all described substances; and PDB files for the presented crystal structures (PDF)

Smiles list, synthesis, and characterization of phenylalanine amides active against Mycobacterium abscessus and other mycobacteria (CSV)

Docking substance **14** (PDB)

Docking substance **20** (PDB)

Docking substance **39** (PDB)

Docking substance MMV688845 (PDB)

## ■ AUTHOR INFORMATION

### Corresponding Author

**Adrian Richter** − *Institut für Pharmazie, Martin-Luther-Universität Halle-Wittenberg, Halle (Saale) 06120,*



https://doi.org/10.1021/acs.jmedchem.3c00009
*J. Med. Chem.* 2023, 66, 5079−5098

*Germany*; orcid.org/0000-0002-0062-7896; Email: adrian.richter@pharmazie.uni-halle.de

**Authors**

**Markus Lang** – *Institut für Pharmazie, Martin-Luther-Universität Halle-Wittenberg, Halle (Saale) 06120, Germany*

**Uday S. Ganapathy** – *Center for Discovery and Innovation, Hackensack Meridian Health, Nutley, New Jersey 07110, United States*

**Lea Mann** – *Institut für Pharmazie, Martin-Luther-Universität Halle-Wittenberg, Halle (Saale) 06120, Germany*

**Rana Abdelaziz** – *Institut für Pharmazie, Martin-Luther-Universität Halle-Wittenberg, Halle (Saale) 06120, Germany*

**Rüdiger W. Seidel** – *Institut für Pharmazie, Martin-Luther-Universität Halle-Wittenberg, Halle (Saale) 06120, Germany*; orcid.org/0000-0003-3438-4666

**Richard Goddard** – *Max-Planck-Institut für Kohlenforschung, Mülheim an der Ruhr 45470, Germany*; orcid.org/0000-0003-0357-3173

**Ilaria Sequenzia** – *Institut für Pharmazie, Martin-Luther-Universität Halle-Wittenberg, Halle (Saale) 06120, Germany*

**Sophie Hoenke** – *Institut für Chemie, Martin-Luther-Universität Halle-Wittenberg, Halle (Saale) 06120, Germany*

**Philipp Schulze** – *Max Planck Institut für Kohlenforschung, Mülheim an der Ruhr 45470, Germany*

**Wassihun Wedajo Aragaw** – *Center for Discovery and Innovation, Hackensack Meridian Health, Nutley, New Jersey 07110, United States*

**René Csuk** – *Institut für Chemie, Martin-Luther-Universität Halle-Wittenberg, Halle (Saale) 06120, Germany*; orcid.org/0000-0001-7911-290X

**Thomas Dick** – *Center for Discovery and Innovation, Hackensack Meridian Health, Nutley, New Jersey 07110, United States; Department of Medical Sciences, Hackensack Meridian School of Medicine, Nutley, New Jersey 07110, United States; Department of Microbiology and Immunology, Georgetown University, Washington, District of Columbia 20007, United States*

Complete contact information is available at: https://pubs.acs.org/10.1021/acs.jmedchem.3c00009

**Funding**

This work was funded by the Deutsche Forschungsgemeinschaft (DFG, German Research Foundation)—432291016 (to A.R.), the National Institute of Allergy and Infectious Diseases of the National Institutes of Health under award number R01AI132374, and Mukoviszidose Institut gGmbH (Bonn, Germany) project number 2202 (to A.R.), the research and development arm of the German Cystic Fibrosis Association Mukoviszidose e. V.

**Notes**

The authors declare no competing financial interest.

## ■ ACKNOWLEDGMENTS

We would like to thank Dr. Nadine Taudte and Dr. Jens-Ulrich Rahfeld for providing and maintaining the biosafety level 2 facility, Professor Christian W. Lehmann for providing access to the X-ray diffraction facility at the Max-Planck-Institut für Kohlenforschung (Mülheim an der Ruhr, Germany), Elke Dreher and Heike Schucht for technical assistance, Dr. Christian Ihling and Antje Herbrich-Peters for measuring the HRMS spectra, and Gudrun Hahn for specific rotation measurements. We are grateful to Wei Chang Huang (Taichung Veterans General Hospital, Taichung, Taiwan) for providing *M. abscessus* Bamboo. Thanks are due to Dr. Dieter Ströhl for the NMR spectroscopy.

## ■ ABBREVIATIONS

AAP, *Nα*-aroyl-*N*-aryl-phenylalanine amide; ADP, adenosine diphosphate; APT, attached proton test; ATCC, American type culture collection; BINAP, (2,2′-bis(diphenylphosphino)-1,1′-binaphthyl); BLAST, Basic Local Alignment Search Tool; Boc, *tert*-butoxycarbonyl; CES, carboxylesterase; CFU, colony forming units; CLR, clarithromycin; cLogP, calculated logarithmic octanol–water partition coefficient; DCM, dichloromethane; DIPEA, *N*,*N*-diisopropylethylamine; DMF, dimethylformamide; DMSO, dimethylsulfoxide; *ee*-values, enantiomeric excess values; EtOAc, ethyl acetate; EtOH, ethanol; FBS, fetal bovine serum; LogP, logarithmic octanol–water partition coefficient; *Mabs*, *Mycobacterium abscessus*; MAC, *Mycobacterium avium* complex; MBC, minimum bactericidal concentration; m-CPBA, *m*-chloroperbenzoic acid; MDR, multidrug resistant; MHII, Miller-Hinton broth II; MIC, minimum inhibitory concentration; *Mintra*, *Mycobacterium intracellulare*; MMV, medicines for malaria ventures; MOI, multiplicity of infection; *Msmeg*, *Mycobacterium smegmatis*; *Mtb*, *Mycobacterium tuberculosis*; NTM, nontuberculous mycobacteria; OD, optical density; PBS, phosphate buffered saline; PFA, paraformaldehyde; PMA, phorbol-12-myristate-13-acetate; RFB, rifabutin; RFP, red fluorescent protein; RIF, rifampicin; RNAP, RNA polymerase; RT, room temperature; SAR, structure–activity relationship; T3P, *n*-propanephosphonic acid anhydride; TFA, trifluoro acetic acid; THF, tetrahydrofuran; TLC, thin-layer chromatography

## ■ REFERENCES

(1) World Health Organization. *Module 4: Treatment Drug-Susceptible Tuberculosis Treatment*; World Health Organization, 2022. https://www.who.int/publications/i/item/9789240048126 (accessed 2023–02–21).

(2) World Health Organization. *Global Tuberculosis Report 2022*; World Health Organization 2022. https://www.who.int/publications/i/item/9789240061729 (accessed 2023-01-02).

(3) Dartois, V. A.; Rubin, E. J. Anti-Tuberculosis Treatment Strategies and Drug Development: Challenges and Priorities. *Nat. Rev. Microbiol.* **2022**, *20*, 685–701.

(4) Sharma, A.; de Rosa, M.; Singla, N.; Singh, G.; Barnwal, R. P.; Pandey, A. Tuberculosis: An Overview of the Immunogenic Response, Disease Progression, and Medicinal Chemistry Efforts in the Last Decade toward the Development of Potential Drugs for Extensively Drug-Resistant Tuberculosis Strains. *J. Med. Chem.* **2021**, *64*, 4359–4395.

(5) Ahmed, I.; Tiberi, S.; Farooqi, J.; Jabeen, K.; Yeboah-Manu, D.; Migliori, G. B.; Hasan, R. Non-Tuberculous Mycobacterial Infections—A Neglected and Emerging Problem. *Int. J. Infect. Dis.* **2020**, *92*, S46–S50.

(6) Dartois, V.; Dick, T. Drug Development Challenges in Nontuberculous Mycobacterial Lung Disease: TB to the Rescue. *J. Exp. Med.* **2022**, *219*, No. e20220445.

(7) Gupta, R. S.; Lo, B.; Son, J. Phylogenomics and Comparative Genomic Studies Robustly Support Division of the Genus Mycobacterium into an Emended Genus Mycobacterium and Four Novel Genera. *Front. Microbiol.* **2018**, *9*, 67.

(8) Tortoli, E.; Brown-Elliott, B. A.; Chalmers, J. D.; Cirillo, D. M.; Daley, C. L.; Emler, S.; Andres Floto, R.; Garcia, M. J.; Hoefsloot, W.; Koh, W. J.; Lange, C.; Loebinger, M.; Maurer, F. P.; Morimoto, K.; Niemann, S.; Richter, E.; Turenne, C. Y.; Vasireddy, R.; Vasireddy, S.;

Wagner, D.; Wallace, R. J.; Wengenack, N.; van Ingen, J. Same Meat, Different Gravy: Ignore the New Names of Mycobacteria. *Eur. Respir. J.* **2019**, *54*, 1900795.
(9) Koh, W. J.; Jeong, B. H.; Kim, S. Y.; Jeon, K.; Park, K. U.; Jhun, B. W.; Lee, H.; Park, H. Y.; Kim, D. H.; Huh, H. J.; Ki, C. S.; Lee, N. Y.; Kim, H. K.; Choi, Y. S.; Kim, J.; Lee, S. H.; Kim, C. K.; Shin, S. J.; Daley, C. L.; Kim, H.; Kwon, O. J. Mycobacterial Characteristics and Treatment Outcomes in Mycobacterium Abscessus Lung Disease. *Clin. Infect. Dis.* **2017**, *64*, 309−316.
(10) Jarand, J.; Levin, A.; Zhang, L.; Huitt, G.; Mitchell, J. D.; Daley, C. L. Clinical and Microbiologic Outcomes in Patients Receiving Treatment for Mycobacterium Abscessus Pulmonary Disease. *Clin. Infect. Dis.* **2011**, *52*, 565−571.
(11) Jeon, K.; Kwon, O. J.; Nam, Y. L.; Kim, B.-J.; Kook, Y.-H.; Lee, S.-H.; Young, K. P.; Chang, K. K.; Koh, W.-J. Antibiotic Treatment of Mycobacterium Abscessus Lung Disease. *Am. J. Respir. Crit. Care Med.* **2009**, *180*, 896−902.
(12) Stover, C. K.; Warrener, P.; VanDevanter, D. R.; Sherman, D. R.; Arain, T. M.; Langhorne, M. H.; Anderson, S. W.; Towell, J. A.; Yuan, Y.; McMurray, D. N.; Kreiswirth, B. N.; Barry, C. E.; Baker, W. R. A Small-Molecule Nitroimidazopyran Drug Candidate for the Treatment of Tuberculosis. *Nature* **2000**, *405*, 962−966.
(13) Diacon, A. H.; Pym, A.; Grobusch, M. P.; de los Rios, J. M.; Gotuzzo, E.; Vasilyeva, I.; Leimane, V.; Andries, K.; Bakare, N.; de Marez, T.; Haxaire-Theeuwes, M.; Lounis, N.; Meyvisch, P.; de Paepe, E.; van Heeswijk, R. P. G.; Dannemann, B. Multidrug-Resistant Tuberculosis and Culture Conversion with Bedaquiline. *N. Engl. J. Med.* **2014**, *371*, 723−732.
(14) Diacon, A. H.; Pym, A.; Grobusch, M.; Patientia, R.; Rustomjee, R.; Page-Shipp, L.; Pistorius, C.; Krause, R.; Bogoshi, M.; Churchyard, G.; Venter, A.; Allen, J.; Palomino, J. C.; de Marez, T.; van Heeswijk, R. P. G.; Lounis, N.; Meyvisch, P.; Verbeeck, J.; Parys, W.; de Beule, K.; Andries, K.; Neeley, D. F. M. The Diarylquinoline TMC207 for Multidrug-Resistant Tuberculosis. *N. Engl. J. Med.* **2009**, *360*, 2397−2405.
(15) Mudde, S. E.; Upton, A. M.; Lenaerts, A.; Bax, H. I.; de Steenwinkel, J. E. M. Delamanid or Pretomanid? A Solomonic Judgement! *J. Antimicrob. Chemother.* **2022**, *77*, 880−902.
(16) Manjunatha, U.; Boshoff, H. I. M.; Barry, C. E. The Mechanism of Action of PA-824. *Commun. Integr. Biol.* **2009**, *2*, 215−218.
(17) Conradie, F.; Diacon, A. H.; Ngubane, N.; Howell, P.; Everitt, D.; Crook, A. M.; Mendel, C. M.; Egizi, E.; Moreira, J.; Timm, J.; McHugh, T. D.; Wills, G. H.; Bateson, A.; Hunt, R.; van Niekerk, C.; Li, M.; Olugbosi, M.; Spigelman, M. Treatment of Highly Drug-Resistant Pulmonary Tuberculosis. *N. Engl. J. Med.* **2020**, *382*, 893−902.
(18) Brode, S. K.; Daley, C. L.; Marras, T. K. The Epidemiologic Relationship between Tuberculosis and Non-Tuberculous Mycobacterial Disease: A Systematic Review. *Int. J. Tuberc. Lung Dis.* **2014**, *18*, 1370−1377.
(19) Lopeman, R. C.; Harrison, J.; Desai, M.; Cox, J. A. G. *Mycobacterium Abscessus*: Environmental Bacterium Turned Clinical Nightmare. *Microorganisms* **2019**, *7*, 90.
(20) Boudehen, Y. M.; Kremer, L. Mycobacterium Abscessus. *Trends Microbiol.* **2021**, *29*, 951−952.
(21) Victoria, L.; Gupta, A.; Gómez, J. L.; Robledo, J. Mycobacterium Abscessus Complex: A Review of Recent Developments in an Emerging Pathogen. *Front. Cell. Infect. Microbiol.* **2021**, *11*, 338.
(22) Malenfant, J. H.; Brewer, T. F. Rifampicin Mono-Resistant Tuberculosis—A Review of an Uncommon But Growing Challenge for Global Tuberculosis Control. *Open Forum Infect. Dis.* **2021**, *8*, ofab018.
(23) Rominski, A.; Roditscheff, A.; Selchow, P.; Böttger, E. C.; Sander, P. Intrinsic Rifamycin Resistance of Mycobacterium Abscessus Is Mediated by ADP-Ribosyltransferase MAB_0591. *J. Antimicrob. Chemother.* **2017**, *72*, 376−384.
(24) Ganapathy, U. S.; Lan, T.; Krastel, P.; Lindman, M.; Zimmerman, M. D.; Ho, H. P.; Sarathy, J. P.; Evans, J. C.; Dartois, V.; Aldrich, C. C.; Dick, T. Blocking Bacterial Naphthohydroquinone Oxidation and Adpribosylation Improves Activity of Rifamycins against Mycobacterium Abscessus. *Antimicrob. Agents Chemother.* **2021**, *65*, e0097821.
(25) Aziz, D. B.; Low, J. L.; Wu, M. L.; Gengenbacher, M.; Teo, J. W. P.; Dartois, V.; Dick, T. Rifabutin Is Active against *Mycobacterium Abscessus* Complex. *Antimicrob. Agents Chemother.* **2017**, *61*, e00155−e00117.
(26) Dick, T.; Shin, S. J.; Koh, W. J.; Dartois, V.; Gengenbacher, M. Rifabutin Is Active against Mycobacterium Abscessus in Mice. *Antimicrob. Agents Chemother.* **2020**, *64*, e00155−e00117.
(27) Lan, T.; Ganapathy, U. S.; Sharma, S.; Ahn, Y.-M.; Zimmerman, M.; Molodtsov, V.; Hegde, P.; Gengenbacher, M.; Ebright, R. H.; Dartois, V.; Freundlich, J. S.; Dick, T.; Aldrich, C. C. Redesign of Rifamycin Antibiotics to Overcome ADP-Ribosylation-Mediated Resistance. *Am. Ethnol.* **2022**, *134*, No. e202211498.
(28) Paulowski, L.; Beckham, K. S. H.; Johansen, M. D.; Berneking, L.; Van, N.; Degefu, Y.; Staack, S.; Sotomayor, F. V.; Asar, L.; Rohde, H.; Aldridge, B. B.; Aepfelbacher, M.; Parret, A.; Wilmanns, M.; Kremer, L.; Combrink, K.; Maurer, F. P. C25-Modified Rifamycin Derivatives with Improved Activity against Mycobacterium Abscessus. *Proc. Natl. Acad. Sci. U. S. A.* **2022**, *1*, 1−13.
(29) Ballell, L.; Bates, R. H.; Young, R. J.; Alvarez-Gomez, D.; Alvarez-Ruiz, E.; Barroso, V.; Blanco, D.; Crespo, B.; Escribano, J.; González, R.; Lozano, S.; Huss, S.; Santos-Villarejo, A.; Martín-Plaza, J. J.; Mendoza, A.; Rebollo-Lopez, M. J.; Remuiñan-Blanco, M.; Lavandera, J. L.; Pérez-Herran, E.; Gamo-Benito, F. J.; García-Bustos, J. F.; Barros, D.; Castro, J. P.; Cammack, N. Fueling Open-Source Drug Discovery: 177 Small-Molecule Leads against Tuberculosis. *ChemMedChem* **2013**, *8*, 313−321.
(30) Low, J. L.; Wu, M. L.; Aziz, D. B.; Laleu, B.; Dick, T. Screening of TB Actives for Activity against Nontuberculous Mycobacteria Delivers High Hit Rates. *Front. Microbiol.* **2017**, *8*, 1539.
(31) Lin, W.; Mandal, S.; Degen, D.; Liu, Y.; Ebright, Y. W.; Li, S.; Feng, Y.; Zhang, Y.; Mandal, S.; Jiang, Y.; Liu, S.; Gigliotti, M.; Talaue, M.; Connell, N.; Das, K.; Arnold, E.; Ebright, R. H. Structural Basis of Mycobacterium Tuberculosis Transcription and Transcription Inhibition. *Mol. Cell* **2017**, *66*, 169−179.
(32) Ebright, Richard H.; Ebright, Yon W.; Mandal, Soma; Wilde, Richard; Li, S. Preparation of N-Alpha-Aroyl-N-Aryl-Phenylalaninamides as Inhibitors of Bacterial RNA Polymerase and as Antibacterials. WO2015120320 A1 2015-08-13, 2015.
(33) Mann, L.; Lang, M.; Schulze, P.; Halz, J. H.; Csuk, R.; Hoenke, S.; Seidel, R. W.; Richter, A. Racemization-Free Synthesis of Nα-2-Thiophenoyl-Phenylalanine-2-Morpholinoanilide Enantiomers and Their Antimycobacterial Activity. *Amino Acids* **2021**, *53*, 1187−1196.
(34) Mann, L.; Ganapathy, U. S.; Abdelaziz, R.; Lang, M.; Zimmerman, M. D.; Dartois, V.; Dick, T.; Richter, A.; Tiwari, S. In Vitro Profiling of the Synthetic RNA Polymerase Inhibitor MMV688845 against Mycobacterium Abscessus. *Microbiol. Spectrum* **2022**, *10*, e0276022.
(35) Dunetz, J. R.; Xiang, Y.; Baldwin, A.; Ringling, J. General and Scalable Amide Bond Formation with Epimerization-Prone Substrates Using T3P and Pyridine. *Org. Lett.* **2011**, *13*, 5048−5051.
(36) Li, H.; Jiang, X.; Ye, Y.-H.; Fan, C.; Romoff, T.; Goodman, M. 3-(Diethoxyphosphoryloxy)-1,2,3-Benzotriazin-4(3H)-One (DEPBT): A New Coupling Reagent with Remarkable Resistance to Racemization. 1999, *1*, 91−94, .
(37) Brewster, W. K. Thieno-Pyrimidine Compounds Having Fungicidal Activity. US 2006/0089370 A1, 2006.
(38) Allwood, D. M.; Blakemore, D. C.; Brown, A. D.; Ley, S. v. Metal-Free Coupling of Saturated Heterocyclic Sulfonylhydrazones with Boronic Acids. *J. Org. Chem.* **2014**, *79*, 328−338.
(39) Barluenga, J.; Tomás-Gamasa, M.; Aznar, F.; Valdés, C. Metal-Free Carbon−Carbon Bond-Forming Reductive Coupling between Boronic Acids and Tosylhydrazones. *Nat. Chem.* **2009**, *1*, 494−499.
(40) Thiemann, T. Thiophene S-Oxides. *Chalcogen Chem*; IntechOpen 2019, .
(41) Elsawy, M. A.; Hewage, C.; Walker, B. Racemisation of N-Fmoc Phenylglycine under Mild Microwave-SPPS and Conventional Stepwise SPPS Conditions: Attempts to Develop Strategies for Overcoming This. *J. Pept. Sci.* **2012**, *18*, 302−311.



https://doi.org/10.1021/acs.jmedchem.3c00009
J. Med. Chem. 2023, 66, 5079−5098

(42) Sturabotti, E.; Vetica, F.; Toscano, G.; Calcaterra, A.; Martinelli, A.; Migneco, L. M.; Leonelli, F. N-Acetyl-l-Phenylalanine Racemization during TBTU Amidation: An In-Depth Study for the Synthesis of Anti-Inflammatory 2-(N-Acetyl)-l-Phenylalanylamido-2-Deoxy-d-Glucose (NAPA). *Molecules* **2023**, *28*, 581.
(43) Al-Warhi, T. I.; Al-Hazimi, H. M. A.; El-Faham, A. Recent Development in Peptide Coupling Reagents. *J. Saudi Chem. Soc.* **2012**, *16*, 97−116.
(44) Bodanszky, M. *Principles of Peptide Synthesis*; Springer.
(45) Antonovics, I.; Young, G. T. Amino-Acids and Peptides. Part XXV. The Mechanism of the Base-Catalysed Racemisation of the p-Nitrophenyl Esters of Acylpeptides. *J. Chem. Soc. C* **1967**, *99*, 595−601.
(46) García, A. L. L. T3P: A Convenient and Useful Reagent in Organic Synthesis. *Synlett* **2007**, *2007*, 1328−1329.
(47) Harada, H. Azolecarboxamide Derivative. WO 2007/123269 A1, 2017.
(48) Midgley, L.; Bourhis, L. J.; Dolomanov, O. v.; Grabowsky, S.; Kleemiss, F.; Puschmann, H.; Peyerimhoff, N. Vanishing of the Atomic Form Factor Derivatives in Non-Spherical Structural Refinement - a Key Approximation Scrutinized in the Case of Hirshfeld Atom Refinement. *Acta Crystallogr., Sect. A: Found. Adv.* **2021**, *77*, 519−533.
(49) Kleemiss, F.; Dolomanov, O. v.; Bodensteiner, M.; Peyerimhoff, N.; Midgley, L.; Bourhis, L. J.; Genoni, A.; Malaspina, L. A.; Jayatilaka, D.; Spencer, J. L.; White, F.; Grundkötter-Stock, B.; Steinhauer, S.; Lentz, D.; Puschmann, H.; Grabowsky, S. Accurate Crystal Structures and Chemical Properties from NoSpherA2. *Chem. Sci.* **2021**, *12*, 1675−1692.
(50) Chaturvedi, V.; Dwivedi, N.; Tripathi, R. P.; Sinha, S. Evaluation of Mycobacterium Smegmatis as a Possible Surrogate Screen for Selecting Molecules Active against Multi-Drug Resistant Mycobacterium Tuberculosis. *J. Gen. Appl. Microbiol.* **2007**, *53*, 333−337.
(51) T, J. A. S.; J, R.; Rajan, A.; Shankar, V. Features of the Biochemistry of Mycobacterium Smegmatis, as a Possible Model for Mycobacterium Tuberculosis. *J. Infect. Public Health* **2020**, *13*, 1255−1264.
(52) Tortoli, E. Microbiological Features and Clinical Relevance of New Species of the Genus Mycobacterium. *Clin. Microbiol. Rev.* **2014**, *27*, 727−752.
(53) Weiss, C. H.; Glassroth, J. Pulmonary Disease Caused by Nontuberculous Mycobacteria. *Expert Rev. Respir. Med.* **2012**, *6*, 597−613.
(54) Henkle, E.; Hedberg, K.; Schafer, S. D.; Winthrop, K. L. Surveillance of Extrapulmonary Nontuberculous Mycobacteria Infections, Oregon, USA, 2007−2012. *Emerging Infect. Dis.* **2017**, *23*, 1627−1630.
(55) To, K.; Cao, R.; Yegiazaryan, A.; Owens, J.; Venketaraman, V. General Overview of Nontuberculous Mycobacteria Opportunistic Pathogens: Mycobacterium Avium and Mycobacterium Abscessus. *J. Clin. Med.* **2020**, *9*, 2541.
(56) Koh, W. J.; Jeong, B. H.; Jeon, K.; Lee, N. Y.; Lee, K. S.; Woo, S. Y.; Shin, S. J.; Kwon, O. J. Clinical Significance of the Differentiation Between Mycobacterium Avium and Mycobacterium Intracellulare in M Avium Complex Lung Disease. *Chest* **2012**, *142*, 1482−1488.
(57) Ricotta, E. E.; Adjemian, J.; Blakney, R. A.; Lai, Y. L.; Kadri, S. S.; Prevots, D. R. Extrapulmonary Nontuberculous Mycobacteria Infections in Hospitalized Patients, United States, 2009−2014. *Emerging Infect. Dis.* **2021**, *27*, 845−852.
(58) Ollinger, J.; Kumar, A.; Roberts, D. M.; Bailey, M. A.; Casey, A.; Parish, T. A High-Throughput Whole Cell Screen to Identify Inhibitors of Mycobacterium Tuberculosis. *PLoS One* **2019**, *14*, No. e0205479.
(59) Richter, A.; Shapira, T.; Av-Gay, Y. THP-1 and Dictyostelium Infection Models for Screening and Characterization of Anti-Mycobacterium Abscessus Hit Compounds. *Antimicrob. Agents Chemother.* **2019**, *64*, e01601−e01619.
(60) Martin-Smith, M.; Reid, S. T. Biological Activity in Compounds Possessing Thiophen Rings. *J. Med. Chem.* **1959**, *1*, 507−564.
(61) Maurer, F. P.; Bruderer, V. L.; Ritter, C.; Castelberg, C.; Bloemberg, G. v.; Böttger, E. C. Lack of Antimicrobial Bactericidal Activity in Mycobacterium Abscessus. *Antimicrob. Agents Chemother.* **2014**, *58*, 3828−3836.
(62) Heifets, L. Qualitative and Quantitative Drug-Susceptibility Tests in Mycobacteriology. *Am. Rev. Respir. Dis.* **1987**, *137*, 1217−1222.
(63) Bahar, F. G.; Ohura, K.; Ogihara, T.; Imai, T. Species Difference of Esterase Expression and Hydrolase Activity in Plasma. *J. Pharm. Sci.* **2012**, *101*, 3979−3988.
(64) Bathelt, C. M.; Ridder, L.; Mulholland, A. J.; Harvey, J. N. Aromatic Hydroxylation by Cytochrome P450: Model Calculations of Mechanism and Substituent Effects. *J. Am. Chem. Soc.* **2003**, *125*, 15004−15005.
(65) Cerny, M. A. Prevalence of Non-Cytochrome P450-Mediated Metabolism in Food and Drug Administration-Approved Oral and Intravenous Drugs: 2006-2015. *Drug Metab. Dispos.* **2016**, *44*, 1246−1252.
(66) Bradshaw, P. R.; Wilson, I. D.; Gill, R. U.; Butler, P. J.; Dilworth, C.; Athersuch, T. J. Metabolic Hydrolysis of Aromatic Amides in Selected Rat, Minipig, and Human In Vitro Systems. *Sci. Rep.* **2018**, *8*, 2405.
(67) Sommerwerk, S.; Heller, L.; Kuhfs, J.; Csuk, R. Selective Killing of Cancer Cells with Triterpenoic Acid Amides - The Substantial Role of an Aromatic Moiety Alignment. *Eur. J. Med. Chem.* **2016**, *122*, 452−464.
(68) Heller, L.; Knorrscheidt, A.; Flemming, F.; Wiemann, J.; Sommerwerk, S.; Pavel, I. Z.; Al-Harrasi, A.; Csuk, R. Synthesis and Proapoptotic Activity of Oleanolic Acid Derived Amides. *Bioorg. Chem.* **2016**, *68*, 137−151.
(69) Csuk, R.; Barthel, A.; Sczepek, R.; Siewert, B.; Schwarz, S. Synthesis, Encapsulation and Antitumor Activity of New Betulin Derivatives. *Arch. Pharm. Chem. Life Sci.* **2011**, *344*, 37−49.
(70) Savjani, K. T.; Gajjar, A. K.; Savjani, J. K. Drug Solubility: Importance and Enhancement Techniques. *Int. Scholarly Res. Not.* **2012**, *2012*, 1−10.
(71) Congreve, M.; Carr, R.; Murray, C.; Jhoti, H. A "Rule of Three" for Fragment-Based Lead Discovery? *Drug Discovery Today* **2003**, *8*, 876−877.
(72) Bevan, C. D.; Lloyd, R. S. A High-Throughput Screening Method for the Determination of Aqueous Drug Solubility Using Laser Nephelometry in Microtiter Plates. *Anal. Chem.* **2000**, *72*, 1781−1787.
(73) Richter, A.; Strauch, A.; Chao, J.; Ko, M.; Av-Gay, Y. Screening of Preselected Libraries Targeting Mycobacterium Abscessus for Drug Discovery. *Antimicrob. Agents Chemother.* **2018**, *62*, 1−11.
(74) Yang, X.; Wedajo, W.; Yamada, Y.; Dahlroth, S. L.; Neo, J. J. L.; Dick, T.; Chui, W. K. 1,3,5-Triazaspiro[5.5]Undeca-2,4-Dienes as Selective Mycobacterium Tuberculosis Dihydrofolate Reductase Inhibitors with Potent Whole Cell Activity. *Eur. J. Med. Chem.* **2018**, *144*, 262−276.



https://doi.org/10.1021/acs.jmedchem.3c00009
J. Med. Chem. 2023, 66, 5079−5098

## 3.4 Publication III

### Determination of bactericidal activity against 3HC-2-Tre-labelled *Mycobacterium abscessus* (*Mycobacteroides abscessus*) by automated fluorescence microscopy

Lea Mann, Fabienne Siersleben, Markus Lang, Adrian Richter.

Elsevier, Journal of Microbiological Methods, Mann *et al.*, Determination of bactericidal activity against 3HC-2-Tre-labelled *Mycobacterium abscessus* (*Mycobacteroides abscessus*) by automated fluorescence microscopy J Microbiol Methods 224:107002,
 DOI: 10.1016/j.mimet.2024.107002

**Summary**

This paper presents a new method for the determination of MBCs against *M. abscessus*. The method is based on fluorescence microscopy and can be performed in a 96-well plate format. The aim of the work was to establish a method that is simpler, faster and less prone to pipetting errors than plating on agar. A fluorescent dye, a trehalose-coupled chromophore, is used to stain the bacteria. The new method was used to determine the MBC of several antibiotics against *M. abscessus*, with and without bactericidal activity. Rifabutin, moxifloxacin, amikacin, clarithromycin and bedaquiline were analysed. Compounds with bactericidal activity such as MMV688845 and a more active derivative of the compound were characterised. The results were compared with the method of plating on agar and the resulting colony forming unit (CFU) count in the laboratory; data from the literature were used for an independent comparison.

Preliminary work and first data on the staining of *M. abscessus* with 2-(6-(diethylamino)benzofuran-2-yl)-3-hydroxy-4*H*-chromen-4-one-conjugated trehalose (3HC-2-Tre) have been published in the following article:

Richter A, Goddard R, Mann L, Siersleben F, Seidel RW. 2024. Structural characterization of a 3-hydroxychromone dye trehalose conjugate for fluorescent labelling of mycobacteria. J Mol Struct 1298:1–8.

**Own contribution:**

Writing, review & editing, writing of the original draft, visualization, software, methodology, investigation and data curation.

In this publication, all results presented are from experiments carried out by the first author. The method was adopted and further improved for *M. abscessus* on the basis of Fabienne Sierslebens diploma thesis (supervised as part of my PhD).

Journal of Microbiological Methods 224 (2024) 107002

Contents lists available at ScienceDirect

Journal of Microbiological Methods

journal homepage: www.elsevier.com/locate/jmicmeth

# Determination of bactericidal activity against 3HC-2-Tre-labelled *Mycobacterium abscessus* (*Mycobacteroides abscessus*) by automated fluorescence microscopy

Lea Mann, Fabienne Siersleben, Markus Lang, Adrian Richter *

*Institut für Pharmazie, Martin-Luther-Universität Halle-Wittenberg, Wolfgang-Langenbeck-Str. 4, 06120 Halle (Saale), Germany*

ARTICLE INFO

*Keywords:*
*Mycobacterium abscessus*
*Mycobacteroides abscessus*
MBC
Bactericidal activity
2-(6-(diethylamino)benzofuran-2-yl)-3-hydroxy-4H-chromen-4-one Trehalose (3HC-2-Tre)
Fluorescence labelling

ABSTRACT

The minimum bactericidal concentration (MBC) of antibiotics is an important parameter for the potency of a drug in eradicating a bacterium as well as an important measure of the potential of a drug candidate in research and development. We have established a fluorescence-based microscopy method for the determination of MBCs against the non-tuberculous mycobacterium *Mycobacterium abscessus* (*Mycobacteroides abscessus*) to simplify and accelerate the performance of MBC determination compared to counting colony forming units on agar. Bacteria are labelled with the trehalose-coupled dye 3HC-2-Tre and analysed in a 96-well plate. The results of the new method are consistent with MBC determination by plating on agar. The method was used to evaluate the bactericidality of the antibiotics rifabutin, moxifloxacin, amikacin, clarithromycin and bedaquiline. Bactericidal effects against *M. abscessus* were observed, which are consistent with literature data.

## 1. Introduction

*Mycobacterium abscessus* (*Mycobacteroides abscessus*) is a fast-growing, multidrug-resistant mycobacterium classified as a non-tuberculous mycobacterium (NTM). It is an opportunistic pathogen responsible for severe respiratory infections in patients with pre-existing medical conditions such as immunosuppression or cystic fibrosis (Baldwin et al., 2019). In addition, *M. abscessus* can cause skin and soft tissue infections. It is difficult to treat infections caused by *M. abscessus* because the pathogen is resistant to a large number of antibiotics (Boudehen and Kremer, 2021). For example, the cornerstones of tuberculosis therapy, rifampicin and isoniazid, are not effective against *M. abscessus* (Wu et al., 2018) and are not used clinically.

The therapeutic regimen for *M. abscessus* infection depends highly on the subspecies and individual strain (Daley et al., 2020). It usually consists of at least three antibiotics. The combination is based on a macrolide combined with a parenteral aminoglycoside and either cefoxitin, imipenem or tigecycline. The duration of therapy is usually 12 months and the defined end point of sputum conversion is rarely achieved (Wu et al., 2018). This uncertain success in therapy, together with several antibiotics causing side effects negatively affects the patient's adherence and compliance (Wu et al., 2018; Holt and Baird, 2023).

A major challenge in the treatment of *M. abscessus* is the lack of antibiotics with bactericidal activity against the pathogen, *e.g.* clarithromycin and tigecycline, which show no or only weak bactericidal activity (Maurer et al., 2014) against *M. abscessus*. To improve *M. abscessus* therapy and to shorten the duration of treatment, it is necessary to include antibiotics with sterilising properties in the treatment regimen. The established method - determination of bactericidal activity by colony counting on agar - is time-consuming and labour-intensive, which limits its applicability in clinical microbiology, but also during early drug development. The transfer of bacterial suspensions to agar plates restricts the number of replicates and usability. For this reason, we have developed a robust and efficient method to analyse whether substances have bactericidal properties against *M. abscessus*.

The goal of the study is to establish a straightforward experimental procedure that allows efficient analysis of compounds in 96-well plate format without the need for manual plating or colony counting. In order to accomplish this, we use a fluorescent trehalose probe 2-(6-(diethylamino)benzofuran-2-yl)-3-hydroxy-4*H*-chromen-4-one Trehalose (3HC-2-Tre), which is capable of selectively staining mycobacteria, *Mycobacterium tuberculosis*, *Mycobacterium smegmatis*, *Mycobacterium aurum* or *M. abscessus* (Kamariza et al., *2018*; Richter et al., *2024*; Kamariza et al., *2021*). Trehalose conjugates are a recent development

* Corresponding author.
*E-mail address:* adrian.richter@pharmazie.uni-halle.de (A. Richter).

https://doi.org/10.1016/j.mimet.2024.107002
Received 30 May 2024; Received in revised form 18 July 2024; Accepted 18 July 2024
Available online 20 July 2024

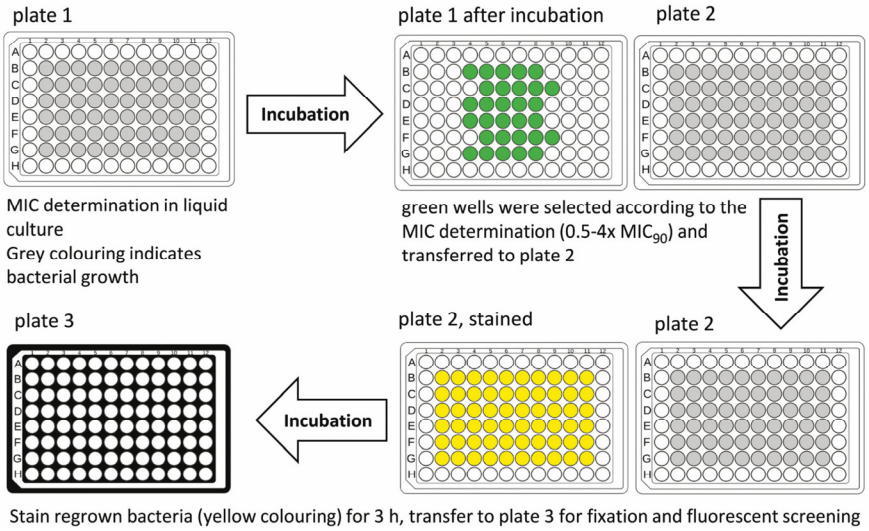


**Fig. 1.** Visualisation of the MBC determination by 3HC-2-Tre staining.

that are of great use for fluorescence microscopic detection of mycobacteria: Kamariza et al. (2018) first published 4-*N*,*N*-Dimethylamino-1,8-naphthalimide conjugate of trehalose (DMN-Tre) as a dye that is selectively incorporated into the mycobacterial cell wall by the enzyme Ag85 (Kamariza et al., 2018). Additionally, DMN-Tre labelling was reported to show comparable results to the commonly used auramine staining. In 2020, Sahile et al. published that DMN-Tre is capable of labelling intracellular *M. tuberculosis* (Sahile et al., 2020). In 2021, Kamariza et al. published two closely related dyes, 3HC-3-Tre and 3HC-2-Tre, for which the fluorescence intensity was further enhanced. Importantly, a straightforward synthetic procedure to make the dyes easily accessible was published (Kamariza et al., 2021). Here we present a method we have developed to simplify the determination of MBC against *M. abscessus*. Results will also be presented to demonstrate that the method provides results comparable to MBC determination by CFU (colony forming units) counting.

## 2. Material and methods

### 2.1. Bacteria and culture medium

Stocks of *M. abscessus* subsp. *abscessus* type strain ATCC 19977 were cultivated in complete 7H9 broth (Sigma Aldrich, St. Louis, MO, USA) and stored as cryo stocks with approximately 15% glycerol at −80 °C. The cryo stocks were used to inoculate complete 7H9 broth supplemented with 10% ADS (ADS supplement is a filter-sterilized solution of 0.8% sodium chloride, 5.0% bovine serum albumin, and 2.0% dextrose in purified water) and 0.05% polysorbate 80. The culture volume was 10 mL in a 50 mL Falcon tube, which was shaken in an incubator at 37 °C. Solid cultures were grown on 7H10 medium supplemented with 0.5% glycerol and 10% ADS (Mann et al., 2022).

### 2.2. $MIC_{90}$ determination in 7H9 by $OD_{600}$ measurement

MICs were determined against *M. abscessus* ATCC 19977 utilizing a broth microdilution method in 7H9 containing 10% ADS and 0.05% polysorbate 80. A nine-point 2-fold serial dilution of each compound was prepared in 96-well flat-bottom plates (Sarstedt, 3924500, Nümbrecht, Germany) with a final volume of 100 µL. Column 2 of the 96-well plate included eight negative controls, column 3 contained eight positive controls. Column 1 contained only medium as a sterile control. The concentration of the inoculum was $5*10^7$ CFU/mL (an $OD_{600}$ (optical density) of 0.1 is equal to $1*10^8$ CFU/mL). The starting inoculum was diluted from a preculture at the mid-log phase ($OD_{600}$, 0.2 to 0.8). The plates were sealed with Parafilm and incubated for 3 days at 37 °C. After incubation, the plates were analysed by OD measurement at 550 nm (BMG labtech Fluostar Optima, Offenburg, Germany). The assay was performed in duplicate.

### 2.3. Calculation of the $MIC_{90}$

Each assay plate contained eight wells with DMSO (1%) as a negative control, which correspond to 100% bacterial growth, and eight wells with amikacin (100 µM) as a positive control, in which 100% inhibition of bacterial growth was reached. The controls were used to monitor assay quality through the determination of the Z score (>0.6) and for normalizing the data. The Z factor was determined using the following formula (Richter et al., 2018):

$$Z' = 1 - \frac{3\left(SD_{\text{positive control}} + SD_{\text{DMSO}}\right)}{M_{\text{positive control}} - M_{\text{DMSO}}}$$

where SD is the standard deviation and M is the mean.

Percent inhibition was calculated as follows:

$$\%\text{inhibition} = -100\% \times \frac{\text{signal(sample)} - \text{signal(DMSO)}}{\text{signal(DMSO)} - \text{signal(positive control)}}$$

The lowest concentration exceeding 90% inhibition was considered as the $MIC_{90}$ value.

### 2.4. MBC determination on agar

For MBC (minimal bactericidal concentration) determination, *M. abscessus* ATCC 19977 was incubated in a microplate assay as described above. Subsequently, the MBC was determined by CFU counting. Petri dishes filled with 7H10 agar supplemented with 0.5% glycerol, 10% ADS were used for this purpose. Serial 10-fold dilutions were prepared in phosphate-buffered saline (PBS) containing 0.025% polysorbate 80. 10 µL of each concentration were pipetted onto the agar

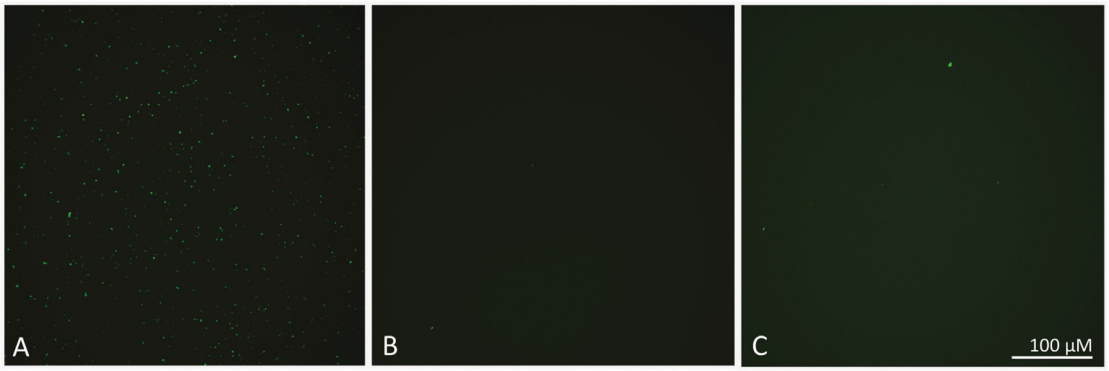


**Fig. 2.** Microscopic images (10× magnification) of fluorescent *M. abscessus* bacteria (green) taken with CX5 (Thermo Fisher Scientific). A: Inoculum, B: 100 µM rifabutin, C: 50 µM MMV688845. (For interpretation of the references to colour in this figure legend, the reader is referred to the web version of this article.)

dish. The colonies were counted after 3 days of incubation at 37 °C and the experiment was performed in triplicate. The concentration in CFU per mL was calculated based on the number of CFU in the inoculum after the three-day incubation from day 0.

### 2.5. Labelling of *M. abscessus* cells with trehalose conjugate 3HC-2-Tre

The synthesis of the compound 3HC-2-Tre was described by Richter et al. 2023 (Richter et al., 2023), following the method previously reported by Kamariza et al. 2021 (Kamariza et al., 2021). After MIC determination (as described above) 1 µL of each well with >90% growth inhibition was transferred in a second 96-well plate containing 100 µL of 7H9 medium supplemented with 10% ADS and 0.05% polysorbate 80 per well. The bacteria were incubated at 37 °C for two days.

Afterwards 1 µL of 3HC-2-Tre (10 mM in DMSO) was added to each well resulting in a final dye concentration of 100 µM followed by incubation at 37 °C for 3 h. After incubation, 1 µL of each well was transferred to a black, clear, flat-bottom 96-well plate (Greiner bio one, 6550909, Frickenhausen, Germany) containing 199 µL of filtered 4% paraformaldehyde solution (PFA) in PBS for fixation. Fluorescence microscopy was then performed using a Thermo Fisher Scientific CellInsight CX5 instrument (Waltham, MA, USA). Samples were analysed at $\lambda_{ex} = 485$ nm and $\lambda_{em} = 510–531$ nm. Images were acquired for 21 fields in one well. The valid object count of the GFP filter was matched to the number of bacteria counted. The valid field count has been used as a check that all fields are in focus of the microscope.

## 3. Results

### 3.1. Preparation of 96-well plates and microscopic readout

The MBC method developed in this study is based on a microplate dilution MIC assay for *M. abscessus*, as shown in Fig. 1. In contrast to the CFU assay, no plating on agar is performed and the bacteria that are still viable after incubation with a drug are cultivated in liquid medium.

After an initial 3-day incubation with a serial drug dilution on plate 1 and determination of $MIC_{90}$ values, the bacteria are resuspended and wells with drug concentrations of 0.5×, at or above the $MIC_{90}$ are transferred to plate 2 containing drug-free medium. This step is followed by a second incubation period of 48 h at 37 °C for growth of any still viable *M. abscessus* cells. During the transfer from plate 1 to plate 2, there is a 100-fold dilution, which reduces the drug concentration below the $MIC_{90}$ to subinhibitory concentrations. In this way, the influence of residual antibiotics can be excluded as an error for drug concentrations close to the MIC.

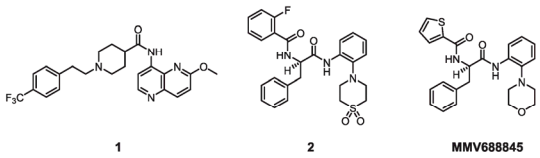


**Scheme 1.** Structures of experimental compounds 1 (Beuchel et al., 2022), 2 (Lang et al., 2023) and MMV688845 (Mann et al., 2022; Ballell et al., 2013).

After the 48 h incubation period of plate 2, 3HC-2-Tre is added at a concentration of 100 µM to stain the bacteria. After 3 h incubation for the sufficient staining the wells are homogenized by pipetting, and an aliquot is transferred to plate 3 containing 4% PFA in PBS for fixation. This second dilution step is necessary to reduce the background fluorescence that is otherwise caused by the dye. Plate 3 (a clear flat-bottom 96-well plate) can be used for analysis by automated fluorescence microscopy.

Automated fluorescence microscopy was performed with a CellInsight CX5 under use of the GFP channel, for determination of the object count (Sahile et al., 2020). However, the method described here is not dependent on a particular dye, and is rather intended to allow a free choice of dye to suit equipment and experience.

To determine the number of bacteria in the inoculum, the inoculum

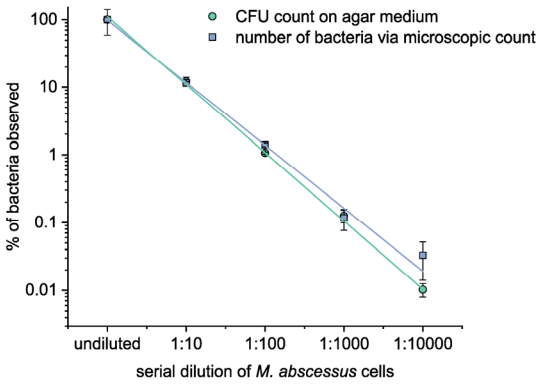


**Fig. 3.** Comparison of CFU with microscopic count of *M abscessus* in a tenfold dilution series.

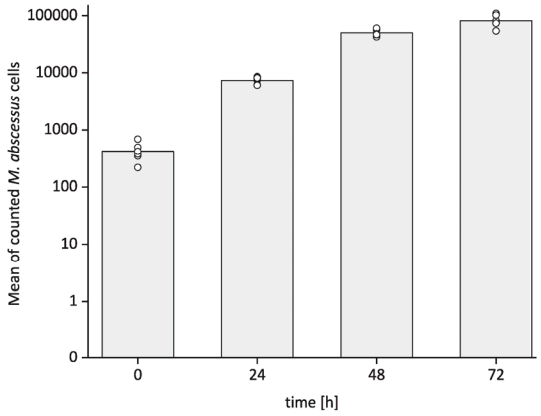


**Fig. 4.** Mean of 3HC-2-Tre labelled *M. abscessus* cells after the respective time of bacterial growth.

is transferred directly to plate 2 without the initial 3-day incubation on plate 1. After two days of incubation, the bacteria are stained and examined microscopically as described. The object count obtained in this way represents 100% viable bacteria and the object counts obtained from the MBC assay are normalised to this value, similar to the evaluation of the CFU assay.

Fig. 2 shows the microscopic images of the bacteria stained with 3HC-2-Tre after incubation with 100 µM rifabutin or 50 µM MMV688845 (Scheme 1) compared to the inoculum. The image data after incubation with the active substances already show a clear decrease in the number of objects, which indicates a bactericidal effect in this assay.

### 3.2. Correlation of CFU on agar and microscopic count

Fig. 3 shows the results of a comparison between the CFU count on agar and the microscopic count of fluorescent labelled bacteria. The aim is to show that, in an identical dilution series, both methods can reliably detect the number of bacteria over the entire dilution range, from undiluted culture to 1:10,000 dilution. The bacterial count in the undiluted culture (determined using CFU count on agar or fluorescence microscopy) is defined as 100%. For the experiment the starting culture was diluted by a factor of 10 and the bacterial count was determined with the respective method. The comparison of the two methods shows that the fluorescence microscopy method can determine the number of bacteria in a similar concentration range as the CFU count after plating, even at high dilutions and low numbers of bacteria.

### 3.3. Determination of regrowth-period

Because mycobacteria grow faster in liquid medium than on agar, the incubation time for regrowth of bacteria on plate 2 is shorter than for bacteria grown on solid agar. Therefore, we adjusted the incubation time for *M. abscessus* based on the measured number of regrown bacteria after 24, 48 and 72 h, as shown in Fig. 4. The inoculum was treated as described above. After fixation, the number of bacterial cells was determined by automated fluorescence microscopy. We chose to incubate for 48 h because the number of bacteria (about 50,000 cells) is 1000 times higher than the number on day 0, which was about 500 cells. Furthermore, with 50,000 cells, individual bacteria can still be detected by microscopic counting, but there are enough cells to detect the low numbers of bacteria within wells containing bactericidal test substances.

### 3.4. Antibiotics analysed for bactericidal activity against M. abscessus

The described assay was used to analyse the bactericidal efficacy of eight different antibiotics against *M. abscessus*. To substantiate the correlation shown in Fig. 2, we wanted to demonstrate the comparability of MBCs determined by CFU count and by fluorescence labelling.

We selected compound 2 and MMV688845 shown in Scheme 1 for which bactericidal activity has already been confirmed in a previous study by CFU counting on agar (Lang et al., 2023). The results for both RNA polymerase inhibitors MMV688845 and compound 2 are shown in Fig. 5. The data obtained by CFU counting (orange bars), showed comparable bactericidal activity to the automated assay based on 3HC-2-Tre labelling (green bars). Both compounds are bactericidal, but compound 2 is a derivative with improved activity, reducing the number of viable bacteria by two log units at 6.3 µM, whereas a considerably higher concentration (25 µM) of MMV688845 is required for a comparable effect.

As the results of the new method described in this study were consistent with the CFU count on agar, we selected additional

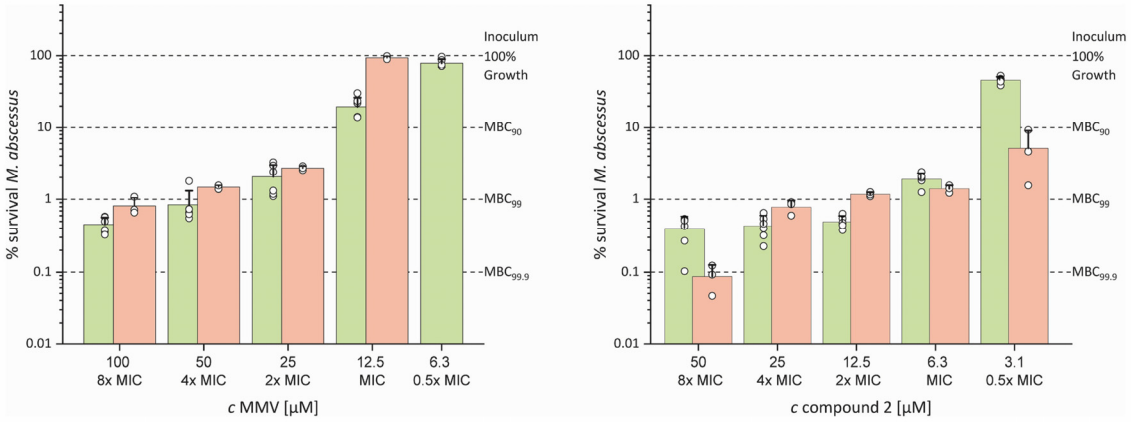


**Fig. 5.** Percentage of viable *M. abscessus*, after incubation with MMV688845 and compound 2. Green bars are determined by fluorescence microscopy, red bars by manual plating on agar and colony counting. (red bars: the experiment was carried put in triplicate, green bars: the experiment was carried out in biological duplicate and technical triplicate). (For interpretation of the references to colour in this figure legend, the reader is referred to the web version of this article.)

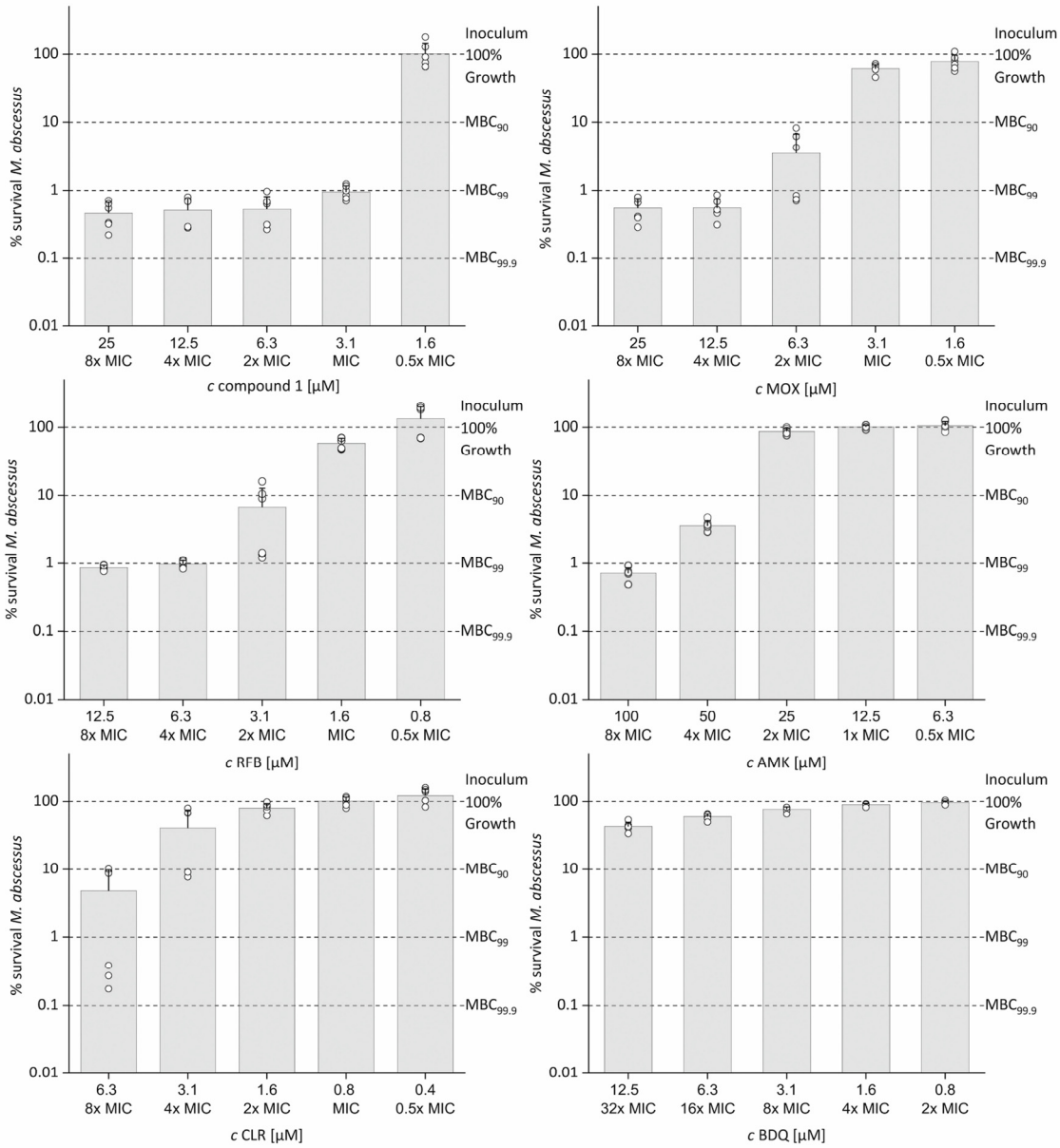


**Fig. 6.** Percentage of viable *M. abscessus*, normalised to the object count of the inoculum. (AMK = amikacin, BDQ = bedaquiline, CLR = clarithromycin, MOX = moxifloxacin, RFB = rifabutin) Experiments were performed in biological duplicates and technical replicate. All six data points and the standard deviation are shown.

antimycobacterial substances and performed further experiments. Six antimycobacterial compounds with different mechanisms of action and known bactericidal or bacteriostatic properties were analysed in the fluorescence based assay. The results are summarized in Fig. 6.

We expected bactericidal activity for the DNA gyrase inhibitors moxifloxacin and the novel bacterial topoisomerase inhibitor compound 1 (Beuchel et al., 2022) (see Scheme 1). As shown by Negatu et al. (Negatu et al., 2021) compound 1 leads to a 90% reduction in CFU of *M. abscessus* ATCC 19977 at 4× MIC and a comparable effect is observed for moxifloxacin at 8× MIC. This corresponds to a compound concentration of 4.5 µM (compound 1) or 9.0 µM (moxifloxacin). We obtained an $MBC_{90}$ for compound 1 at 3.1 µM (1× MIC) and for moxifloxacin at 6.3 µM (2× MIC), reflecting a very similar dose range and also a weaker effect of moxifloxacin compared to compound 1.

For the RNA polymerase inhibitor rifabutin we determined an $MBC_{90}$ at 3.1 µM (2× MIC) and an $MBC_{99}$ from 6.3 µM (4× MIC). In a previous study, we determined an $MBC_{90}$ of 2.4 µM (2× MIC) (Mann et al., 2022) by CFU count on agar. In a publication using *M. abscessus* Bamboo, an

$MBC_{90}$ of 5 μM is reported for rifabutin (Xie et al., 2023). In another study using different strains of *M. abscessus*, including *M. abscessus* subsp. *abscessus* ATCC 19977, rifabutin showed an $MBC_{90}$ of 6 μM (2× MIC) (Dick et al., 2020). The $MBC_{90}$ and $MBC_{99}$ values determined by 3HC-2-Tre labelling are within a similar dose range.

As shown in Fig. 6, amikacin showed a reduction of viable bacteria ($MBC_{90}$) for a rather high concentration of >50 μM, which is consistent with literature reporting an $MBC_{90}$ of 40 μM (Xie et al., 2023) against *M. abscessus* Bamboo. Clarithromycin reduced the bacterial count by 90% at 6.3 μM (8× MIC), which is consistent with literature data reporting a 90% reduction at 12.5 μM (8× MIC) (Aziz et al., 2017). However, clarithromycin shows weak bactericidal activity overall, as it does not achieve a 99% reduction of viable bacteria at 8× MIC.

For bedaquiline, we did not observe a reduction in bacterial counts up to a concentration of 12.5 μM. A publication investigating the activity of bedaquiline also showed no colony-reducing effect against two different *M. abscessus* strains: $MBC_{99.9}$ > 2 μg/mL (3.6 μM) (Aguilar-Ayala et al., 2017). However, it is possible to achieve bactericidal activity against *M. abscessus* with bedaquiline, by extending the incubation period. Xie et al. published an $MBC_{90}$ of 2 μM against *M. abscessus* bamboo with an incubation period of 10 days (Xie et al., 2023).

## 4. Discussion

We developed a method to determine the bactericidal activity of antibiotics against *M. abscessus* using automated fluorescence microscopy with the trehalose conjugate 3HC-2-Tre. Automated evaluation based on bacterial staining provides a straightforward method for analysing the effect of antibiotics on the ability of bacterial cells to divide. Compared to plating on agar, this method saves time and material, which leads to a higher throughput during substance characterisation. The method also allows a greater number of objects to be analysed than with colony counting and requires fewer dilution steps. We are confident that the method described here represents an improvement over CFU assays performed by plating on agar, particularly in terms of sample throughput, accurate quantification of residual antibiotic concentration and robustness of results.

A study based on fluorescence to facilitate the determination of the MBC against *Escherichia coli* and *Pseudomonas aeruginosa* was carried out by Bär et al. in 2009 (Bär et al., 2009) using propidium iodide and SYTO™ 9 for staining. Here, however, two dyes are used to determine a ratio of viable to non-viable bacteria and an algorithmic evaluation is proposed. The staining with propidium iodide and SYTO™ 9 is based on the membrane integrity of the cell. The method described in our study is based on the ability of bacteria to grow in a liquid medium after exposure to antibiotics and determines an absolute number of bacteria.

In our experiments, we observed that propidium iodide stains viable and non-viable bacteria non-selectively, as described in Bärs study. For this reason, we decided to quantify the growth capacity of the cells after exposure to an antibiotic in liquid medium, rather than to differentiate between viable and non-viable bacteria by staining.

Another advantage of our method is that it does not require genetic modification of the bacteria. There are a number of methods for labelling mycobacteria, including episomal labelling or integration into the bacterial genome (Takaki et al., 2013; Biegas and Swarts, 2021; Sorrentino et al., 2016). However, this method is limited to genetically modified strains of bacteria, *e.g.* clinical isolates from patients cannot be analysed in this way without prior manipulation. When bacteria are modified with a plasmid, there is always a risk that the cells will lose the plasmid during the assay procedure and become undetectable by fluorescence microscopy (Wein et al., 2020). Another advantage of the method described in this study is that the unmodified wild-type bacteria can be used for substance testing, as the bacteria are not stained until the final step of the assay. Therefore, interference between the staining method or genetic modification and substance activity is rather unlikely.

The possibility of staining different types of mycobacteria, such as *M. tuberculosis* (Sahile et al., *2020*) or *M. aurum* (Richter et al., *2023*), with trehalose dyes has already been published. We therefore assume, even if this was not shown in the present study, that this assay can also be realised with the other subspecies of *M. abscessus*.

To summarise, our results show that the described method is suitable for determining the bactericidal properties of substances against the pathogenic mycobacterium *M. abscessus*.The method can discriminate between bacteriostatic and bactericidal effects of drugs and delivers equivalent results in comparison to the conventional method of plating on agar, while It is less time and material consuming. Since 3HC-2-Tre stains various mycobacterial species, the protocol described here can be adapted to other mycobacterial species, *e.g. M. tuberculosis*, by adjusting the incubation times.

## CRediT authorship contribution statement

**Lea Mann:** Writing – review & editing, Writing – original draft, Visualization, Software, Methodology, Investigation, Data curation. **Fabienne Siersleben:** Methodology, Investigation, Data curation. **Markus Lang:** Writing – review & editing, Investigation. **Adrian Richter:** Writing – review & editing, Supervision, Project administration, Funding acquisition, Formal analysis, Data curation, Conceptualization.

## Declaration of competing interest

The authors declare the following financial interests/personal relationships which may be considered as potential competing interests:

Adrian Richter reports financial support was provided by German Research Foundation. Adrian Richter reports financial support was provided by Deutsche Mukoviszidose Stiftung. If there are other authors, they declare that they have no known competing financial interests or personal relationships that could have appeared to influence the work reported in this paper.

## Data availability

Data will be made available on request.

## Acknowledgements

We would like to thank Dr. Nadine Taudte and Dr. Jens-Ulrich Rahfeld for providing and maintaining the biosafety level 2 facility.

This work was funded by the Deutsche Forschungsgemeinschaft (DFG, German Research Foundation) - 432291016 and Mukoviszidose Institut gGmbH project no. 2202 (Bonn, Germany), the research and development arm of the German Cystic Fibrosis Association Mukoviszidose e. V.

## References

Aguilar-Ayala, D.A., Cnockaert, M., André, E., Andries, K., Gonzalez-Y-merchand, J.A., Vandamme, P., Palomino, J.C., Martin, A., 2017. In vitro activity of Bedaquiline against rapidly growing nontuberculous mycobacteria. J. Med. Microbiol. 66 (8), 1140–1143. https://doi.org/10.1099/jmm.0.000537.

Aziz, D.B., Low, J.L., Wu, M.-L., Gengenbacher, M., Teo, J.W.P., Dartois, V., Dick, T., 2017. Rifabutin is active against *Mycobacterium Abscessus* complex. Antimicrob. Agents Chemother. 61 (6) https://doi.org/10.1128/AAC.00155-17.

Baldwin, S.L., Larsen, S.E., Ordway, D., Cassell, G., Coler, R.N., 2019. The complexities and challenges of preventing and treating nontuberculous mycobacterial diseases. PLoS Negl. Trop. Dis. 13 (2), e0007083 https://doi.org/10.1371/journal.pntd.0007083.

Ballell, L., Bates, R.H., Young, R.J., Alvarez-Gomez, D., Alvarez-Ruiz, E., Barroso, V., Blanco, D., Crespo, B., Escribano, J., González, R., Lozano, S., Huss, S., Santos-Villarejo, A., Martín-Plaza, J.J., Mendoza, A., Rebollo-Lopez, M.J., Remuiñan-Blanco, M., Lavandera, J.L., Pérez-Herran, E., Gamo-Benito, F.J., García-Bustos, J.F., Barros, D., Castro, J.P., Cammack, N., 2013. Fueling open-source drug discovery: 177 small-molecule leads against tuberculosis. ChemMedChem 8 (2), 313–321. https://doi.org/10.1002/cmdc.201200428.

Bär, W., Bäde-Schumann, U., Krebs, A., Cromme, L., 2009. Rapid method for detection of minimal bactericidal concentration of antibiotics. J. Microbiol. Methods 77 (1), 85 89. https://doi.org/10.1016/j.mimet.2009.01.010.

Beuchel, A., Robaa, D., Negatu, D.A., Madani, A., Alvarez, N., Zimmerman, M.D., Richter, A., Mann, L., Hoenke, S., Csuk, R., Dick, T., Imming, P., 2022. Structure-activity relationship of anti-*Mycobacterium Abscessus* Piperidine-4-Carboxamides, a new class of NBTI DNA gyrase inhibitors. ACS Med. Chem. Lett. 13 (3), 417–427. https://doi.org/10.1021/acsmedchemlett.1c00549.

Biegas, K.J., Swarts, B.M., 2021. Chemical probes for tagging mycobacterial lipids. Curr. Opin. Chem. Biol. 65, 57–65. https://doi.org/10.1016/j.cbpa.2021.05.009.

Boudehen, Y.-M., Kremer, L., 2021. Mycobacterium abscessus. Trends Microbiol. 29 (10), 951–952. https://doi.org/10.1016/j.tim.2021.06.006.

Daley, C.L., Iaccarino, J.M., Lange, C., Cambau, E., Wallace, R.J., Andrejak, C., Böttger, E.C., Brozek, J., Griffith, D.E., Guglielmetti, L., Huitt, G.A., Knight, S.L., Leitman, P., Marras, T.K., Olivier, K.N., Santin, M., Stout, J.E., Tortoli, E., van Ingen, J., Wagner, D., Winthrop, K.L., 2020. Treatment of nontuberculous mycobacterial pulmonary disease: an official ATS/ERS/ESCMID/IDSA clinical practice guideline. Clin. Infect. Dis. 71 (4), e1–e36. https://doi.org/10.1093/cid/ciaa241.

Dick, T., Shin, S.J., Koh, W.-J., Dartois, V., Gengenbacher, M., 2020. Rifabutin is active against *Mycobacterium Abscessus* in mice. Antimicrob. Agents Chemother. 64 (2) https://doi.org/10.1128/AAC.01943-19.

Holt, M.R., Baird, T., 2023. Treatment approaches to *Mycobacterium Abscessus* pulmonary disease. Clin. Chest Med. 44 (4), 785–798. https://doi.org/10.1016/j.ccm.2023.06.010.

Kamariza, M., Shieh, P., Ealand, C.S., Peters, J.S., Chu, B., Rodriguez-Rivera, F.P., Babu Sait, M.R., Treuren, W.V., Martinson, N., Kalscheuer, R., Kana, B.D., Bertozzi, C.R., 2018. Rapid detection of *Mycobacterium Tuberculosis* in sputum with a Solvatochromic Trehalose probe. Sci. Transl. Med. 10 (430) https://doi.org/10.1126/scitranslmed.aam6310.

Kamariza, M., Keyser, S.G.L., Utz, A., Knapp, B.D., Ealand, C., Ahn, G., Cambier, C.J., Chen, T., Kana, B., Huang, K.C., Bertozzi, C.R., 2021. Toward point-of-care detection of *Mycobacterium Tuberculosis*: a brighter Solvatochromic probe detects mycobacteria within minutes. JACS Au 1 (9), 1368–1379. https://doi.org/10.1021/jacsau.1c00173.

Lang, M., Ganapathy, U.S., Mann, L., Abdelaziz, R., Seidel, R.W., Goddard, R., Sequenzia, I., Hoenke, S., Schulze, P., Aragaw, W.W., Csuk, R., Dick, T., Richter, A., 2023. Synthesis and characterization of phenylalanine amides active against *Mycobacterium Abscessus* and other mycobacteria. J. Med. Chem. 66 (7), 5079–5098. https://doi.org/10.1021/acs.jmedchem.3c00009.

Mann, L., Ganapathy, U.S., Abdelaziz, R., Lang, M., Zimmerman, M.D., Dartois, V., Dick, T., Richter, A., 2022. In vitro profiling of the synthetic RNA polymerase inhibitor MMV688845 against *Mycobacterium Abscessus*. Microbiol. Spectr. 10 (6) https://doi.org/10.1128/spectrum.02760-22.

Maurer, F.P., Bruderer, V.L., Ritter, C., Castelberg, C., Bloemberg, G.V., Böttger, E.C., 2014. Lack of antimicrobial bactericidal activity in *Mycobacterium Abscessus*. Antimicrob. Agents Chemother. 58 (7), 3828–3836. https://doi.org/10.1128/AAC.02448-14.

Negatu, D.A., Beuchel, A., Madani, A., Alvarez, N., Chen, C., Aragaw, W.W., Zimmerman, M.D., Laleu, B., Gengenbacher, M., Dartois, V., Imming, P., Dick, T., 2021. Piperidine-4-Carboxamides target DNA gyrase in *Mycobacterium Abscessus*. Antimicrob. Agents Chemother. 65 (8) https://doi.org/10.1128/AAC.00676-21.

Richter, A., Strauch, A., Chao, J., Ko, M., Av-Gay, Y., 2018. Screening of preselected libraries targeting *Mycobacterium Abscessus* for drug discovery. Antimicrob. Agents Chemother. 62 (9), 1–11. https://doi.org/10.1128/AAC.00828-18.

Richter, A., Goddard, R., Siersleben, F., Mann, L., Seidel, R.W., 2023. Structural Elucidation of 2-(6-(Diethylamino)Benzofuran-2-Yl)-3-Hydroxy-4H-Chromen-4-One and Labelling of *Mycobacterium Aurum* Cells. Molbank 2023, M1647. https://doi.org/10.3390/M1647. Page M1647 2023, 2023 (2).

Richter, A., Goddard, R., Mann, L., Siersleben, F., Seidel, R.W., 2024. Structural characterization of a 3-Hydroxychromone dye Trehalose conjugate for fluorescent labelling of mycobacteria. J. Mol. Struct. 1298, 137010 https://doi.org/10.1016/J.MOLSTRUC.2023.137010.

Sahile, H.A., Rens, C., Shapira, T., Andersen, R.J., Av-Gay, Y., 2020. DMN-Tre labeling for detection and high-content screening of compounds against intracellular mycobacteria. ACS Omega 5 (7), 3661–3669. https://doi.org/10.1021/acsomega.9b04173.

Sorrentino, F., Del Rio, R.G., Zheng, X., Matilla, J.P., Gomez, P.T., Hoyos, M.M., Herran, M.E.P., Losana, A.M., Av-Gay, Y., 2016. Development of an intracellular screen for new compounds able to inhibit *Mycobacterium Tuberculosis* growth in human macrophages. Antimicrob. Agents Chemother. 60 (1), 640–645. https://doi.org/10.1128/AAC.01920-15/FORMAT/EPUB.

Takaki, K., Davis, J.M., Winglee, K., Ramakrishnan, L., 2013. Evaluation of the pathogenesis and treatment of *Mycobacterium Marinum* infection in zebrafish. Nat. Protoc. 8 (6), 1114–1124. https://doi.org/10.1038/nprot.2013.068.

Wein, T., Wang, Y., Hülter, N.F., Hammerschmidt, K., Dagan, T., 2020. Antibiotics interfere with the evolution of plasmid stability. Curr. Biol. 30 (19), 3841–3847.e4. https://doi.org/10.1016/j.cub.2020.07.019.

Wu, M.-L., Aziz, D.B., Dartois, V., Dick, T., 2018. NTM drug discovery: status, gaps and the way forward. Drug Discov. Today 23 (8), 1502–1519. https://doi.org/10.1016/j.drudis.2018.04.001.

Xie, M., Ganapathy, U.S., Lan, T., Osiecki, P., Sarathy, J.P., Dartois, V., Aldrich, C.C., Dick, T., 2023. ADP-Ribosylation-resistant Rifabutin analogs show improved bactericidal activity against drug-tolerant *M. Abscessus* in Caseum surrogate. Antimicrob. Agents Chemother. 67 (9) https://doi.org/10.1128/aac.00381-23.

# 4 Discussion

## 4.1 In depth characterisation of the assay hit MMV688845

The publication listed in this dissertation as Publication I: '*In Vitro Profiling of the Synthetic RNA Polymerase Inhibitor MMV688845 against Mycobacterium abscessus*' aimed to investigate the suitability of the substance MMV688845 as a drug candidate against *M. abscessus*. For this purpose, various assays were carried out which, as explained in section 1.2, enable a comprehensive and targeted analysis of the substances adapted to the properties of NTM. In addition, checkerboard assays were performed. Figure 8 is intended to illustrate the progress made in the context of Publication I. In comparison to Figure 5 (chapter 1.2), the sub-items of the figure for which results have been published are highlighted in blue.

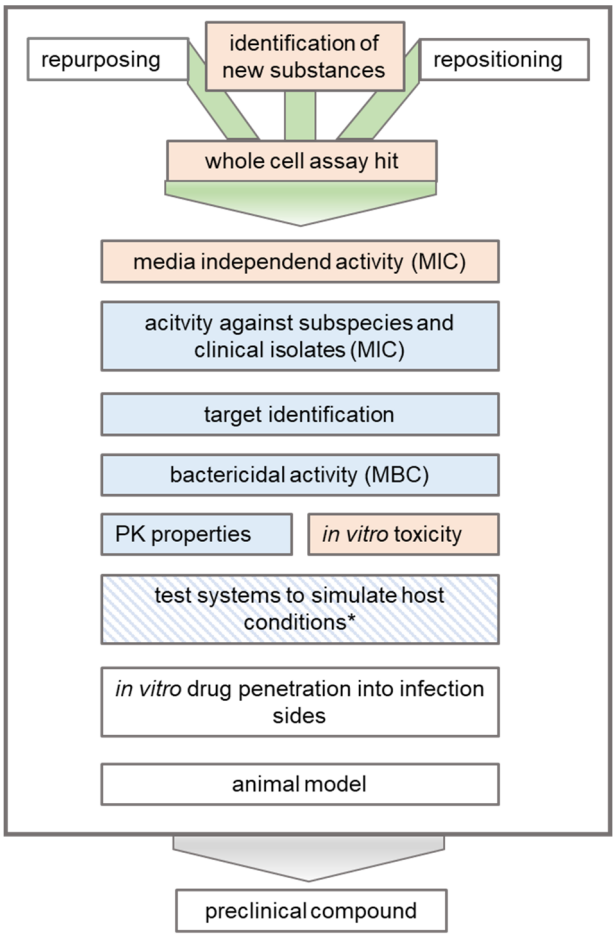


**Figure 8** *NTM drug discovery workflow II.*
*Adapted from* (Wu *et al.*, 2018). *In comparison to Figure 5, what has already been analysed for the substance MMV688845 in previous studies is highlighted in orange, what was analysed in Publication I in blue. *Test systems to simulate host conditions, i.e. tests such as: non-replicating assays, macrophage infection assays, caseum assay or persister-specific assays. As only the macrophage infection assay was examined in this publication, this point is only partially emphasized.*

In the publication, the activity against subspecies of *M. abscessus* and clinical isolates of the bacterium was assessed (Table 1, Publication I). The bactericidal activity of MMV688845 was determined against *M. abscessus* and published for the first time (Table 2, Publication I). The target RNA polymerase was reconfirmed by sequencing resistant mutants of *M. abscessus*, which was done in the laboratories of Prof. Thomas Dick. In order to investigate the activity of MMV688845 under host conditions, MIC determinations were carried out in the macrophage infection model (Tables 2, 4 and 5, Figure 3, Publication I). In addition, investigation of the oral bioavailability was carried out but showed rapid metabolism of the substance, as only a plasma concentration of 0.1 µM could be achieved when a dose of 25 mg/kg was administered orally to mice (Figure 4, Publication I). These results emphasise the value of investigating pharmacokinetic properties in addition to activity in the early stages of drug development. For the further development of the substance class, it will be important to optimise the pharmacokinetics in addition to improve the activity. To this end, it is important to investigate the target of the compound in order to understand the binding interactions in detail. Further investigations, such as modelling studies, can significantly facilitate chemical synthesis to find optimised compounds.

Since a combination therapy with at least three antibiotics is considered the standard therapy for *M. abscessus*, the combination of MMV688845 with various antibiotics of different classes used against NTM and *M. abscessus* was already investigated at this early stage of drug development. Drug interactions can reveal connections between processes in the cell and are, therefore, of interest for basic research in microbial cell physiology (Hsieh *et al.*, 1993). However, the study reveals weaknesses that point to recommendations for future improvements. For the combinations that showed synergy in the determined MIC, a determination of the MBC at which cell viability is detected could have further clarified the efficacy of the drug combination (Gómara and Ramón-García, 2019). It would, therefore, be interesting to test the combination of clarithromycin and MMV688845 for its bactericidal properties and to determine whether there is synergy in terms of bacterial count reduction.

Overall, the study is comparable to other *M. abscessus* drug development literature studies, in terms of the assays performed and the approach used. Examples include a publication on the investigation of benzoxaboroles against *M. abscessus* (Ganapathy, González del Rio, *et al.*, 2021), another on the characterisation of Decaprenylphosphoryl-β-D-ribofuranose 2′-oxidase (DprE1) (Sarathy *et al.*, 2022) and a third on new F-ATP Synthase inhibitors (Ragunathan, Dick and Grüber, 2022). In these studies, tests were carried out on various strains or clinical isolates, the bactericidal properties of the substances were investigated and target validations were performed. Two of the publications show initial pharmacokinetic

data (Ganapathy, González del Rio, *et al.*, 2021; Sarathy *et al.*, 2022), and the interaction with other drugs was investigated (Ragunathan, Dick and Grüber, 2022; Sarathy *et al.*, 2022). Publication I is, thus, considered an important step towards the development of drugs against *M. abscessus.* It collects important data for the characterisation of the AAP substance class.

## 4.2 Characterisation of AAP derivatives in broth and in the macrophage infection assay

Publication II was included in the series of listed papers on drug development against *M. abscessus* on the basis of the investigations of Publication I: Testing against various non-tuberculous mycobacteria, including different strains of *M. abscessus* in different liquid media and in the macrophage infection model (Table 2, Publication II); determination of bactericidal activity (Figure 7, Publication II); toxicity testing (Table 5, Publication II); pharmacokinetic testing (Figure 8, Table 4, Publication II). Importantly, based on Publication I, this paper presents analogues of MMV688845 with improved activity. In addition to the above-mentioned investigations, the paper presents more extensive results, such as the synthesis and, with regard to the properties of the compounds, investigations on solubility and plasma/microsomal stability. Of approximately 100 different derivatives tested during this doctoral thesis, 26 derivatives with activity against *M. abscessus* are presented in the publication. Some of the substances show improved activity compared to the hit substance, as listed in Table 2 (Publication II).

In addition to the tests in broth, tests in the macrophage infection model were carried out for the 26 derivatives in the publication, as mentioned above. The assay-results and evaluation of the data are described in Section 2.3.1 (Publication II) and Sections 4.12.1-4.12.3 and 4.12.6 (Publication II) and also in Publication I.

Table 2 (Publication II) shows the results of the compounds tested in the liquid medium and in the macrophage infection model for *M. abscessus* ATCC 19977. The results of the macrophage infection assay show higher MIC values compared to the values determined in bacterial growth medium.

In general, intracellular *M. abscessus* is less susceptible to treatment with inhibitors (Molina-Torres *et al.*, 2018). It is hypothesised that the conditions within the macrophage, such as ROS, nitric oxide, low pH and a lipid-rich environment, lead to bacterial adaptation and the induction of drug tolerance (Wu *et al.*, 2018). As mentioned in section 1.2, the macrophage infection assay can be used as a model to simulate the bacterial environment in the host. The protocol used in our laboratories (again Section 4.12.6, Publication II), which is based on fluorescence evaluation, is a high-content screening approach. Figure 9 shows overlaid fluorescence images taken for image-based analysis. The method enables the screening of drugs against *M. abscessus in vitro*, taking into account drug permeability, host effects or macrophage inactivation (Richter, Shapira and Av-Gay, 2019). Some clinically used antibiotics for *M. abscessus* therapy have intracellular activity against the bacterium, such as bedaquiline, tigecycline and macrolides (Molina-Torres *et al.*, 2018) (see Table 4, Publication I).

After the hit substance MMV688845 was shown to be active in the macrophage infection model (Richter, Shapira and Av-Gay, 2019), the corresponding derivatives were characterised for their intracellular activity. The fact that the derivatives of the substance MMV688845 with improved MIC against *M. abscessus* in liquid medium (Table 2, e.g. substances 20,24, 28, 29) maintain the improvement in the macrophage infection model is to be regarded as positive. In general, the efficacy in macrophages is an outstanding property for the substance class, as it could help to eradicate infections more effectively.

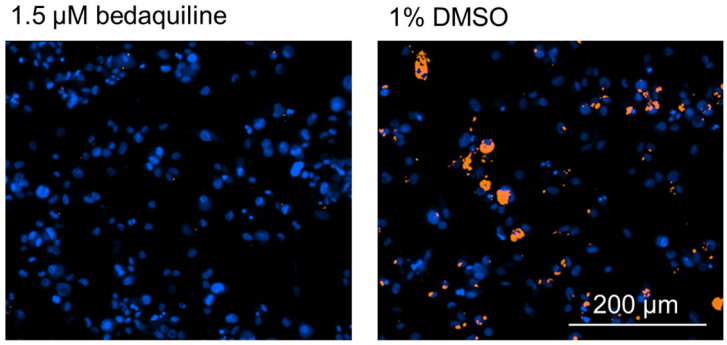


**Figure 9** *Overlay of fluorescence microscopic images.*
*DAPI stained nuclei (blue) and red fluorescent protein of M. abscessus pTEC27 ATCC 19977 (red). Image acquired with CX5 by Lea Mann, 2023.*

It would be interesting to investigate the extent to which the efficacy of a substance against bacteria growing in macrophages actually correlates with its efficacy in the clinic, although this may be difficult to determine due to additional pharmacokinetic parameters during clinical administration.

For the future, a more comprehensive characterisation of the bactericidal activity of the substances should be added to the results currently obtained. The bactericidal effect on bacteria in macrophages was determined for the lead substance (Publication I, Table 2), but no such study was carried out for the optimised derivatives. Due to the necessary fixation prior to the final evaluation, which was obligatory due to the location of the fluorescence microscope outside the S2 laboratory, no *in vitro* live cell imaging could be performed to gain more insight into the dynamic process of phagocytosis.

Overall, the macrophage infection model for testing substances under simulated conditions of human infection with the pathogen is a useful method for determining the efficacy of substances against *M. abscessus*. This work generated important data for two papers (Publication I and Publication II). By using this model, it was possible to simulate the host conditions and make progress in the early process of drug development.

## 4.3 Development of a new fluorescence-based method for MBC determination

Bactericidal activity of the agents used against NTM is considered to be crucial for the success of the therapy: To sterilise persisters in biofilms, but to eradicate *M. abscessus* bacilli in immunocompromised patients, where bacteriostatic antibiotics may not be sufficient (Dartois and Dick, 2022). The lack of success in treating *M. abscessus* can be attributed to the lack of bactericidal activity of the drugs (Dartois and Dick, 2024b). As the clinically used drugs tigecycline and amikacin have weak bactericidal activity against *M. abscessus* (Maurer *et al.*, 2014). Bactericidal properties are therefore essential for the development of new drugs.

The determination of MBC is not a standardised method (Greendyke and Byrd, 2008), so the definitions for the evaluation of bactericidal activity differ. In this work, the MBC is defined as the minimum concentration to reduce viability, measured in CFU, by 90% or 99% compared to the initial inoculum.

Initially, a method for determining MBC by plating substances on agar was established in the laboratories. This conventional method was developed based on protocols found in literature and methodically adapted to further optimise the method (Franzblau *et al.*, 2012; Maurer *et al.*, 2014; Ganapathy, Del Rio, *et al.*, 2021).

Due to the constant adaptation of the MBC method during my doctoral work, different methods of MBC determination are described in the publications I-III. They do not differ in quality, but in efficiency in terms of the time required per substance to be tested, which could be reduced. During the process of compound characterisation of AAPs, we constantly optimised the methods in order to accelerate the process. In retrospect, the performance of the MBC determination on agar medium has provided important results for all three publications included in the dissertation. See Publication I, Figure 1 and Table 2, Publication II Figure 7, Section 2.3.2 and 4.12.7, and Publication III Figure 2 and Section 2.4.

The third publication, however, deals with a novel method of MBC determination using fluorescence microscopy in a 96-well format in liquid culture. The approach taken was to automate the analysis by software-assisted counting of CFUs. To obtain an optimally analysable microscopic image for evaluation, different growth times, dilutions and dyes were investigated as part of the method development, leading to the method described in publication III. All results presented in the publication were carried out by myself. The method was adopted and further improved for *M. abscessus* on the basis of the results obtained in Fabienne Siersleben's diploma thesis for testing *Mycobacterium aurum* (supervised by me).

Overall, the development of an improved method should lead to progress within the drug development process (Figure 5) in order to accelerate bactericidal testing and, thus, the

entire drug development process. MBC determinations are usually performed at a later stage of drug development as they are very time consuming. Using an automated high-throughput method for this step will help to perform the MBC assessment at an early stage. Since information about the bactericidal activity of a drug is very important, especially for bacteria that tend to develop resistance during therapy, it is valuable to check the bactericidal properties of a drug at an early stage of drug development.

Another approach to determine MBCs more quickly, was found in the literature (Bär *et al.*, 2009). However, this is based on a relative ratio of viable to non-viable bacteria determined by differential staining, requiring the use of two dyes that can reliably differentiate bacteria based on viability. In addition, the evaluation is based on graphical extrapolation and a mathematical approximation method, which makes the evaluation more complicated than the method presented in Publication III.

In the newly developed method (Publication III), a single dye: 3HC-2-Tre is used for coloring and whose chemical structure is shown in Figure 10. Unlike structurally related dyes, it is not capable of selectively staining viable bacteria (Kamariza *et al.*, 2021).

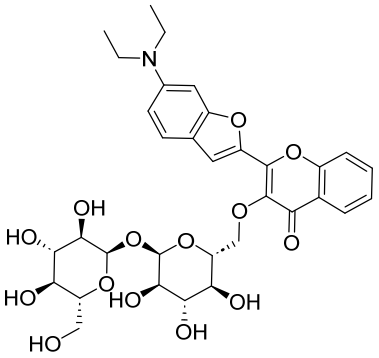


**Figure 10** *Chemical diagram of 3HC-2-Tre.*

For trehalose-conjugated dyes, the mycolation to trehalose mycolates by antigen 85 and its subsequent insertion into the mycobacterial membrane by MmpL transport are described in literature. However, a second, unknown mechanism has been described for the 3HC-2-Tre dye used, which can stain bacteria regardless of their viability and enzyme activity. Due to the solvatochromic property of the dye, the fluorescence should be particularly intense within the lipophilic mycobacterial cell wall compared to the aqueous medium (Kamariza *et al.*, 2018, 2021). However, during work with the dye, it was found that a washing/diluting step was necessary to obtain an image with the low background fluorescence required for analysis. To ensure sufficient reduction of the background, a final dilution step was, therefore, implemented in the method to dilute the dye so that the contrasting bacteria could then be sufficiently focused.

To stain bacteria in the new method, only one dye is needed that can reliably stain the viable bacteria present in a sample. An advantage of the method is that the dye can be selected to

match the fluorescence filter of the device used for the evaluating measurement. Although an RFP-expressing strain of *M. abscessus* was used in this work, a wild-type strain was deliberately used for this study (the RFP strain was used for validation purposes only). The aim was to show that the MBC test presented here can be carried out with clinical isolates and can generally be performed independently of genetic modification.
As mentioned in Publication III, the method described allows an improvement in throughput due to the simplified quantification compared to counting CFU after plating on agar.
Another advantage is the dilution of the drugs during the transfer to the second 96-well plate, so that interfering, residual concentrations of drug do not interfere with the bactericidal test.

Due to the simplification and acceleration of the method for the determination of MBC, the fluorescence-based assay is already being used in our laboratory. However, this newly developed, improved method for MBC determination, adapted to *M. abscessus*, has contributed to improving the drug development process, which will hopefully be used in other laboratories, as it will be possible to perform the assay with other NTM after adjusting the incubation times.

# 5 Summary

In general, this work demonstrates the potential of the *N*α-aroyl-*N*-aryl-phenylalanine amides (AAPs) of compounds as antimycobacterial agents.
The testing of the substance MMV688845 and AAP derivatives against various NTM made an important contribution to the optimisation and further development of the substance class.

The compound MMV688845, which was originally identified by testing compound libraries (see Section 1.3), has been comprehensively characterised in this work (Publication I). In particular, checkerboard assays were used to investigate the effect (synergistic, additive, antagonistic) of a combination of MMV688845 with antimycobacterial agents against *M. abscessus*. A synergistic effect was observed in the combination of clarithromycin with MMV688845. A similar behaviour is described in the literature for the combination of the RNA polymerase inhibitor rifabutin with clarithromycin (Aziz, Go and Dick, 2020). The synergistic effect may be caused by the suppression of inducible macrolide resistance in *erm41*-positive *M. abscessus* by the combination of an RNA polymerase inhibitor with clarithromycin. In addition, the bactericidal properties of the substance MMV688845 were determined for the first time and compared with the activity of rifabutin. For this purpose, a colony count was performed on agar medium after incubation of *M. abscessus* in 7H9 and also after incubation in the macrophage infection model. It was shown that in both cases a reduction of colony forming units of 99% ($MBC_{99}$) was achieved.

Due to the interdisciplinarity within our working group, the activities of the newly synthesised MMV688845 derivatives could be very quickly and directly reproduced by *in vitro* testing of the mycobacteria, which accelerated the optimisation process. For the further development of the substance class, approximately 100 derivatives were tested and analysed against *M. abscessus* ATCC19977 (subsp. *abscessus*), *M. smegmatis* mc2 155 and *M. intracellulare* ATCC 35761, as well as against *M. abscessus* in the macrophage infection model. The derivatives with improved properties (such as increased activity) have been published in Publication II. In addition, the bactericidal properties of some derivatives were also analysed and lower MBC values were found in comparison with the lead compound.

With the establishment and improvement of a method for the determination of MBC, an assay was developed. The results shown in Publication III are based on the approach of simplifying the process of determining colony-forming units by plating on agar medium and alternatively testing the growth capacity of the bacteria in 96-well plates in liquid culture. For evaluation,

an automated, fluorescence microscopic quantification of the bacteria was established, which is preceded by the staining of the bacteria with a trehalose dye 3HC-2-Tre (2-(6-(diethylamino)benzofuran-2-yl)-3-hydroxy-4*H*-chromen-4-one-conjugated trehalose). This new method was used to determine the bactericidal activity of various antibiotics against *M. abscessus* and the results were compared with literature data or verified by plating on agar. It was shown that the new fluorescence-based method gives comparable results to the enumeration of the colony-forming unit on agar.

In the future, synthetic optimisation of the AAP derivatives will be necessary in order to reduce the metabolisation of the substances. *In vitro* testing against mycobacteria (MIC/MBC, macrophage infection assay) will continue to be an important aspect in order to understand the influence of the structural change on the effect in the whole cell assay and to optimise both parameters (activity and stability).

There are various approaches for further development of the presented method of MBC determination in liquid culture. For example, the attempt to use it in another laboratory, where a transfer to other mycobacteria as well as to clinical isolates is also conceivable. Another idea would be to carry out the assay following an *in vitro* combination test. In addition, the use for the time-dependent determination of bactericidal activity, which could be realised by evaluation at different points in time.

For the further development of the substance class, the parameters of antimycobacterial efficacy and metabolic stability must be considered equally in order to establish the active substance class of AAPs as preclinical candidates and to prove their efficacy in a suitable *in vivo* model.

## 5 Zusammenfassung

Grundsätzlich zeigt diese Arbeit das Potential der Substanzklasse der *N*α-aroyl-*N*-aryl-phenylalanin amide (AAPs) als antimykobakterielle Wirkstoffe auf. Die Testung der Substanz MMV688845 und AAP-Derivate gegen verschiedene NTM leistet einen wichtigen Beitrag zur Optimierung und Weiterentwicklung der Substanzklasse.

Die Verbindung MMV688845, welche ursprünglich durch die Testung von Substanzbibliotheken identifiziert wurde (siehe Abschnitt 1.3), ist in dieser Arbeit (Publikation I) umfassend charakterisiert worden. Hierfür wurden insbesondere Checkerboard-Assays herangezogen, um den Effekt (synergistisch, additiv, antagonistisch) einer Kombination von MMV688845 mit antimykobakteriellen Wirkstoffen gegen *M. abscessus* zu untersuchen. Es konnte ein synergistischer Effekt in der Kombination von Clarithromycin mit MMV688845 festgestellt werden. Ein ähnliches Verhalten ist für die Kombination des RNA-Polymerase Hemmstoffes Rifabutin mit Clarithromycin in der Literatur beschrieben (Aziz, Go and Dick, 2020). Der synergistische Effekt kann mit der Suppression der induzierbaren Makrolidresistenz bei *erm*41-positiven *M. abscessus* durch die Kombination eines RNA-Polymerase Hemmstoffs mit Clarithromycin verursacht werden. Zudem wurde erstmals eine Bestimmung der bakteriziden Eigenschaften für die Substanz MMV688845 untersucht und mit der Aktivität von Rifabutin verglichen. Hierfür wurde eine Koloniezählung auf Agar-Medium durchgeführt, nach Inkubation von *M. abscessus* in 7H9 und ebenfalls nach der Inkubation im Makrophagen-Infektionsmodell. Es konnte gezeigt werden, dass in beiden Fällen eine Reduktion der koloniebildenden Einheiten von 99% ($MBC_{99}$) erreicht wird.

Durch die Interdisziplinarität innerhalb unserer Arbeitsgruppe konnten Aktivitäten der neu synthetisierten MMV688845-Derivate durch *in vitro* Testung der Mykobakterien sehr schnell und direkt nachvollzogen werden, was den Optimierungs-Prozess beschleunigte. Für die Weiterentwicklung der Substanzklasse wurden für ca. 150 Derivate gegen *M. abscessus* ATCC19977 (subsp. *abscessus*), *M. smegmatis* $mc^2$ 155 und *M. intracellulare* ATCC 35761, sowie gegen *M. abscessus* im Makrophagen-Infektions-Modell getestet und ausgewertet. Die Derivate mit verbesserten Eigenschaften (wie unter anderem erhöhte Aktivität) sind in Publikation II veröffentlicht worden. Zudem wurden auch hier die bakteriziden Eigenschaften einiger Derivate untersucht und im Vergleich der Leitsubstanz geringere MBC-Werte festgestellt.

Mit der Etablierung und Verbesserung einer Methode zur Bestimmung der MBC wurde zusätzlich ein Assay entwickelt. Die in Publikation III gezeigten Ergebnisse basieren auf dem Ansatz, den Prozess der Bestimmung koloniebildender Einheiten über Platierung auf Agar Medium zu vereinfachen und die Prüfung der Wachstumsfähigkeit der Keime alternativ in 96-Well Platten in Flüssigkultur durchzuführen. Zur Auswertung wurde eine automatisierte, fluoreszenzmikroskopische Quantifizierung der Keime etabliert, der die Färbung der Bakterien mit einem Trehalose-Farbstoff 3HC-2-Tre (2-(6-(diethylamino)benzofuran-2-yl)-3-hydroxy-4*H*-chromen-4-on-konjugierte Trehalose) vorausgeht. Diese neue Methode wurde zur Bestimmung der Bakterizidie verschiedener Antibitoika gegen *M. abscessus* genutzt und die Ergebnisse wurden mit Literaturdaten verglichen bzw. mittels Platierung auf Agar verifiziert. Dabei zeigte sich das die neue fluoreszenzbasierte Methode vergleichbare Ergebnisse wie die Auszählung der koloniebildenden Einheit auf ergibt.

Zukünftig wird synthetische Optimierung der AAP-Derivate notwendig sein, um die Metabolisierung der Substanzen zu verringern. Dabei wird die *in vitro* Testung gegen Mykobakterien (MHK/MBC, Makrophagen-Infektionsassay) auch weiterhin einen wichtigen Aspekt darstellen um den Einfluss der Strukturveränderung auf die Wirkung im Ganzzellassay nachvollziehen zu können und beide Parameter (Aktivität und Stabilität) zu optimieren.

Für die vorgestellte Methode der MBC Bestimmung in Flüssigkultur gibt es verschiedene Ansätze der Weiterentwicklung. Zum Beispiel den Versuch der Anwendung in einem anderen Labor, bei der eine Übertragung auf andere Mykobakterien wie auch auf klinische Isolate, ebenfalls denkbar ist. Eine Durchführung im Anschluss einer *in vitro* Kombinationstestung wäre eine weitere Idee. Außerdem die Nutzung zur Zeit-abhängigen Bestimmung der bakteriziden Aktivität, die durch Auswertung zu verschiedenen Zeitpunkten zu realisieren wäre.

Für die weitere Entwicklung der Stoffklasse müssen die Parameter antimykobakterielle Wirksamkeit und metabolische Stabilität gleichermaßen berücksichtigt werden, um die Wirkstofflasse der AAPs als präklinische Kandidaten zu etablieren und ihre Wirksamkeit in einem geeigneten *in vivo* Modell nachzuweisen.

## 6 References


Abdelaal, H.F.M. *et al.* (2022) 'Mycobacterium abscessus: It's Complex', *Microorganisms*, 10(1454), pp. 1–24. Available at: https://doi.org/10.3390/microorganisms10071454.

Agustí, G. *et al.* (2008) 'Surface spreading motility shown by a group of phylogenetically related, rapidly growing pigmented mycobacteria suggests that motility is a common property of mycobacterial species but is restricted to smooth colonies', *Journal of Bacteriology*, 190(20), pp. 6894–6902. Available at: https://doi.org/10.1128/JB.00572-08.

Armstrong, D.T., Eisemann, E. and Parrish, N. (2023) 'A Brief Update on Mycobacterial Taxonomy, 2020 to 2022', *Journal of Clinical Microbiology*. Edited by R.M. Humphries, 61(4), pp. 1–3. Available at: https://doi.org/10.1128/jcm.00331-22.

Aziz, D.B. *et al.* (2017) 'Rifabutin Is Active against Mycobacterium abscessus Complex', *Antimicrobial Agents and Chemotherapy*, 61(6), pp. 1–10. Available at: https://doi.org/10.1128/AAC.00155-17.

Aziz, D.B., Go, M.L. and Dick, T. (2020) 'Rifabutin Suppresses Inducible Clarithromycin Resistance in Mycobacterium abscessus by Blocking Induction of whiB7 and erm41', Antibiotics, 9(72), pp. 1–7. Available at: https://doi.org/10.3390/antibiotics9020072.

Baldwin, S.L. *et al.* (2019) 'The complexities and challenges of preventing and treating nontuberculous mycobacterial diseases', *PLOS Neglected Tropical Diseases*. Edited by D. Laouini, 13(2), pp. 1–23. Available at: https://doi.org/10.1371/journal.pntd.0007083.

Ballell, L. *et al.* (2013) 'Fueling Open-Source Drug Discovery: 177 Small-Molecule Leads against Tuberculosis', *ChemMedChem*, 8(2), pp. 313–321. Available at: https://doi.org/10.1002/cmdc.201200428.

Bär, W. *et al.* (2009) 'Rapid method for detection of minimal bactericidal concentration of antibiotics', *Journal of Microbiological Methods*, 77(1), pp. 85–89. Available at: https://doi.org/10.1016/j.mimet.2009.01.010.

Belisle, J.T. and Brennan, P.J. (1989) 'Chemical basis of rough and smooth variation in mycobacteria', *Journal of Bacteriology*, 171(6), pp. 3465–3470. Available at: https://doi.org/10.1128/jb.171.6.3465-3470.1989.

Bernut, A. *et al.* (2016) 'Insights into the smooth-to-rough transitioning in Mycobacterium bolletii unravels a functional Tyr residue conserved in all mycobacterial MmpL family members', *Molecular Microbiology*, 99(5), pp. 866–883. Available at: https://doi.org/10.1111/mmi.13283.

Boudehen, Y.-M. and Kremer, L. (2021) 'Mycobacterium abscessus.', *Trends in microbiology*, 29(10), pp. 951–952. Available at: https://doi.org/10.1016/j.tim.2021.06.006.

Brodhun, B. *et al.* (2020) *Bericht zur Epidemiologie der Tuberkulose in Deutschland für 2020*, *Sustainability (Switzerland)*. Available at: https://doi.org/10.25646/8772.

Carter, G., Young, L.S. and Bermudez, L.E. (2004) 'A Subinhibitory Concentration of Clarithromycin Inhibits Mycobacterium avium Biofilm Formation', *Antimicrobial Agents and Chemotherapy*, 48(12), pp. 4907–4910. Available at: https://doi.org/10.1128/AAC.48.12.4907-4910.2004.

Chun, J.J. (2017) Bacterial species concept explained. Available at: https://help.ezbiocloud.net/bacterial-species-concept-explained/.

CLSI (2011) 'M24-A2 Susceptibility Testing of Mycobacteria, Nocardiae, and Other Aerobic Actinomycetes; Approved Standard-Second Edition A standard for global application developed through the Clinical and Laboratory Standards Institute consensus process', in. Wayna, PA. Available at: www.clsi.org.

Collins, F.M. (1988) 'AIDS-related mycobacterial disease', *Springer Seminars in Immunopathology*, 10(4), pp. 375–391. Available at: https://doi.org/10.1007/BF02053847.

Corbett, C. *et al.* (2023) 'Development of prevalence and incidence of non-tuberculous mycobacteria in German laboratories from 2016 to 2020', *Emerging Microbes and Infections*, 12(2). Available at: https://doi.org/10.1080/22221751.2023.2276342.

Cowman, S. *et al.* (2019) 'Non-tuberculous mycobacterial pulmonary disease.', *The European respiratory journal*, 54(1), p. 1900250. Available at: https://doi.org/10.1183/13993003.00250-2019.

Cudahy, P. and Shenoi, S. V (2016) 'Diagnostics for pulmonary tuberculosis', *Postgrad Med J*, 92, pp. 187–193. Available at: https://doi.org/10.1136/postgradmedj-2015-133278.

Daley, C.L. *et al.* (2020) 'Treatment of Nontuberculous Mycobacterial Pulmonary Disease: An Official ATS/ERS/ESCMID/IDSA Clinical Practice Guideline.', *Clinical infectious diseases : an official publication of the Infectious Diseases Society of America*, 71(4), pp. e1–e36. Available at: https://doi.org/10.1093/cid/ciaa241.

Dartois, V. and Dick, T. (2022) 'Drug development challenges in nontuberculous mycobacterial lung disease: TB to the rescue', *Journal of Experimental Medicine*, 219(6), pp. 1–4. Available at: https://doi.org/10.1084/jem.20220445.

Dartois, V. and Dick, T. (2024a) 'Therapeutic developments for tuberculosis and nontuberculous mycobacterial lung disease', *Nature Reviews Drug Discovery*, 23(5), pp. 381–403. Available at: https://doi.org/10.1038/s41573-024-00897-5.

Dartois, V. and Dick, T. (2024b) 'Toward better cures for Mycobacterium abscessus lung disease', *Clinical microbiology reviews*. Edited by F.C. Fang. American Society for Microbiology, pp. 1–29. Available at: https://doi.org/10.1128/cmr.00080-23.

D Chan, E. and Bai, X. (2016) 'Animal Models of Non-Tuberculous Mycobacterial Infections', *Mycobacterial Diseases*, 6(3), pp. 1–7. Available at: https://doi.org/10.4172/2161-1068.1000216.

Dulberger, C.L., Rubin, E.J. and Boutte, C.C. (2020) 'The mycobacterial cell envelope — a moving target', *Nature Reviews Microbiology*, 18(1), pp. 47–59. Available at: https://doi.org/10.1038/s41579-019-0273-7.

Ebright, R.H. *et al.* (2015) 'ANTIBACTERIAL AGENTS: N(ALPHA)-AROYL-N-ARYL PHENYLALANINAMIDES'.

Feazel, L.M. *et al.* (2009) 'Opportunistic pathogens enriched in showerhead biofilms', *Proceedings of the National Academy of Sciences*, 106(38), pp. 16393–16399. Available at: https://doi.org/10.1073/pnas.0908446106.

Forbes, B.A. (2017) 'Mycobacterial Taxonomy', *Journal of Clinical Microbiology*, 55(2), pp. 380–383. Available at: https://doi.org/10.1128/JCM.01287-16.

Franzblau, S.G. *et al.* (2012) 'Comprehensive analysis of methods used for the evaluation of compounds against Mycobacterium tuberculosis', *Tuberculosis*, 92(6), pp. 453–488. Available at: https://doi.org/10.1016/j.tube.2012.07.003.

Fritsche, O. (2016) *Mikrobiologie*. Berlin, Heidelberg: Springer Berlin Heidelberg. Available at: https://doi.org/10.1007/978-3-662-49729-6.

Ganapathy, U.S., González del Rio, R., *et al.* (2021) 'A Leucyl-tRNA Synthetase Inhibitor with Broad-Spectrum Antimycobacterial Activity', *Antimicrobial Agents and Chemotherapy*, 65(5), pp. 1–13. Available at: https://doi.org/10.1128/AAC.02420-20.

Ganapathy, U.S., Del Rio, R.G., *et al.* (2021) 'A leucyl-tRNA synthetase inhibitor with broad-spectrum antimycobacterial activity', *Antimicrobial Agents and Chemotherapy*, 65(5), pp. 1–13. Available at: https://doi.org/10.1128/AAC.02420-20.

Ganapathy, U.S. and Dick, T. (2022) 'Why Matter Matters: Fast-Tracking Mycobacterium abscessus Drug Discovery', *Molecules*, 27(6948), pp. 1–13. Available at: https://doi.org/10.3390/molecules27206948.

Gómara, M. and Ramón-García, S. (2019) 'The FICI paradigm: Correcting flaws in antimicrobial in vitro synergy screens at their inception', *Biochemical Pharmacology*, 163(2019), pp. 299–307. Available at: https://doi.org/10.1016/j.bcp.2019.03.001.

Greendyke, R. and Byrd, T.F. (2008) 'Differential Antibiotic Susceptibility of Mycobacterium abscessus Variants in Biofilms and Macrophages Compared to That of Planktonic Bacteria', *Antimicrobial Agents and Chemotherapy*, 52(6), pp. 2019–2026. Available at: https://doi.org/10.1128/AAC.00986-07.

De Groote, M.A. *et al.* (2006) 'Relationships between Mycobacterium Isolates from Patients with Pulmonary Mycobacterial Infection and Potting Soils', *Applied and Environmental Microbiology*, 72(12), pp. 7602–7606. Available at: https://doi.org/10.1128/AEM.00930-06.

Holt, M.R. and Baird, T. (2023) 'Treatment Approaches to Mycobacterium abscessus Pulmonary Disease', *Clinics in Chest Medicine*, 44(4), pp. 785–798. Available at: https://doi.org/10.1016/j.ccm.2023.06.010.

Hsieh, M.H. *et al.* (1993) 'Synergy assessed by checkerboard', *Diagnostic Microbiology and Infectious Disease*, 16(4), pp. 343–349. Available at: https://www.sciencedirect.com/science/article/pii/073288939390087N?via%3Dihub.

Van Ingen, J. *et al.* (2012) 'Resistance mechanisms and drug susceptibility testing of nontuberculous mycobacteria', *Drug Resistance Updates*, 15(3), pp. 149–161. Available at: https://doi.org/10.1016/j.drup.2012.04.001.

van Ingen, J. *et al.* (2018) 'A definition of the Mycobacterium avium complex for taxonomical and clinical purposes, a review', *International Journal of Systematic and Evolutionary Microbiology*, 68(11), pp. 3666–3677. Available at: https://doi.org/10.1099/ijsem.0.003026.

van Ingen, J. *et al.* (2024) 'Rifampicin has no role in treatment of Mycobacterium avium complex pulmonary disease and bactericidal sterilising drugs are needed: a viewpoint', *European Respiratory Journal*, 63(5), pp. 1–4. Available at: https://doi.org/10.1183/13993003.02210-2023.

Jarand, J. *et al.* (2011) 'Clinical and microbiologic outcomes in patients receiving treatment for Mycobacterium abscessus pulmonary disease', *Clinical Infectious Diseases*, 52(5), pp. 565–571. Available at: https://doi.org/10.1093/cid/ciq237.

Jeong, J. *et al.* (2018) 'Pathogen Box screening for hit identification against Mycobacterium abscessus', *PLoS ONE*, 13(4), pp. 1–10. Available at: https://doi.org/10.1371/journal.pone.0195595.

Johansen, M.D., Herrmann, J.-L. and Kremer, L. (2020) 'Non-tuberculous mycobacteria and the rise of Mycobacterium abscessus', *Nature Reviews Microbiology*, 18(7), pp. 392–407. Available at: https://doi.org/10.1038/s41579-020-0331-1.

Johnson, J.S. et al. (2019) 'Evaluation of 16S rRNA gene sequencing for species and strain-level microbiome analysis', Nature Communications, 10(5029), pp. 1–11. Available at: https://doi.org/10.1038/s41467-019-13036-1.

Kamariza, M. *et al.* (2018) 'Rapid detection of Mycobacterium tuberculosis in sputum with a solvatochromic trehalose probe', *Science Translational Medicine*, 10(430), pp. 1–12. Available at: https://doi.org/10.1126/scitranslmed.aam6310.

Kamariza, M. *et al.* (2021) 'Toward Point-of-Care Detection of Mycobacterium tuberculosis: A Brighter Solvatochromic Probe Detects Mycobacteria within Minutes', *JACS Au*, 1(9), pp. 1368–1379. Available at: https://doi.org/10.1021/jacsau.1c00173.

Kim, Y. *et al.* (2023) 'Gastroesophageal Reflux Disease Increases Susceptibility to Nontuberculous Mycobacterial Pulmonary Disease', *Chest*, 163(2), pp. 270–280. Available at: https://doi.org/10.1016/j.chest.2022.08.2228.

Kirsch, S.H., Haeckl, F.P.J. and Müller, R. (2022) 'Beyond the approved: target sites and inhibitors of bacterial RNA polymerase from bacteria and fungi', *Natural Product Reports*, 39(6), pp. 1226–1263. Available at: https://doi.org/10.1039/d1np00067e.

Kumar, K. *et al.* (2022) 'Management of Mycobacterium avium complex and Mycobacterium abscessus pulmonary disease: therapeutic advances and emerging treatments', *European Respiratory Review*, 31(163), pp. 1–17. Available at: https://doi.org/10.1183/16000617.0212-2021.

Kumar, P. *et al.* (2017) 'Mycobacterium abscessus L,D-transpeptidases are susceptible to inactivation by carbapenems and cephalosporins but not penicillins', *Antimicrobial Agents and Chemotherapy*, 61(10), pp. 1–13. Available at: https://doi.org/10.1128/AAC.00866-17.

Lanni, F. *et al.* (2023) 'Adaptation to the intracellular environment of primary human macrophages influences drug susceptibility of Mycobacterium tuberculosis', *Tuberculosis*, 139(102318), pp. 1–9. Available at: https://doi.org/10.1016/j.tube.2023.102318.

Lan, T. *et al.* (2022) 'Redesign of Rifamycin Antibiotics to Overcome ADP-Ribosylation-Mediated Resistance', *Angewandte Chemie International Edition*, 61(45), pp. 1–7. Available at: https://doi.org/10.1002/anie.202211498.

Lin, W. *et al.* (2017) 'Structural Basis of Mycobacterium tuberculosis Transcription and Transcription Inhibition', *Molecular Cell*, 66(2), pp. 169-179.e8. Available at: https://doi.org/10.1016/j.molcel.2017.03.001.

Low, J.L. *et al.* (2017) 'Screening of TB actives for activity against nontuberculous mycobacteria delivers high hit rates', *Frontiers in Microbiology*, 8(1539), pp. 2–9. Available at: https://doi.org/10.3389/fmicb.2017.01539.

Machelart, A. *et al.* (2017) 'Host-directed therapies offer novel opportunities for the fight against tuberculosis', *Drug Discovery Today*, 22(8), pp. 1250–1257. Available at: https://doi.org/10.1016/j.drudis.2017.05.005.

Maurer, F.P. *et al.* (2014) 'Lack of antimicrobial bactericidal activity in Mycobacterium abscessus', *Antimicrobial Agents and Chemotherapy*, 58(7), pp. 3828–3836. Available at: https://doi.org/10.1128/AAC.02448-14.

Molina-Torres, C.A. *et al.* (2018) 'Evaluation of the intracellular activity of drugs against Mycobacterium abscessus using a THP-1 macrophage model', *Journal of Microbiological Methods*, 148(March), pp. 29–32. Available at: https://doi.org/10.1016/j.mimet.2018.03.020.

NCT04922554 (2021) *Oral Omadacycline Vs. Placebo in Adults with NTM Pulmonary Disease Caused by Mycobacterium Abscessus Complex*. Available at: https://clinicaltrials.gov/study/NCT04922554.

NCT05327803 (2022) *Study of Epetraborole in Patients With Treatment-refractory MAC Lung Disease*. Available at: https://clinicaltrials.gov/study/NCT05327803.

NCT05496374 (2022) *A Study to Evaluate the Efficacy, Safety, Tolerability, and Pharmacokinetics of SPR720 as Compared With Placebo for the Treatment of Participants With Mycobacterium Avium Complex (MAC) Pulmonary Disease*. Available at: https://clinicaltrials.gov/study/NCT05496374.

Nguyen, M.-V.H. and Daley, C.L. (2023) 'Treatment of Mycobacterium avium Complex Pulmonary Disease: When Should I Treat and What Therapy Should I Start?', *Clinics in Chest Medicine*, 44(4), pp. 771–783. Available at: https://doi.org/10.1016/j.ccm.2023.06.009.

Oren, A. and Garrity, G. (2018) 'List of new names and new combinations previously effectively, but not validly, published', *International Journal of Systematic and Evolutionary Microbiology*, 68(5), pp. 1411–1417. Available at: https://doi.org/10.1099/ijsem.0.002711.

Parmar, S. and Tocheva, E.I. (2023) 'The cell envelope of Mycobacterium abscessus and its role in pathogenesis', *PLOS Pathogens*. Edited by C. Dehio, 19(5), pp. 1–14. Available at: https://doi.org/10.1371/journal.ppat.1011318.

Poirier, V. and Av-Gay, Y. (2015) 'Intracellular Growth of Bacterial Pathogens: The Role of Secreted Effector Proteins in the Control of Phagocytosed Microorganisms', *Microbiology Spectrum*, 3(6), pp. 1–16. Available at: https://doi.org/10.1128/microbiolspec.vmbf-0003-2014.

Prevots, D.R. et al. (2023) 'Global Epidemiology of Nontuberculous Mycobacterial Pulmonary Disease: A Review', Clinics in Chest Medicine, 44(4), pp. 675–721. Available at: https://doi.org/10.1016/J.CCM.2023.08.012.

Prevots, D.R. and Marras, T.K. (2015) 'Epidemiology of Human Pulmonary Infection with Nontuberculous Mycobacteria', *Clinics in Chest Medicine*, 36(1), pp. 13–34. Available at: https://doi.org/10.1016/j.ccm.2014.10.002.

Ragunathan, P., Dick, T. and Grüber, G. (2022) 'Anti-Mycobacterium abscessus Activity of Tuberculosis F-ATP Synthase Inhibitor GaMF1.', *Antimicrobial agents and chemotherapy*, 66(5), pp. 1–5. Available at: https://doi.org/10.1128/aac.00018-22.

Richter, A. *et al.* (2018) 'Screening of preselected libraries targeting mycobacterium abscessus for drug discovery', *Antimicrobial Agents and Chemotherapy*, 62(9), pp. 1–11. Available at: https://doi.org/10.1128/AAC.00828-18.

Richter, A., Shapira, T. and Av-Gay, Y. (2019) 'THP-1 and Dictyostelium Infection Models for Screening and Characterization of Anti-Mycobacterium abscessus Hit Compounds',

*Antimicrobial Agents and Chemotherapy*, 64(1), pp. 1–12. Available at: https://doi.org/10.1128/AAC.01601-19.

Rogall, T. *et al.* (1990) 'Towards a phylogeny and definition of species at the molecular level within the genus Mycobacterium', *International Journal of Systematic Bacteriology*, 40(4), pp. 323–330. Available at: https://doi.org/10.1099/00207713-40-4-323.

Rosselló-Mora, R. (2001) 'The species concept for prokaryotes', FEMS Microbiology Reviews, 25(1), pp. 39–67. Available at: https://doi.org/10.1016/S0168-6445(00)00040-1.

Roux, A.L. *et al.* (2016) 'The distinct fate of smooth and rough Mycobacterium abscessus variants inside macrophages', *Open Biology*, 6(160185), pp. 1–12. Available at: https://doi.org/10.1098/rsob.160185.

Rüger, K. *et al.* (2014) 'Characterization of rough and smooth morphotypes of mycobacterium abscessus isolates from clinical specimens', *Journal of Clinical Microbiology*, 52(1), pp. 244–250. Available at: https://doi.org/10.1128/JCM.01249-13.

Sarathy, J.P. *et al.* (2016) 'Prediction of Drug Penetration in Tuberculosis Lesions', *ACS Infectious Diseases*, 2(8), pp. 552–563. Available at: https://doi.org/10.1021/acsinfecdis.6b00051.

Sarathy, J.P. *et al.* (2022) 'Mycobacterium tuberculosis DprE1 Inhibitor OPC-167832 Is Active against Mycobacterium abscessus In Vitro', *Antimicrobial Agents and Chemotherapy*, 66(12), pp. 1–7. Available at: https://doi.org/10.1128/aac.01237-22.

Sarathy, J.P. and Dartois, V. (2020) 'Caseum: A niche for mycobacterium tuberculosis drug-tolerant persisters', *Clinical Microbiology Reviews*, 33(3), pp. 1–19. Available at: https://doi.org/10.1128/CMR.00159-19.

Spero Therapeutics (2025) Spero Therapeutics Announces SPR720 Phase 2a Interim Results and Provides a Business Update. Available at: https://s3.amazonaws.com/b2icontent.irpass.cc/2748/rl139704.pdf.

Teng, R. and Dick, T. (2003) 'Isoniazid resistance of exponentially growing Mycobacterium smegmatis biofilm culture', *FEMS Microbiology Letters*, 227(2), pp. 171–174. Available at: https://doi.org/10.1016/S0378-1097(03)00584-6.

Thomson, R. *et al.* (2013) 'Isolation of nontuberculous mycobacteria (NTM) from household water and shower aerosols in patients with pulmonary disease caused by NTM', *Journal of Clinical Microbiology*, 51(9), pp. 3006–3011. Available at: https://doi.org/10.1128/JCM.00899-13.

Tortoli, E. *et al.* (2019) 'Same meat, different gravy: Ignore the new names of mycobacteria', *European Respiratory Journal*, 54(1), pp. 19–21. Available at: https://doi.org/10.1183/13993003.00795-2019.

Victoria, L. *et al.* (2021) 'Mycobacterium abscessus complex: A Review of Recent Developments in an Emerging Pathogen', *Frontiers in Cellular and Infection Microbiology*, 11(659997), pp. 1–8. Available at: https://doi.org/10.3389/fcimb.2021.659997.

Weiss, G. and Schaible, U.E. (2015) 'Macrophage defense mechanisms against intracellular bacteria', *Immunological Reviews*, 264(1), pp. 182–203. Available at: https://doi.org/10.1111/imr.12266.

Wengenack, N.L. *et al.* (2024) 'This is giving me a complex: a practical attempt to streamline nontuberculous mycobacteria nomenclature for clinical purposes', *Journal of Clinical Microbiology*, 62(3), pp. 1–5. Available at: https://doi.org/10.1128/jcm.01531-23.

Wu, M.-L. *et al.* (2018) 'NTM drug discovery: status, gaps and the way forward', *Drug Discovery Today*, 23(8), pp. 1502–1519. Available at: https://doi.org/10.1016/j.drudis.2018.04.001.

Wu, M.L., Gengenbacher, M. and Dick, T. (2016) 'Mild nutrient starvation triggers the development of a small-cell survival morphotype in mycobacteria', *Frontiers in Microbiology*, 7(947), pp. 1–11. Available at: https://doi.org/10.3389/fmicb.2016.00947.

Xie, M. *et al.* (2023) 'ADP-ribosylation-resistant rifabutin analogs show improved bactericidal activity against drug-tolerant M. abscessus in caseum surrogate', *Antimicrobial Agents and Chemotherapy*. Edited by K.E. Dooley, 67(9), pp. 1–8. Available at: https://doi.org/10.1128/aac.00381-23.

Yam, Y.-K.K. *et al.* (2020) 'Extreme Drug Tolerance of Mycobacterium abscessus "Persisters"', *Frontiers in Microbiology*, 11(359), pp. 1–9. Available at: https://doi.org/10.3389/fmicb.2020.00359.

Yan, M., Brode, S.K. and Marras, T.K. (2023) 'Treatment of the Less Common Nontuberculous Mycobacterial Pulmonary Disease', *Clinics in Chest Medicine*, 44(4), pp. 799–813. Available at: https://doi.org/10.1016/j.ccm.2023.06.011.

# Supporting Information

## Supplemental Material Publication II

The supplement has been shortened accordingly, with a focus on the sections relevant to the present work.

jm3c00009_si_001.pdf (acs.org)

# Supplementary Information

## Synthesis and characterization of phenylalanine amides active against *Mycobacterium abscessus* and other mycobacteria

Markus Lang[a], Uday S. Ganapathy[b], Lea Mann[a], Rana Abdelaziz[a], Rüdiger W. Seidel[a], Richard Goddard[c], Ilaria Sequenzia[a], Sophie Hoenke[f], Philipp Schulze[c], Wassihun Wedajo Aragaw[b], René Csuk, Thomas Dick[b,d,e], Adrian Richter[a]*

[a]Institut für Pharmazie, Martin-Luther-Universität Halle-Wittenberg, Wolfgang-Langenbeck-Str. 4, 06120 Halle (Saale), Germany

[b]Center for Discovery and Innovation, Hackensack Meridian Health, 111 Ideation Way, 07110 Nutley, New Jersey, USA

[c]Max-Planck-Institut für Kohlenforschung, Kaiser-Wilhelm-Platz 1, 45470 Mülheim an der Ruhr, Germany

[d]Department of Medical Sciences, Hackensack Meridian School of Medicine, 123 Metro Blvd, 07110 Nutley, New Jersey, USA

[e]Department of Microbiology and Immunology, Georgetown University, 3900 Reservoir Road, N.W., 20007 Washington DC, USA

[f]Institut für Chemie, Martin-Luther-Universität Halle-Wittenberg, Kurt-Mothes-Str. 2, 06120 Halle (Saale), Germany

*Corresponding author:

Dr. Adrian Richter

Wolfgang-Langenbeck-Str. 4

06120 Halle (Saale)

Germany

adrian.richter@pharmazie.uni-halle.de

## Table of Contents

## 3. Antimycobacterial activity of MMV688845 derivatives, additional data

**Table S4** Antimycobacterial activity of MMV688845 derivatives[A], OD measurements

| | | | | | $MIC_{90}$ | | | |
|---|---|---|---|---|---|---|---|---|
| | | | | | ***Msmeg* mc² 155[B]** | ***Mabs ATCC19977*[B]** | **Mabs ATCC19977[B]** | ***Mintra* ATCC 35761[B]** |
| | | | | | 7H9 | 7H9 | MHII | 7H9 |
| | $R^1$ | $R^2$ | X, Y | $R^3$ | OD | OD | OD | OD |
| **MMV845** | Phenyl | H | O, N | 2-Thiophenoyl | 0.78 | 6.25 | 12.5 | 0.39 |
| **6** | Phenyl | H | S, N | 2-Thiophenoyl | 3.13 | 6.25 | > 100 | 0.39 |
| **7** | Phenyl | H | S, N | 2-F-Benzoyl | 3.13 | 6.25 | > 100 | 0.78 |
| **11** | Phenyl | F | S, N | 2-Thiophenoyl | 3.13 | 25 | > 100 | 1.56 |
| **12** | Phenyl | F | S, N | 2-F-Benzoyl | 3.13 | 25 | > 100 | 1.56 |
| **14** | Phenyl | H | S=O, N | 2-Thiophenoyl | 1.56 | 3.13 | 6.25 | 0.1 |
| **15** | Phenyl | H | S=O, N | 2-F-Benzoyl | 0.7 | 6.25 | 6.25 | 0.1 |
| **17** | Phenyl | F | S=O, N | 2-Thiophenoyl | 1.56 | 1.56 | 6.25 | 0.2 |
| **18** | Phenyl | F | S=O, N | 2-F-Benzoyl | 1.56 | 3.13 | 3.13 | 0.39 |
| **20** | Phenyl | H | O=S=O, N | 2-Thiophenoyl | 1.56 | 1.56 | 3.13 | 0.1 |
| **24** | Phenyl | H | O=S=O, N | 2-F-Benzoyl | 0.78 | 0.78 | 1.56 | 0.1 |
| **28** | Phenyl | F | O=S=O, N | 2-Thiophenoyl | 1.56 | 3.13 | 1.56 | 0.1 |
| **29** | Phenyl | F | O=S=O, N | 2-F-Benzoyl | 1.56 | 3.13 | 1.56 | 0.2 |
| **32** | Phenyl | H | S, CH | 2-Thiophenoyl | 6.25 | 50 | 100 | 12.5 |
| **34** | Phenyl | H | S=O, CH | 2-Thiophenoyl | 3.13 | 25 | 25 | 3.13 |
| **36** | p-Hydroxyphenyl | F | S, N | 2-Thiophenoyl | 12.5 | 25 | 25 | 0.2 |
| **37** | p-Hydroxyphenyl | F | S, N | 2-F-Benzoyl | 6.25 | 25 | 50 | 0.39 |
| **39** | p-Hydroxyphenyl | F | O=S=O, N | 2-Thiophenoyl | 6.25 | 12.5 | 3.13 | 0.05 |
| **40** | p-Hydroxyphenyl | F | O=S=O, N | 2-F-Benzoyl | 6.25 | 6.25 | 6.25 | 0.2 |
| **42** | 3-Thiophenyl | H | O, N | 2-Thiophenoyl | 1.56 | 12.5 | 25 | 1.56 |
| **43** | 3-Thiophenyl | H | O, N | 2-F-Benzoyl | 1.56 | 6.25 | 12.5 | 1.56 |
| **45** | 2-Thiophenyl | H | O, N | 2-Thiophenoyl | 1.56 | 12.5 | 25 | 1.56 |
| **46** | 2-Thiophenyl | H | O, N | 2-F-Benzoyl | 1.56 | 12.5 | 12.5 | 1.56 |
| **50** | 3-Thiophenyl | H | S=O, N | 2-Thiophenoyl | 1.56 | 6.25 | 12.5 | 0.39 |
| **51** | 3-Thiophenyl | H | S=O, N | 2-F-Benzoyl | 1.56 | 6.25 | 12.5 | 0.39 |
| **53** | 2-Thiophenyl | H | S=O, N | 2-Thiophenoyl | 3.13 | 6.25 | 25 | 0.39 |
| **54** | 2-Thiophenyl | H | S=O, N | 2-F-Benzoyl | 1.56 | 6.25 | 12.5 | 0.39 |

[A]For detailed information on the methodology of the assays see supporting information. [B]Incubated for three days at 37 °C (*M. smegmatis* and *M. abscessus*) or five days (*M. intracellulare*). Performed in duplicate, results were averaged. Data was obtained via OD measurements.



d

# Appendix

## Angaben zur Person und zum Bildungsgang

---

**Name/Geburtsname:** Mann

**Vorname:** Lea

**Geschlecht:** weiblich

**Staatsangehörigkeit:** deutsch

**Akademischer Grad:**

Approbation als Apothekerin

Diplom: Martin-Luther-Universität Halle-Wittenberg

---

**Fachgebiet der Promotion:** Charakterisierung von antimykobakteriellen Substanzen

---

**Besuchte Hochschule und abgelegten Abschlussprüfungen:**

Studium der Pharmazie an der Martin-Luther-Universität Halle-Wittenberg

3. Staatsexamen

2. Staatsexamen

1. Staatsexamen

---

**List of Publications**

1. **Mann L**, Lang M, Schulze P, Halz JH, Csuk R, Hoenke S, Seidel RW, Richter A. 2021. Racemization-free synthesis of Nα-2-thiophenoyl-phenylalanine-2-morpholinoanilide enantiomers and their antimycobacterial activity. Amino Acids 53:1187–1196.

2. Sirak B, **Mann L**, Richter A, Asres K, Imming P. 2021. In Vivo Antimalarial Activity of Leaf Extracts and a Major Compound Isolated from Ranunculus multifidus Forsk. Molecules 26:1–16.

3. Beuchel A, Robaa D, Negatu DA, Madani A, Alvarez N, Zimmerman MD, Richter A, **Mann L**, Hoenke S, Csuk R, Dick T, Imming P. 2022. Structure-Activity Relationship of Anti-Mycobacterium abscessus Piperidine-4-carboxamides, a New Class of NBTI DNA Gyrase Inhibitors. ACS Med Chem Lett 13:417–427.

4. Richter A, Seidel RW, Goddard R, Eckhardt T, Lehmann C, Dörner J, Siersleben F, Sondermann T, **Mann L**, Patzer M, Jäger C, Reiling N, Imming P. 2022. BTZ-Derived Benzisothiazolinones with In Vitro Activity against Mycobacterium tuberculosis. ACS Med Chem Lett 13:1302–1310.

5. **Mann L**, Ganapathy US, Abdelaziz R, Lang M, Zimmerman MD, Dartois V, Dick T, Richter A. 2022. In Vitro Profiling of the Synthetic RNA Polymerase Inhibitor MMV688845 against Mycobacterium abscessus. Microbiol Spectr 10:1–14.

6. Lang M, Ganapathy US, **Mann L**, Abdelaziz R, Seidel RW, Goddard R, Sequenzia I, Hoenke S, Schulze P, Aragaw WW, Csuk R, Dick T, Richter A. 2023. Synthesis and Characterization of Phenylalanine Amides Active against Mycobacterium abscessus and Other Mycobacteria. J Med Chem 66:5079–5098.

7. Abdelaziz R, Di Trani JM, Sahile H, **Mann L**, Richter A, Liu Z, Bueler SA, Cowen LE, Rubinstein JL, Imming P. 2023. Imidazopyridine Amides: Synthesis, Mycobacterium smegmatis CIII 2 CIV 2 Supercomplex Binding, and In Vitro Antimycobacterial Activity. ACS Omega 8:19081–19098.

8. Richter A, Goddard R, Siersleben F, **Mann L**, Seidel RW. 2023. Structural Elucidation of 2-(6-(Diethylamino)benzofuran-2-yl)-3-hydroxy-4H-chromen-4-one and Labelling of Mycobacterium aurum Cells. Molbank 2023:M1647.

9. Courbon GM, Palme PR, **Mann L**, Richter A, Imming P, Rubinstein JL. 2023. Mechanism of mycobacterial ATP synthase inhibition by squaramides and second generation diarylquinolines. EMBO J 42:1–12.

10. Richter A, Goddard R, **Mann L**, Siersleben F, Seidel RW. 2024. Structural characterization of a 3-hydroxychromone dye trehalose conjugate for fluorescent labelling of mycobacteria. J Mol Struct 1298:1–8.

11. Lang M, Ganapathy US, **Mann L**, Seidel RW, Goddard R, Erdmann F, Dick T, Richter A. 2024. Synthesis and in vitro Metabolic Stability of Sterically Shielded Antimycobacterial Phenylalanine Amides. ChemMedChem 19:1–13.

12. **Mann L**, Siersleben F, Lang M, Richter A. 2024. Determination of bactericidal activity against 3HC-2-Tre-labelled Mycobacterium abscessus (Mycobacteroides abscessus) by automated fluorescence microscopy. J Microbiol Methods 224:1–7.

## Contribution to Conferences

### Talks

*Antimycobacterial drug discovery: Synthetic chemistry and antimycobacterial characterization.*
Pharmaceutical research day, July 2023 (Halle)

*Assay Development and Microbiological Characterization against Mycobacterium abscessus.*
Research Symposium on: "Novel Antimicrobial Agents: A Medicinal Chemistry Perspective", August 2023 (Kairo)

*Mycobacterium abscessus assay development.*
Conference: Targets and inhibitors of Mycobacteria including Non-Tuberculous Mycobacteria,
July 2024 (Toronto)

---

### Poster

**Mann L**, Richter A. *Synergy testing of the RNA polymerase inhibitor MMV688845 against Mycobacterium abscessus.*
Colorado Mycobacteria Conference, May 2022 (Fort Collins)

**Mann L**, Richter A. *Synergy testing of the RNA polymerase inhibitor MMV688845 against Mycobacterium abscessus.*
Pharmaceutical research day, July 2022 (Halle)

**Mann L**, Richter A. *Activity of antibiotic combinations with a synthetic RNA polymerase inhibitor against Mycobacterium abscessus.*
DPhG DoktorandInnen Tagung, March 2023 (Bonn)

**Mann L**, Siersleben F, Richter A. *Fluorescence based method for determination of minimal bactericidal concentration against Mycobacteria.*
Tuberculosis Drug Discovery and Development Gordon Research Conference,
July 2023 (Barcelona)

**Mann L**, Siersleben F, Lang M, Richter A. *Fluorescence based method for determination of minimal bactericidal concentration against Mycobacteria.*
Pharmaceutical research day, July 2023 (Halle)

**Mann L**, Siersleben F, Lang M, Richter A. *Fluorescence-based assay for the determination of the minimum bactericidal concentration against Mycobacterium abscessus.*
ECFS Basic Science Conference, March 2024 (Malta)

## Eidesstattliche Erklärung

Hiermit erkläre ich gemäß § 5 der Promotionsordnung der Naturwissenschaftlichen Fakultät I (Biowissenschaften) der Martin-Luther-Universität Halle-Wittenberg, dass ich die vorliegende Dissertation selbständig und ohne fremde Hilfe verfasst habe. Ferner habe ich keine anderen als die angegebenen Quellen und Hilfsmittel benutzt und die Stellen, die wörtlich oder inhaltlich aus anderen Werken entnommen wurden, als solche kenntlich gemacht.

Darüber hinaus wurden keine weiteren Promotionsversuche unternommen.

Die Dissertation wurde ausschließlich der Mathematisch-Naturwissenschaftlichen Fakultät I der Martin-Luther-Universität Halle-Wittenberg vorgelegt und ist an keiner anderen Hochschule in Deutschland oder im Ausland zur Erlangung des Doktorgrades eingereicht worden.

Halle (Saale), 10.12.2024 _____

Ort, Datum Unterschrift